The identification of fatty acids in deep-sea sponge *Geodia barretti*, and its response to an acute crude oil exposure

Elise Tvinnereim Otnes

Master Thesis
Department of Chemistry
University of Bergen

Aknowledgements

Sonnich Meier, my supervisor at the Institute of Marine Research, thank you for all interesting discussions and guidance in the field of lipid chemistry and PAHs. Thank you for encouraging me, for having large expectations for me and for allowing me to deep dive into a field no one has ever investigated before. Not only did this give me extra agitation for this work. It also gave me the opportunity to present my results at an international conference, a great experience in which I am grateful to have.

Svein Are Mjøs, my supervisor at the University of Bergen, thank you for supervising my thesis and giving me advice along the way. The precise identification of my fatty acids would not have been possible without *ChromBox* and the fact that the door was always open when I had struggles regarding this or other aspects of my thesis. His help throughout this period has been irreplaceable.

Anders Thorsen, thank you for helping me planning the microscopy during the experimental work at Austevoll Research Station and for photographing all my TLC plates. Thank you, Bjarte Holmelid, for performing LC-MS analyses on my lipid fractions.

Thank you so much, to all who helped me with the experimental work. Thank you, Raymond Bannister, for giving letting me join the sponge harvesting, for enriching my understanding of sponges with such enthusiasm and positivity and for all the work performed at Austevoll Research Station. Thank you, Chloè Stevenne, for the time we spent working together, for her company and her results regarding the biological response of the sponges. Thank you Cathinka Krogness and Annhild Engevik, for all help with the experimental setup and sampling. Also, to all, thanks for your kindness, the laughs and the dinners we shared way passed working hours.

Thank you to all employees at the Chemistry Laboratory at the Institute of Marine Research. It has been a pleasure working with you and amongst you. A special thanks goes to Carey Donald, for all the learning-by-doing process of PAH body burden extraction, and for all help at the instrument and at data handling. Your ever-helpful presence at the lab has been more than expected. Patient guidance from Arve Fossen also requires a special thanks. Without your help, the data handling of my fatty acid results would be a never-ending story. Also, a large hand to Therese Aase and Grete Tveit for showing me extraction procedures on fatty acids from tissue samples and PAHs from water samples respectively, and for helping me find my way around the lab.

Thanks to my uncle, Jan, who helped me with the boring yet necessary work formatting to presenting my result in the best possible way and to Elin Sørhus for guidance regarding citeing.

Last, I would like to thank my family and friends for supporting me through this, at times, stressful period of my life. Thank you for all the good memories, advice, kindness and craziness that has brought a smile to my face. Finally, I would like to thank Sindre for his continuous support, kind words and for his effort at times I had no opportunity to contribute at home.

Contents

Abstract

Globally, offshore oil explorations are moving into deeper locations and to more extreme latitudes. In Norway, this means that oil exploration is being extended northwards to the areas around the Lofoten Islands, the Norwegian Arctic and the Barents Sea. The extraction of oil in this area is often undertaken by subsea installation, increasing the concern of accidental release of hydrocarbons into deep-sea ecosystems. Surprisingly, the impacts of oil on deep-sea sponges remain unexplored, despite sponges being particularly dominant near oil and gas exploration locations in the Northern Atlantic.

The sponge *Geodia barretti* is a filter-feeding sedentary organism dominating the Norwegian continental shelf and surrounding areas. Sponges carry out important functional roles in the deep-sea benthic environment, including providing habitat and shelter for a variety of marine organisms, substrate stabilising and as a direct food source. More importantly, sponges link pelagic and benthic food webs through their ability to filter copious amounts of water and together with their symbiosis with complex microbial communities carry out carbon and nutrient cycling through aerobic and anaerobic pathways.

This master thesis presents the findings from a mesocosm study, where sponge explants of *G. barretti* were exposed to three concentrations of dispersed oil and compared with control treatments (0 µg/L, 33 µg/L, 100 µg/L and 300 µg/L). Sponge explants were exposed to oil for a duration of 8 days, followed by a recovery period of 30 days. Both the effect of duration and intensity of the exposure were investigated. The effect parameters were focused on measuring tissue uptake of polyaromatic hydrocarbons (PAH) and changes in physiology (lipid composition). The identification of the lipid profile of *G. barretti* was an important part of the thesis in conjunction to investigate the changes in lipid composition.

Results demonstrate that PAH compounds from the medium and high treatments did accumulate in the sponge explant with a clear gradient considering both time and intensity. After the 30-day recovery, concentrations went back to control levels for the medium treatment. The levels decreased drastically for the high treatment as well, however the levels were still significantly higher than control levels. The lipid profile was found to consist of mainly saturated fatty acids where a large share were mono branched, and di-unsaturated fatty acids where a large share was found to be very long chained and possibly branched fatty acids. Lipid composition was slightly affected by the PAH accumulation, but no drastic changes were found. These findings are amplified by the findings in changes of the sponge-associated microbiome and the lack other strong physiological effects on the oil exposed sponges.

Even though PAH does accumulate in sponge *G. barretti*, it does not seem to cause acute or long-term effects on the sponge's mortality, and it seems to have a certain resilience to crude oil exposure.

Sammendrag

Verden over utvides oljeleting mot dypere farvann og mer ekstreme breddegrader. I Norge betyr dette at oljevirksomheten ekspanderes nordover mot områdene rundt Lofoten, Barentshavet og den norske delen av Arktis. Oljeutvinningen blir ofte gjort ved bruk av undersjøiske installasjoner på dype farvann. Dette øker faren for ulykker som slipper ut hydrokarboner til økosystemene som befinner seg her. Selv om svamper er dominerende organismer rundt olje- og gassområder i Nord-Atlanteren, har likevel ingen undersøkt effekten av olje på dyphavssvamp.

Svampen *Geodia barretti* er en filterende og stillesittende organisme som dominerer den norske kontinentalsokkelen og omliggende områder. Svamp har flere viktige roller i det bentiske miljøet. De fungerer som habitat og skjul for en rekke marine organismer, stabiliserer havbunnen og er en direkte kilde til mat. Enda viktigere er det likevel at de bilder sammen den pelagiske og bentiske næringskjeden ved å filtrere enorme mengder vann. En symbiose med komplekse bakteriekulturer gjør at de på denne måten resirkulerer både karbon og andre næringsmidler gjennom aerobe og anaerobe prosesser.

Denne masteroppgaven presenterer resultatene fra et tank-forsøk der replikaer av *G. barretti* ble eksponert for tre konsentrasjoner (33 µg/L, 100 µg/L and 300 µg/L) av disperserte oljedråper og sammenlignet med kontrollbehandlinger (0 µg/L). Eksponeringstiden var over en periode på 8 dager, etterfulgt av en rekonvalensperiode på 30 dager. Effekten av både behandlingens varighet og intensitet ble undersøkt. Parameterene som det ble fokusert på var opptaket av polyaromatiske hydrokarboner (PAH) i svampvev og fysiologiske endringer i form av endring av lipidsammensetning. Identifisering av lipidprofilen til *G. barretti* var en viktig den av arbeidet i sammenheng med å undersøke endringen i lipidsammensetning.

Resultatene viser at PAH akkumulerte i svampvev ved den mellomste og høye behandlingen. De hadde en gradient bade med tanke på intensitet og varighet. Etter en 30 dagers rekonvalensperiode falt konsentrasjonen tilbake til kontrollnivå for den mellomste behandlingen. For den høye behandlingen falt nivået drastisk, men det var signifikant forskjellig fra kontrollnivået. Lipidprofilen ble stort sett funnet til å bestå av mettede fettsyrer der et stort innslag av den var mono-forgrenede, og av di-umettede fettsyrer, der en stor del av den var svært lange og muligens forgrenede. Lipidsammensetningen fremstod som relativt upåvirket av akkumuleringen av PAH, men små endringer ble observert. Disse resultatene er forsterket av de fraværende endringene i svampens bakterieflora og andre sterke fysiologiske effekter hos den olje-eksponerte svampen.

Selv om PAH akkumulerer i G. barretti fører sannsynligvis ikke dette til en akutt eller langtidseffekt på svampens dødelighet, og den synes a ha en viss motstandsdyktighet mot eksponering av råolje.

List of abbreviations

APPEA – Australian Petroleum Production & Exploration Association
AW – Ash weight
BFPC - Benzothiophenes, fluorenes, pyrenes and chrysenes
CL – Cardiolipin
DAF – Dry ash free
DCM – Dichloromethane
DUFA – Diunsaturated fatty acids
DW – Dry weight
DWH – Deepwater Horizon
ECL – Equivalent chain length
EEZ – Exclusive economic zone
EI – Electron ionization
ESI – Electrospray ionization
FA – Fatty acid(s)
FAME – Fatty acid methyl ester(s)
FCL – Fractional chain length
FFA – Free fatty acid
FID – Flame ionization detector
GC – Gas Chromatography
GL – Glycerolipids
HC – Hydrocarbons
HPLC – High performance liquid chromatography
IMR – Institute of Marine Research
LC – Liquid chromatography
LC-FA – Long chain fatty acid(s)
LMS – Lysosomal membrane stability
m/z – Mass-to-charge ratio
M^+ - Molecular ion
MS – Mass Spectrometry
MUFA – Monounsaturated fatty acid(s)
NCS – Norwegian continental shelf
NMI – Non-methylene interrupted
NPD - Naphthalenes, phenanthrenes and dibenzothiophenes
PA – Phosphatidic acid
PAH – Polycyclic aromatic hydrocarbon
PC - Phosphatidylcholine
PCA – Principal component analysis
PE – Phosphatidylethanolamine
PG – Phosphatidylglycerol
PI - Phosphatidylinositol
PL – Phospholipid(s)
PS - Phosphatidylserine
PUFA – Polyunsaturated fatty acid(s)
r – Correlation coefficient
rpm – rounds per minute
RSD – Relative standard deviation

RT – retention time
SM - Sphingomyelin
SL – Sphingolipid(s)
TAG - Triacylglycerols
TLC – Thin layer chromatography
TOF – Time of flight
t_R – Retention time
TSS – Total Suspended Solids
VLC-FA – Very long chain fatty acid(s)
VOC – Volatile organic compound(s)
WW – Wet weight

1. Introduction

1.1. Background

Norwegian offshore oil exploration is being extended northwards to the area around the Lofoten Islands, the Norwegian Arctic and the Barents Sea. These areas are important spawning areas for several species, including economically important species such as cod (Sundby, 2013). Little research has been performed on the consequences of a major oil spill or blowout in northern cold seawaters and how it affects the species in these areas. To enhance our understanding of the vulnerability of these ecosystems to oil exposure, the Norwegian Institute of Marine Research (IMR) are performing research on several key organisms. This thesis will contribute to a comprehensive understanding by looking on the effects of oil exposure to the abundant and ecologically important deep-sea sponge *Geodia Barretti*. The results will enhance our understanding of the vulnerability and/or resilience of deep-sea sponges to hydrocarbon exposure and provide useful data for risk assessment associated with oil and gas exploration in the Northern Atlantic.

1.2. Oil spills in the marine environment

1.2.1. The petroleum industry in Norway and the world

According to the Australian Petroleum Production & Exploration Association (APPEA), *"Oil is the world's most important fuel and underpins our high standard of living. It provides modern convenience and freedom of movement and is crucial to transport systems." (APPEA, 2019)*. Oil and its associated by-products are essential for modern convenience as it is crucial for transport systems and to produce a variety of products such as plastics, lubricants, asphalts, pesticides and fertilisers (APPEA, 2019). In 2018 the global consumption was estimated to 99.2 million barrels per day (Statista, 2019), and is expected to rise in the years to come (OPEC, 2018). As the demand is steadily increasing exploration for new sites are taking place. The offshore oil and gas industry have experienced rapid growth in the recent decades and, now representing more than 30% of the global oil production. Due to a decline in easily accessible resources, oil drilling in deeper offshore areas are increasing (Bennear, 2015).

About 2% of the global reserves are extracted in Norway, making Norway is the world's 15th most important producer of petroleum (EIA, 2019). Figure 1 shows the Norwegian Exclusive Economic Zone (EEZ) that spread over 3 large marine ecosystems open to Norwegian petroleum activities. These include the North Sea, the Norwegian Sea and that Barents Sea, and by the end of 2018 it included 83 active fields and 8800 km of pipeline network (Ministry of Petroleum and Energy, 2019). The Lofoten area, located between the Norwegian Sea and the Barents Sea (Figure 1), is yet unexploited but is at the centre of an ongoing debate as it contains promising oil and gas reservoirs. This region has a high ecological value with a rich bird life, important spawning and nursery areas for abundant fish stocks, and important benthic communities such as sponge and coral aggregations (Blanchard et al., 2014). Few studies have evaluated the impacts of accidental oil spills in northern ecosystems. The vulnerability of the Lofoten area and the Barents Sea to oil spills have previously been investigated, and these ecosystems were found to be fragile to accidental spills. Oil degradation is slowed down by cold water temperature, darkness and ice. Some species confer less resilience to the ecosystem and some key organisms including benthos are thought to be particularly vulnerable to oil exposure (Forsgren, 2009). The effect of oil exposure on deep-sea benthic fauna along the Norwegian continental shelf (NCS) is, however, still relatively unexplored.

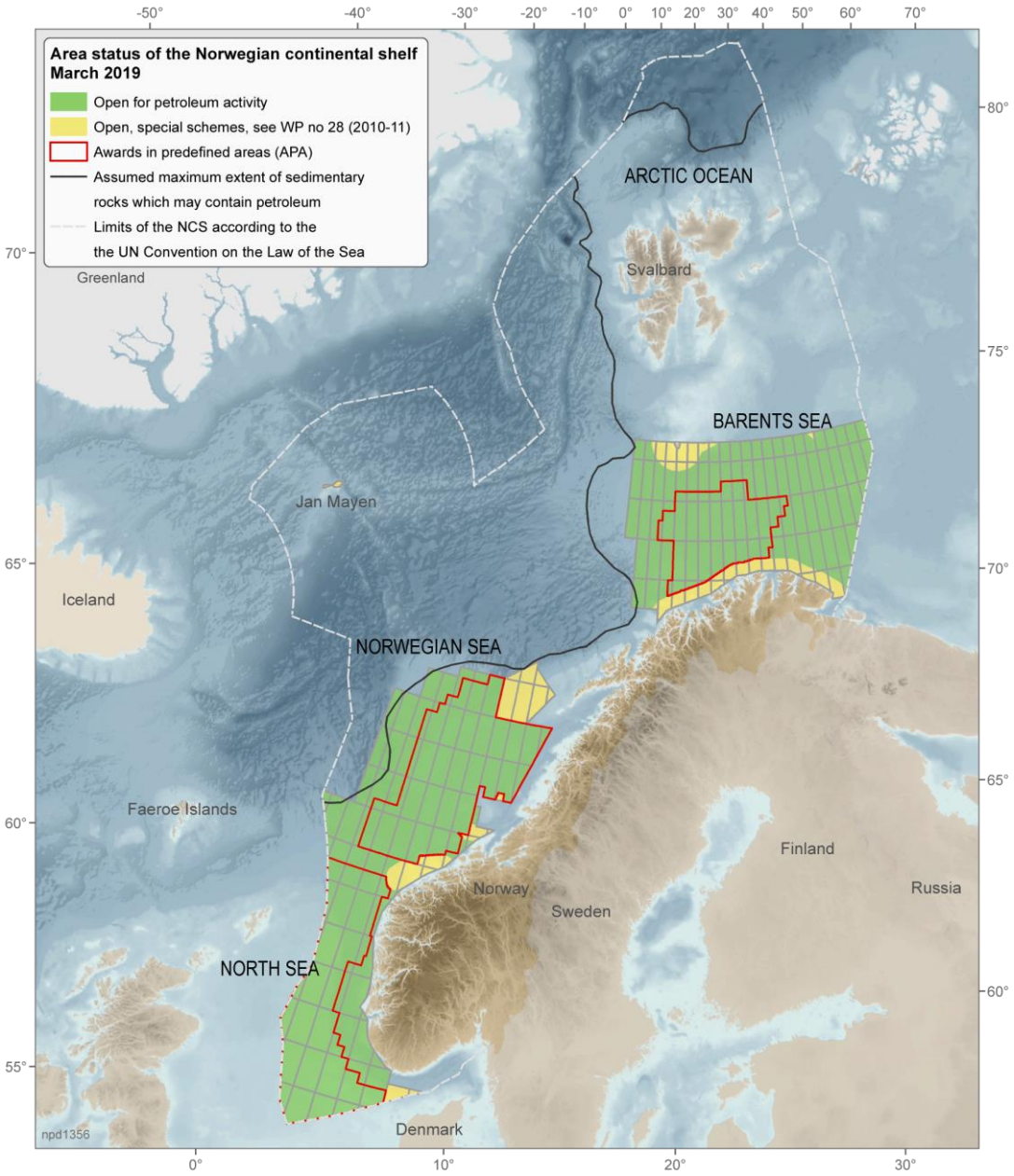

Figure 1: Petroleum licensing distribution on the Norwegian continental shelf. The Norwegian EEZ encompasses the North Sea, the Norwegian Sea and the Barents Sea. The Lofoten area is currently closed for petroleum activities but is at the centre of on-going debates (Norwegian Petroleum Directorate, 2019).

1.2.2. Types of oil and oil composition

Oil and gas, generally referred to as petroleum, are formed by millions of years of decomposition and pressurization of organic material. They are trapped in geological basins formed by a combination of source rock, reservoir rock, cap rock and a trap in the area. On the NCS, most petroleum deposits lie several thousand meters under the seabed (Norwegian Petroleum Directorate, 2019). Oils are composed by a range of organic compounds, but the content of each type of oil varies greatly. Oils are classified in four main types: very light (e.g. gasoline), light (e.g. diesel), medium (most crude oils) and heavy (heavy crude oils) (Shobert, 2013). Each of the different chemical compounds have their own toxicity and behave differently if released in the marine environment. Lighter and medium oils endanger the water column and intertidal areas. Heavy oils also impact the intertidal resources, but additionally, they contaminate sediments on the long term as their decomposition, evaporation and dissolution is slow (NOAA, 2019). Some of the compound classes found within crude oils are e.g.

polycyclic aromatic hydrocarbons (PAH), which present a high resilience in the environment (Hodson, 2017). PAHs are a class of organic compounds containing, with some exceptions, only carbon and hydrogen. They consist of two or more aromatic rings, and may be linear, angular or clustered. A range of PAHs are shown in figure 2, and they may be methylated on several sites or have benzo isomers (Achten and Andersson, 2015).The size and shape decide characteristics such as volatility and solubilization, and the largest molecules are the most persistent (Achten and Andersson, 2015).

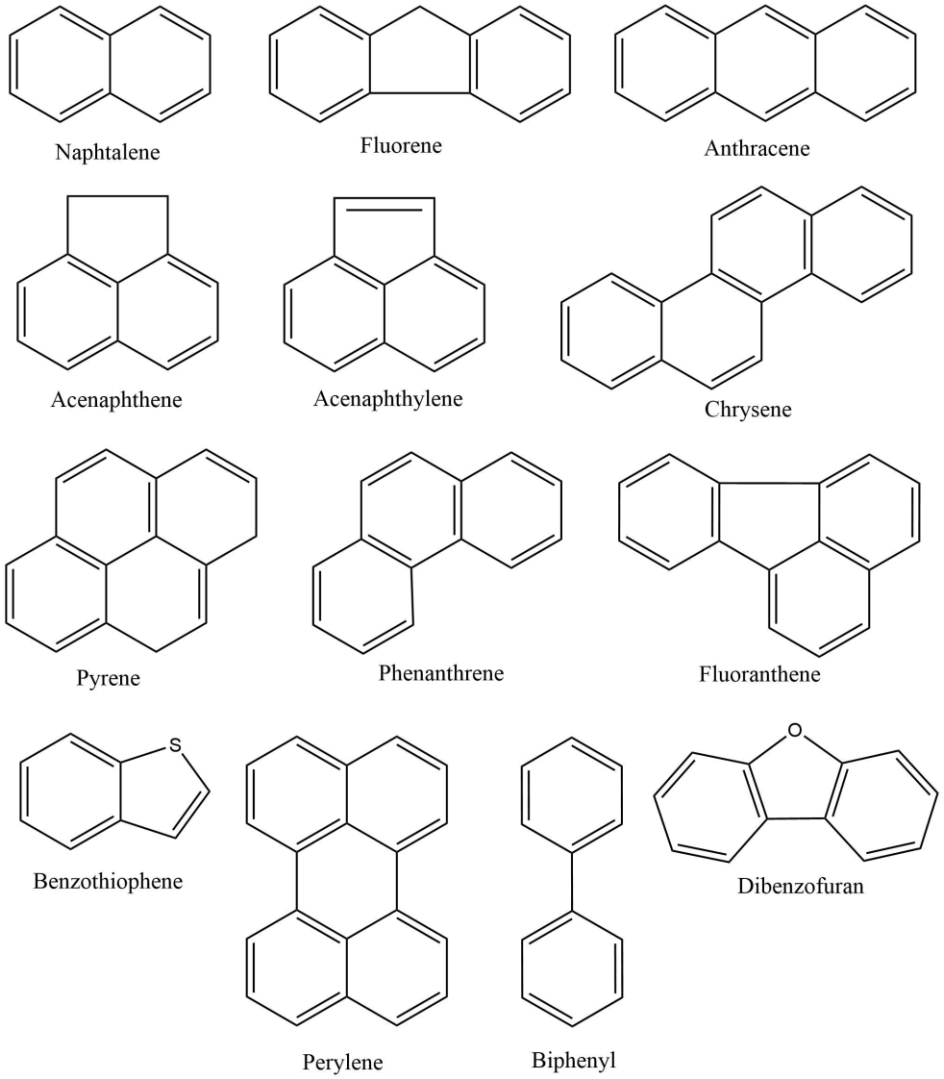

Figure 2: Some main groups of PAHs. The PAHs may be methylated at several sites and/or have benzo-isomers.

PAHs are considered the main class of oil-related compounds responsible for toxic effects in marine organisms (Sorensen et al., 2017) (Adams et al., 2014). They have been found to be effectively incorporated in the tissues of filter feeding organisms as their aggregation potential with particular matter are enhanced by their low solubility in water(Batista et al., 2013).

1.2.3. Oil in marine ecosystems and benthic communities

As an increasing part of the global petroleum production is carried out offshore (Bennear, 2015), there are eligible concerns about loss of hydrocarbons to the marine environment. Between 1990 and 1999, an annual average of 1 300 000 metric tons of petroleum were released to the sea worldwide (Transportation Research Board and National Researh Council, 2003). Depending on factors such as size, rates of release and location of the spill, the impacts on the environment varies (Transportation Research Board and National Research Council, 2003). Natural seeps and petroleum

consumption contribute to 45% and 40% of the inputs to the marine environment respectively, but the release rates are slow and chronic, hence the surrounding biota can adapt and survive. The most hazardous releases are related to petroleum extraction and petroleum transportation. They respectively account for only 3% and 12% of oil released to the marine environment per year. However, their potential for large accidental spills makes them a real threat to the surrounding environment. If they happen close to coastal areas, they may be catastrophic (Transportation Research Board and National Research Council, 2003). Oil spills may originate from tanker incidents or from leakages or blowouts from extraction platforms or transportation pipelines, and the likelihood of accidental blowout/leakages increase with the increasing depth of the operation (Muehlenbachs et al., 2013). Different organisms, and consequently ecosystem functioning, can experience varying consequences from such incidents.

One of the most dramatic oil production incidents in the history is the Deepwater Horizon (DWH) blowout that occurred in the Gulf of Mexico in April 2010. The well was capped for 87 days, releasing enormous amounts of oil to the surrounding area (Beyer et al., 2016). Out of the 4,9 million barrels of oil originally released, 3,7 million barrels remained in the environment despite efforts to contain the spill (Murawski et al., 2016). Due to a rapid pressure drop at the exit point, the oil was physically dispersed into small droplets ranging from 10 µm to several mm. As oil generally has lower density than seawater, it generally moves upwards to the surface. Larger droplets rise more rapidly than smaller ones, and droplets smaller than 70 µm tend to have a neutral relative buoyancy that will let them remain in the water column until they coagulate to form larger droplets. An additional use of dispersing agents at the blowout point contributed to the formation of large plumes with HC rich water that spread laterally in the water column (Beyer et al., 2016). HC trapped in marine snow also reached the seabed ecosystems (Murawski et al., 2016). Effects on the benthic communities were found as far as 14 km away from the spilling site (Fisher et al., 2016). Notable changes in micro- and macrofauna abundance and diversity lasted for at least four years, and an increase in oxygen consumption and denitrification indicated that that a change in the nature of the microbial communities might had occurred. Tissue necrosis was also observed on deep-sea corals (Fisher et al., 2016).

Water-soluble PAHs have been believed to be responsible for crude oil toxicity in marine systems (Carls et al., 2008) (Nordtug et al., 2011b). However, some observations suggests that the formation of oil micro droplets may increase the bioavailability of oil to marine organisms(Hansen et al., 2012) (Sorhus et al., 2015), leading to more severe effects than if only the water accommodated fraction was present (Gonzalez-Doncel et al., 2008).

1.3. Benthic deep-sea environments

1.3.1. Ecology of deep-sea benthic ecosystem and the role of benthic communities

The deep-sea is the Earth's largest ecosystem, with the pelagic deep-sea below 200 m representing about 95% of the total volume of the ocean (Thurber et al., 2014). Nevertheless, it remains one of the least explored, thus least understood regions of the world. The dysphotic zone comprised between 200 m and 1000 m is characterized by rapid dissipation of light, thus also the possibility of photosynthesis, as depth increases (NOAA, 2019). Due to the high pressure and absence of light combined with nutrient-low, cold water, the physical environment of the deep-sea floor is considered extreme (Thistle, 2003). However, the species found in the deep-sea has lately been recognized as rich, diversified habitats with unique ecosystems that can support high biodiversity (Ramirez-Llodra et al., 2011). Animals nourishing on nutrition from sediment, plankton, bacteria or dead biomass dominate in the deep-sea (Thistle, 2003).

Deep-sea benthic communities, including sponges, often form biogenic habitats, defined as *"areas of extensive three-dimensional structure created by organisms themselves"* which *"can cover tens of square kilometres of the deep seafloor" (Thurber et al., 2014)*. They carry out vital functional roles in the environment including providing habitat and shelter for a variety of marine organisms, stabilising the seafloor and a critical part of the base of the food web through their biomass production. More importantly, they comprise active organic decomposers which regenerate nutrients and are home to complex microbial communities with an important role in waste detoxification (Fisher et al., 2016).

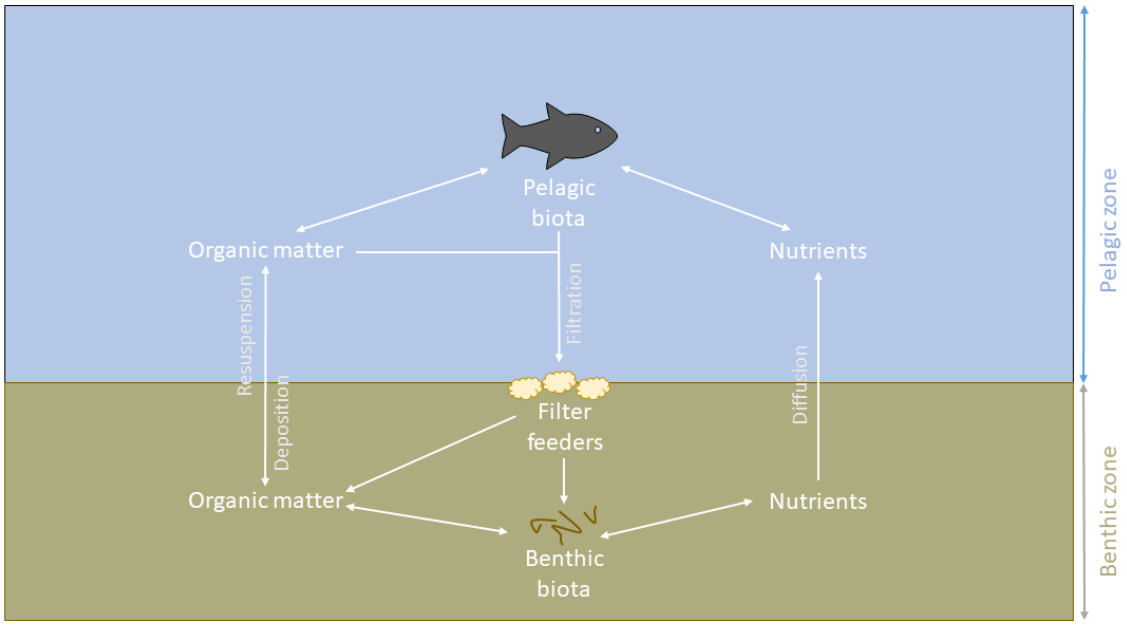

Figure 3: Deep-sea benthic filter-feeding communities, including sponges contribute to benthic-pelagic coupling by carbon and nutrient recycling when filtering the surrounding waters.

Deep-sea benthic ecosystems depend on organic waste produced at shallower waters where photosynthesis occurs. Suspension and epibenthic feeders such as sponges actively participate to benthic-pelagic coupling (Figure 3) by consuming organic matter and releasing by-products such as suspended particles and dissolved nutrients which can be used by other organisms (Soetaert and van Oevelen, 2009) (Ludeman et al., 2017).

1.3.2. An introduction to sponges

Sponges are important members of benthic communities, and found in a range of marine and freshwater benthic environments all over the world (Bell and Carballo, 2008). Both soft- and hard-bottom environments are successfully colonized by sponges, and they are found in various habitats in both coastal and deep-sea environments (Thakur and Singh, 2016). They are strictly aquatic, multicellular organisms that evolved from the Precambrian era (Carballo and Bell, 2017). Despite their sessile nature, they are highly efficient at capturing food by filter-feeding activity, filtering up to 900 times their body volume of water per hour (Ludeman et al., 2017). Sponge communities may look like the ones presented in figure 4.

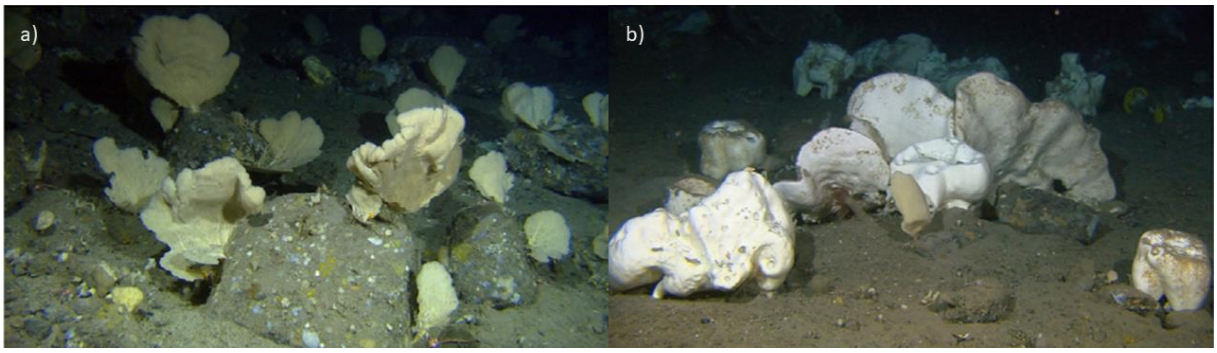

Figure 4: Sponge grounds on the Norwegian continental shelf. Different kinds of sponges dominate the areas of which a) and b) is taken, *G. barretti* is almost absent in a), but one of the dominating species in b). Modified from (Kutti et al., 2013).

Based on the nature of their skeleton, sponges are grouped into four distinct classes: Demospongiae, Hexatinellida and Homoscleromorpha have siliceous spicules, whereas Calcarea harbour spicules of calcium-carbonate (Van Soest et al., 2012). Sponges have a simple level of organization, with specialised cells for a variety of life functions. None of these are organised into tissues or organs but to an outer layer of flattened cells (pinacocytes) and inner canals and chambers lined with choanocytes, flagella-bearing cells that create water currents for the sponges filtering activity (Van Soest et al., 2012). Sponge cells are mobile and totipotent, meaning that they are capable of cellular rearrangement (Bond, 1992) and tissue regeneration (Wulff, 2010). Their evolutionary success are undoubtedly liked to the simplicity and adaptability of their body plan, but is also linked to the intricate symbiosis with bacteria, which can represent between 40% and 60% of the sponge total biomass (Carballo and Bell, 2017). Sponge microbial communities are specific and often differ greatly from those of the surrounding water and sediment (Schottner et al., 2013). Its metabolism is intricately linked to the activities of its associated microbiome. Metabolites produced by bacteria that oxidize/reduce nutrients have been observed to benefit sponges, as well as e.g. cyanobacteria for shallow water aggregations (Webster and Blackall, 2009). Therefore, the term “holobiont” is a more accurate way to describe the ecological unit formed by the sponge and its associated symbiotic microorganisms, especially regarding responses to environmental factors (Webster and Taylor, 2012).

1.3.3. Geodia barretti

The demosponge aggregations on the NCS is dominated by species from the Geodiidae family, including boreal demosponge *Geodia barretti (Kutti et al., 2013)*. *G. barretti* thrives at depths from 30 to 2000 m and temperatures from 3 to 9°C. Specimen have been found from the Mediterranean to north of Svalbard (Cardenas et al., 2013), and is abundant in Norwegian fjords (Commission, 2010). *G. barretti* is a leucon type sponge of spherical or irregular shape that can grow up to at least 80 cm in diameter and 38 kg wet weight (WW). It is usually white or light brown/yellow in colour (Cardenas et al., 2013). The sponge possesses one to several preoscules, depressions protecting the true oscules (Figure 5a). They are located on the cortex, an outer layer protecting the sponge interior (Figure 5b) which is rich in narrow filter canals called mesophylls, and silica spicules (Cardenas et al., 2013). Water pumping rates of 3000 L/kg dry weight (DW) has been shown in the wild. This is lower than shallow water species, but is believed to increase the contact time of seawater with the sponge and its associated microbiome (Kutti et al., 2013).

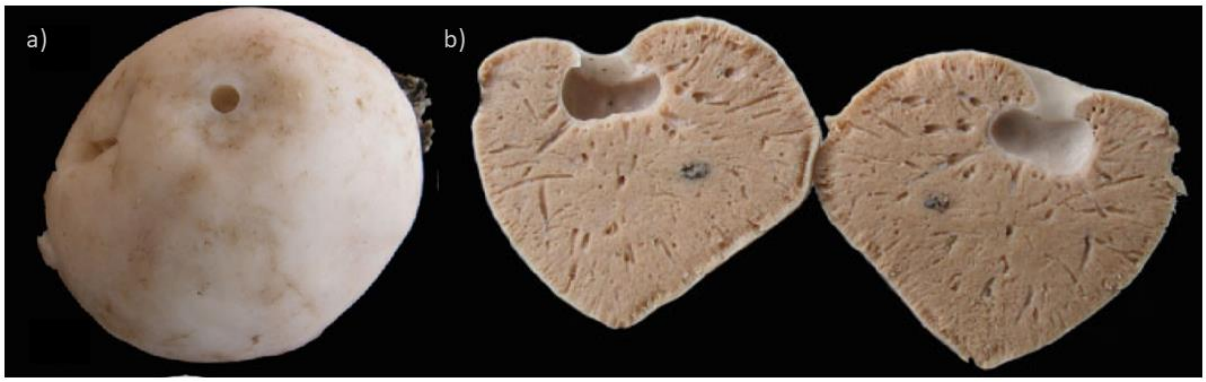

Figure 5: *Geodia barretti*: a) External morphology of a 10 cm specimen. The sponge present a round shape with a round opening: the preoscule. b) Internal morphology of a 14 cm wide specimen cut in half. The sponge presents an opening on a cavity (the preoscule), an internal matrix of spicules-rich sponge tissue and canals (the mesophyll) and a thin external cortex. Modified from (Cardenas et al., 2013).

High filtration rates combined with a sessile nature makes *G. barretti* and other sponges highly susceptible to pollution. Signs of compromised health, such as necrotic tissues in *G. barretti* have been characterised by (Luter et al., 2017). Sub-lethal stress responses have been observed after exposure to suspended sediments, mine tailings, drill cutting (Kutti et al., 2015), drilling muds (Edge et al., 2016), oil drilling waste (Fang et al., 2018) and thermal stress (Strand et al., 2017). It has been shown that sponges can accumulate anthropogenic contaminants such as PAHs (Batista et al., 2013), but few studies have investigated the impact of oil spills on their health. Sponges dominate areas where oil and gas exploration are taking place (Bell et al., 2015) and as they are of great importance of marine ecosystems, it is essential that the impacts of petroleum activities on their health is investigated (Edge et al., 2016).

1.4. Lipids

1.4.1. Definition and classes of lipids

Lipids are an important class of biological molecules and found in all living organisms. They consist of mostly carbon and hydrogen, together with oxygen, phosphorous and nitrogen. All lipids have a hydrophobic character, as most lipids include long chains of hydrocarbons, but they exhibit a great structural variety (Voet, 2013). There is no accurate definition of lipids. Some are based on its characteristics, others on its structure. One definition based on the structure is that *"Lipids are a group of naturally occurring molecules that include fatty acids, its derivatives and closely related species." (Christie, 2019)*. . However, this definition does not cover all species commonly defined as lipids, such as sterols. The HC group in sterols in figure 6 are marked as R_1 since it differs drastically from the structure of fatty acid carbon chains. Anyhow, it is classified as a lipid by using a definition based on the characteristics of lipids. The most widespread characteristic perceptions are that *"Lipids are substances of biological origins that solve in organic solvents such as chloroform and methanol."* (Voet, 2013). Lipids can be parted in classes, and some of the main classes are shown in figure 5. The polarity of lipids is an important characteristic, and decisive for its functional roles in an organism. When classified by polarity, triglycerides (TAG) and sterols are classified as neutral/non-polar lipids, whereas free fatty acids (FFA), monoglycerides (MAG), diglycerides (DAG) and phospholipids (PL) are classified as polar lipids. Partly because of this, triacylglycerols function as energy reserves, whereas phospholipids and sphingolipids are important in biological membranes. In mammals, sterols are the metabolic precursor of hormones that regulate a variety of physiological functions (Voet, 2013).

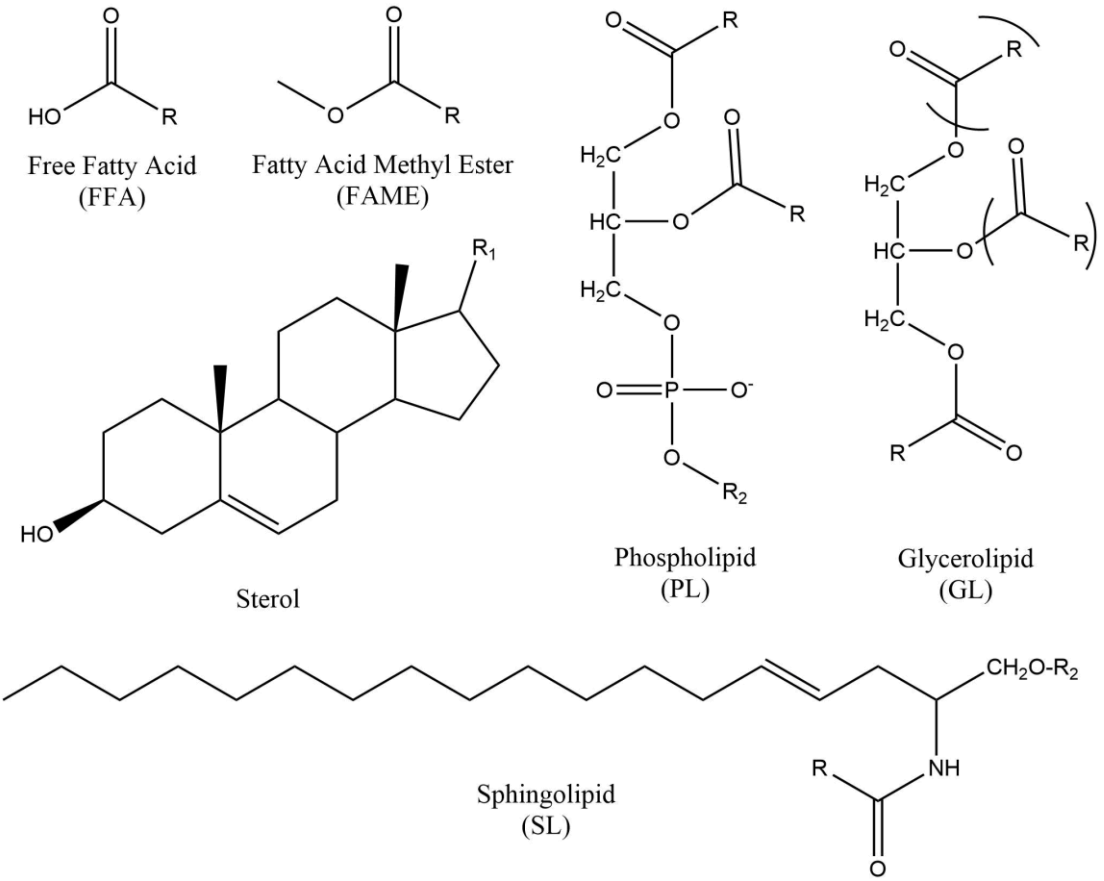

Figure 6: Some lipid classes, including free fatty acids (FFA), fatty acid methyl esters (FAME), sterols, phospholipids (PL) and sphingolipids (SL). Within the classes there may be a variety of subclasses.

Within the different classes of lipids there may be a variety of subclasses. R_2 in SL may be varied from H to different kinds of sugar and to phosphor choline (the latter forming sphingomyelin (SM)). R_2 in PL may also vary a lot, giving the various kinds of PL in figure 7.

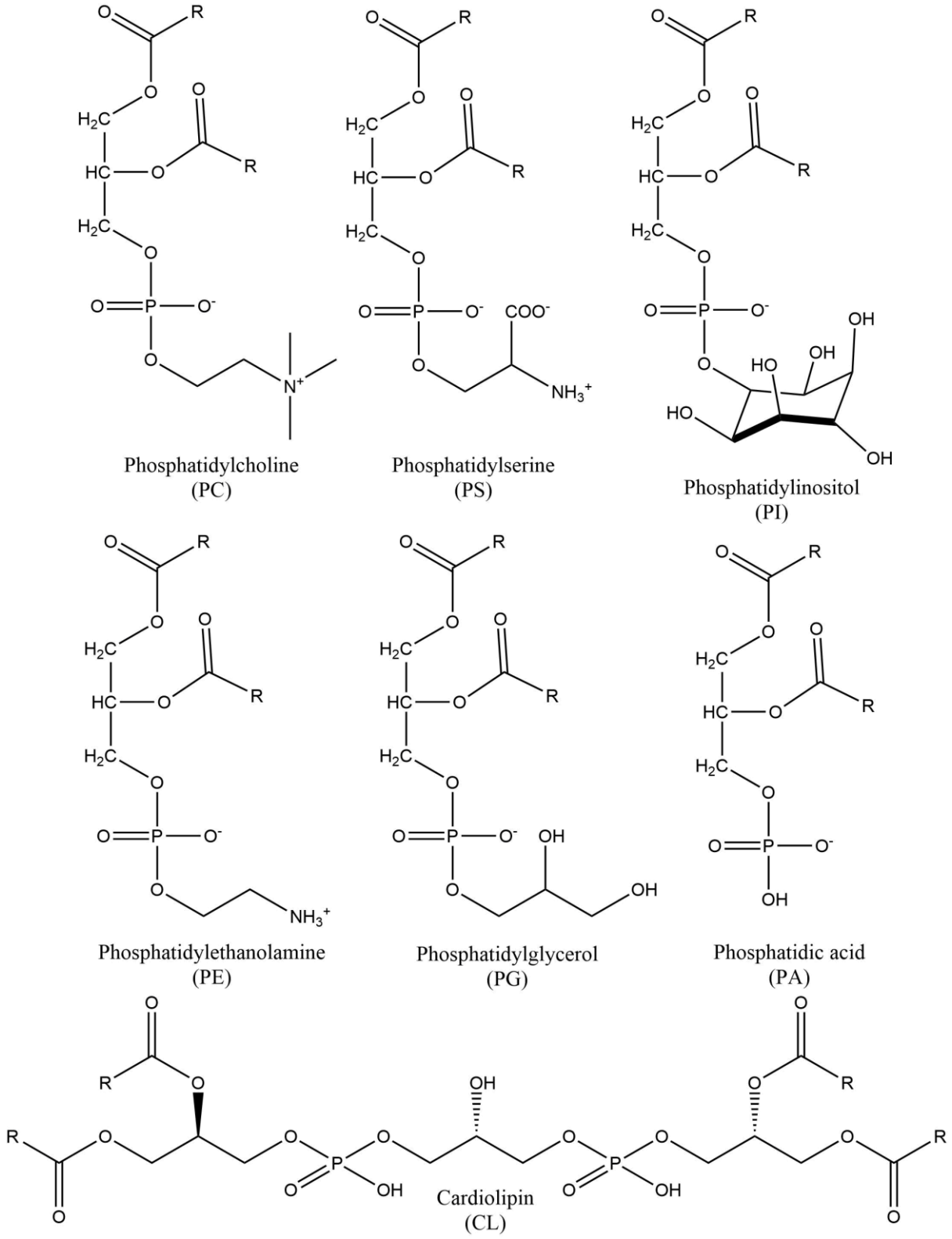

Figure 7: Different classes of phospholipids.

Fatty acids, carboxylic acids with long chain hydrocarbon side groups are the building blocks of most lipid classes, as the hydrocarbon groups (R) are connected to the rest of the molecule by an ester or amide bond. PL are, as mentioned, the building blocks for biological membranes and FA provide their hydrophobic interior. The membrane properties such as membrane fluidity are determined by the different FA components in the lipid membrane. FA may be long, short, saturated, mono-, di- or polyunsaturated, branched, halogenated, hydroxylated, methoxylated and so on. Analysing FA may

reflect an organisms metabolism and/or special conditions in its environment (Berge and Barnathan, 2005), and changes in FA composition may give information on the organisms response to changes (Denich et al., 2003).

1.4.2. The structure of fatty acids

Free fatty acids (FFA) are carboxylic acids with long -chain hydrocarbon side groups(Voet, 2013). Most naturally occurring fatty acids (FA) have a chain length of 4-24 carbons, with 14-20 carbons as the most common ones. However, FA with longer chain lengths (up to 34 carbons) have been observed in some marine organisms such as sponges (Berge and Barnathan, 2005). Most FA have an even number of carbons (Voet, 2013), but bacterial FA biomarkers are typically odd-numbered (Dalsgaard et al., 2003).

FA normally contain 0-6 double bonds with cis geometry, but trans geometry may also occur. The distance between double bonds may vary, but if the fatty acid contains more than one double bond, they will be separated with one methylene group or more. Branching on one or several sites is also common. Some fatty acids may also feature other elements or structures in the carbon chain, such as oxygen or triple bonds. Some contain ring structures such as furan fatty acids.

1.4.3. Fatty acids nomenclature

Mainly three systems are used in the naming of fatty acids: They can be named from the IUPAC system, from where the fatty acid is commonly found, or one can give them short names explaining the number of carbons, the number of double bonds and the double bonds position and geometry. The placement of branching point etc. is indicated too. All three systems have benefits and disadvantages. The one used throughout this thesis is the latter. It will be explained in this section.

The short name of any unsaturated fatty acid is given as A:B n-C. A give the number of carbons, B give the number of double bonds and C gives the position of the first double bond counted from the methyl end of the carbon chain (Anon., 1978). The mono-unsaturated free fatty acid shown in figure 7b) will hence get the name 18:1 n-9. If the fatty acid is di- or poly-unsaturated, one assumes that all double bonds are separated by a methylene group. Then, only the position of the first double bond is necessary. In some occasions, ω (omega) is used rather than n. this is the origin to the designation of omega-3 and omega-6 fatty acids.

The position of every double bond can alternatively be given, but if so, they are counted from the carboxyl group, and the position of the double bond is given prior to the short name. 18:3 n-3 is written as 9, 12, 15-18:3. If the double bonds are not separated by a methylene group, the fatty acid must be named this way. Non-methylene interrupted (NMI) fatty acids are examples of this, since the distance between double bonds are greater than a methylene group.

If the fatty acids contain double bonds with trans geometry, the geometry must be given by the name. There are several ways of doing this, but the following method is used throughout this thesis. If the double bond in the omega-3 position in 18:3 n-3 has trans geometry, it will be named c9,c12,t15-18:3 or 18:3 n-3-cct, where c indicate cis and t indicate trans.

Fatty acids may be branched. In branched fatty acids, A give the number of carbons in the fatty acid. However, the longest carbon chain is shorter than A, depending on how many carbons are “lost” to branching. Branching on position 2 and 3 from the methyl end are called iso and ante-iso branching respectively. Branching on other sites of the carbon chain is normally denoted like DMI fatty acids, as shown in figure 8i). If the methyl group is exchanged with another group such as ethyl or hydroxy, this is shown as Et or OH instead of Me.

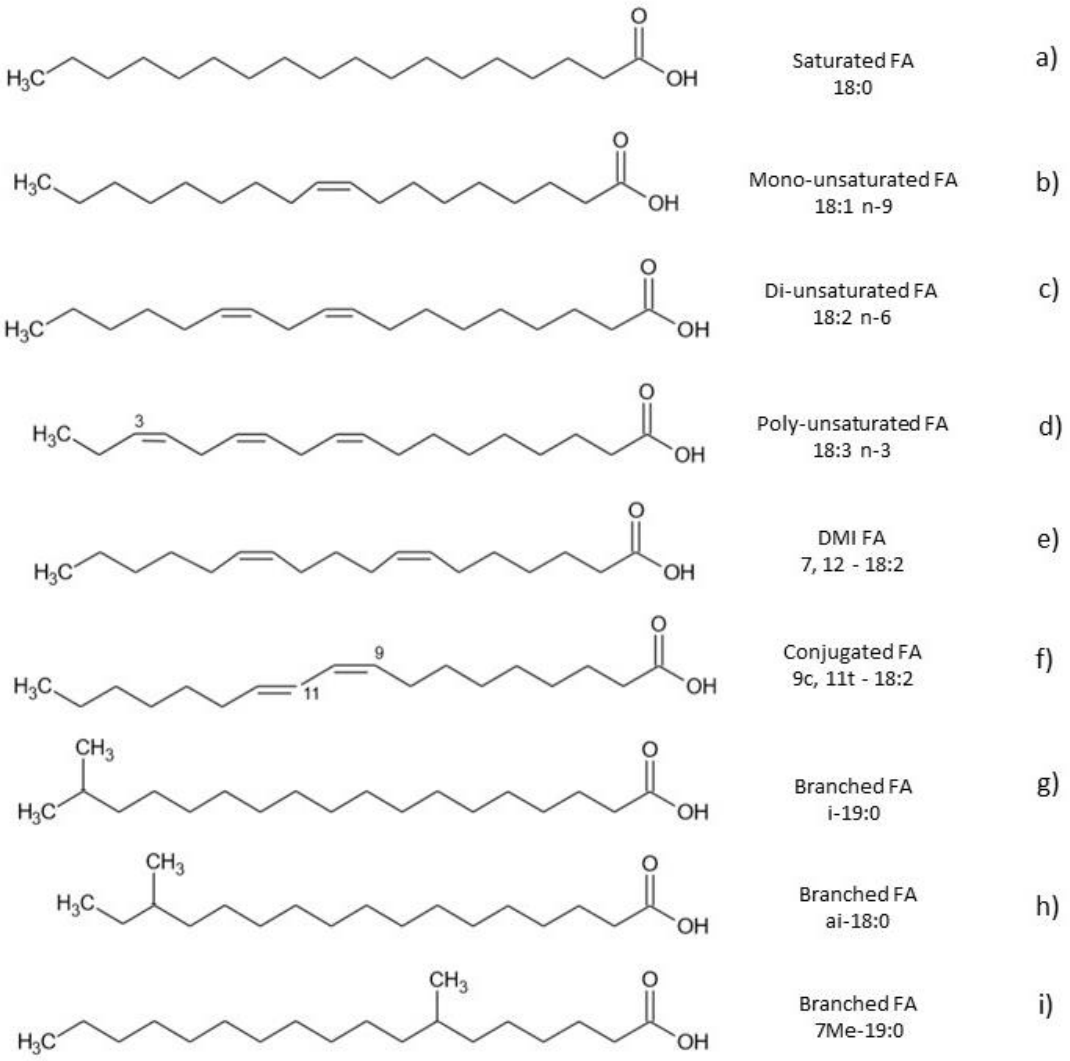

Figure 8: Examples of the structure and nomenclature of some free fatty acids.

1.5. Hypotheses

PAH may or may not accumulate in the tissue of deep-sea sponge *Geodia barretti*, and this may or may not affect the sponge and its associated microbiome. Three possible hypotheses are considered as possible outcome for this experiment:

1. PAH accumulates in the tissue of deep-sea sponge *Geodia barretti* after an acute exposure to crude oil and the sponge and its associated microbial community is negatively impacted in terms of physiology (change of lipid composition).
2. PAH may accumulate in the tissue of deep-sea sponge *Geodia barretti* but the sponge and its associated microbiome does not seem to be negatively impacted in terms of physiology (change of lipid composition).
3. PAH does not accumulate in the tissue of deep-sea *Geodia barretti*, hence no conclusions can be drawn considering the effect of oil exposure on the sponge and its associated microbial community.

1.6. Objectives of the thesis

There are two main objectives of this master thesis.

No former work has previously presented a complete view of the lipid composition of *G. barretti*, and how the different FA are distributed within the lipid classes. The first aim of the thesis is to identify the FA profile of *G. barretti* and the distribution amongst lipid classes. In addition to providing us with valuable information about the species itself, new FA may be identified. This work will be performed by analysing lipid extracts using gas chromatography with mass spectrometric detection (GC-MS).

The second aim of this thesis is to examine the sponge's response to an acute oil exposure. This will provide valuable data that will enhance our understanding of the vulnerability of deep-sea benthic ecosystems to hydrocarbon exposure. Such data is useful for risk assessments and ecosystem forecasting following oil spills in Northern Atlantic seas where oil and gas exploration are prevalent. More specifically, the aim is to measure *G. barretti's* uptake of PAH and response measured as the change in lipid composition during an acute exposure to oil of 8 days at 3 different oil concentrations, and after a recovery period of 30 days. The quantitative measurements will be approached using gas chromatography with flame ionization detection (GC-FID)

The sponge's uptake of PAH from oil exposure will be examined both visually by fluorescence microscopy and analytically by body burden extraction and GC-MS analysis.

2. Theory

During the work on this thesis, several techniques were used for the qualitative and quantitative analysis. The GC's primary task is to separate the different species from one another, and the MS and FID give information used for qualitative/quantitative analysis. There is direct connection between the GC, the detection units and the computer. Additionally, fluorescence microscopy was used to support the chemical analysis. The theory of the instrumentation used throughout this thesis are described in sections 2.1-2.5.

2.1. Separation techniques

2.1.1. An introduction to chromatography

Separation methods are an important part of chemical analysis, and during the work on this thesis, several chromatographic techniques has been used. Chromatography s defined by IUPAC as *"… a physical method of separation in which the components to be separated are distributed between two phases, one of which is stationary while the other moves in a definite direction." (IUPAC, 1993)*. The mobile phase is usually a gas or a liquid, and the stationery phase is usually solid particles, or a viscous liquid chemically bonded to a surface of solid particles (Harris, 2010). If two species A and B in a mixed sample have different affinity for the two phases, it will distribute differently between them. Eventually, since the mobile phase is moving, the two species will be separated (Figure 8). Chromatography can be used for separation of complex mixtures for analytical or work-up purposes and may also give identifying information about the contents in a sample (Braithwaite, 1996).

2.1.1.1 Chromatographic separation

Figure 9 illustrates how two compounds, A and B, elute through a capillary column. Say, A has 80% affinity for the mobile phase and B 30%. Then A is likely to stay in the mobile phase 80% of the time, and in the stationary phase 20% of the time, but the molecules in a dynamic equilibrium an are continuously exchanged between the mobile phase and the stationary phase. Likewise, B stay in the mobile phase 30% of the time and in the stationary phase 70% of the time. The molecules of a species will have a speed, or retention, through the chromatographic system that equals the mobile

phase velocity multiplied by the share of molecules from that species present in the mobile phase. Equation 1 show one way to calculate the retention factor *k*.

$$k = \frac{time\ solute\ spends\ in\ stationary\ phase}{time\ solute\ spends\ in\ mobile\ phase} \qquad \text{Equation 1}$$

Since A has a greater affinity for the mobile phase than B, it moves faster through the column than B. Hence, the two compounds get separated eventually (Harris, 2010).

Both A and B are spread over a certain area in the capillary column. Two factors lead to this: diffusion and slowness in the mass transfer between the two phases. Random movement of each molecule cause a net transport of the solute from regions of high concentration to regions with lower concentrations. This is called diffusion (Harris, 2010). When the molecules continuously change between the two phases, the molecules that stay in the stationary phase will lag slightly compared to the molecules in the mobile phase, which will also cause a spread sidewise. This phenomenon is most clearly shown for B and is called slowness in the mass transfer between phases, or finite equilibrium time between phases (Harris, 2010). The faster the mobile phase moves, the bigger the effect of slowness in mass transfer between phases. Simultaneously, the faster the mobile phase moves, the less the effect of diffusion. In packed columns different molecules may also choose different flow paths through the columns. Some flow paths are longer than other, which also contribute to band spreading.

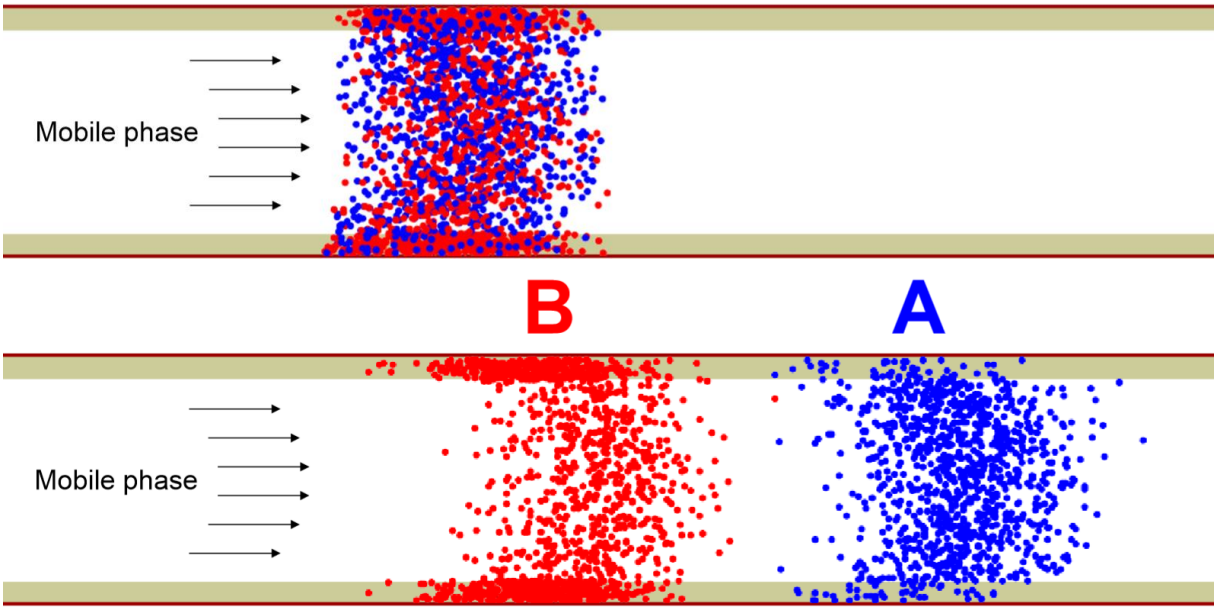

Figure 9: A capillary column with two compounds A and B with different affinities towards the two phases. A has greater affinity to the mobile phase than B. Lecture by Svein A. Mjøs, University of Bergen.

The detector at the end of the capillary column measure the amount of compound that elute on a given time. The result is given as a chromatogram like the one shown in figure 10, where the detector signal is plotted against the time since the sample was injected to the column (t_0). Because of the spread during the elution, each peak will have a shape close to the shape of a normal distribution curve. The retention time (t_R) of a certain compound equals the time of the compound maxima. Since t_R depend on the affinity of the compound to the mobile phase, it will be characterizing and give information about the compounds structure. t_M in figure 10 equals the time the mobile phase uses through the column. Species with no interactions with the stationary phase will elute simultaneously with the mobile phase, and thereby have retention time t_M.

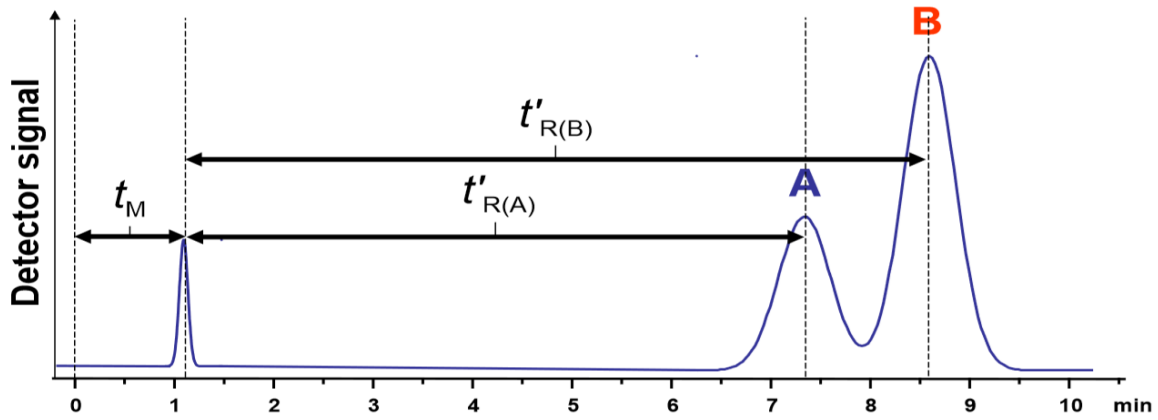

Figure 10: A chromatogram of the two compounds A and B from figure 9, where B has a longer retention than A. Lecture by Svein A. Mjøs, University of Bergen.

The adjusted retention time t'_R is calculated using equation 2, and another way to calculate the retention factor *k* from equation 1 is given in equation 3.

$$t'_R = t_R - t_M \qquad \text{Equation 2}$$

$$\mathrm{k} = \frac{\mathrm{t'_R}}{\mathrm{t_M}} \qquad \text{Equation 3}$$

The amount of a certain compound is calculated from the area of the chromatographic peaks. To be able to calculate the area of a chromatographic peak correctly, it should not overlap with other peaks. Say, the peaks must be satisfactorily separated. The separation, or resolution (R_S) between to chromatographic peaks depend on the distance between the peak maxima's (the retention times) and the width of the peaks at the base live (w_b). If the peak is normally distributed, the width at base line is defined as four times the standard deviation (4σ) to the associated normal distribution curve (Ettre, 1993). The chromatographic resolution is calculated using equation 4, amongst others.

$$R_S = \frac{t_{R(B)} - t_{R(A)}}{\frac{1}{2}\left(w_{b(A)} + w_{b(B)}\right)} \qquad \text{Equation 4}$$

Two peaks are said to have proper resolution if R_S equals 1.5 or more. Proper resolution depends on three factors: retention (Equation 1 and 3), efficiency and selectivity. Figure 11a) show two overlapping chromatographic peaks. A better chromatographic resolution can be achieved by b) increasing the distance between the peak maxima's (increased selectivity) or c) decreasing the width (increased effectivity) (Anderson, 2015).

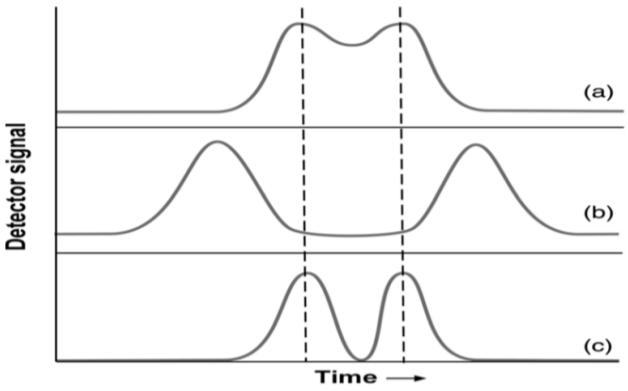

Figure 11: Two overlapping chromatographic peaks (a), and the effect of increased chromatographic selectivity (b) and increased chromatographic effectivity (c). (Anderson, 2015).

Separation between two peaks depend on the two compounds to have different retention. Chromatographic selectivity (α) is a measure of this. Equation 5 show the calculation of the selectivity. The more the retention differ, the higher the selectivity gets. Chromatographic selectivity can be altered by changing the mobile or stationary phase.

$$\alpha = \frac{k_B}{k_A}$$ Equation 5

Chromatographic efficiency is a measure of how much the peaks spread compared to the amount of time they spend in the columns and is measured in number of theoretical plates (N) that can fit between two peaks. If the plate number is high, the chromatographic efficiency is good. The chromatographic efficiency is calculated by using equation 6. The chromatographic efficiency can be altered by adjusting e.g. the columns length or the flow rate of the mobile phase.

$$N = 16 \cdot \left(\frac{t_R}{w_b}\right)^2$$ Equation 6

In addition to being calculated by equation 4, the resolution can be calculated using the Purnell equation (Equation 7). The Purnell equation applies only for chromatography with isothermal/isocratic conditions.

$$R_S = \frac{\sqrt{N_B}}{4} \cdot \frac{\alpha - 1}{\alpha} \cdot \frac{k_B}{k_B + 1}$$ Equation 7

2.1.1.3 Retention indexes

A retention index is a way to express retention relative to a series of reference compounds from the same series. It is a way to measure chromatographic selectivity, as it describes how compounds elute compared to each other (Ettre, 1993). The most common system, the Kováts index (Kovats, 1958) uses n-alkanes as the reference system. When analysing FAME, equivalent chain lengths (ECL) is the preferred system (Woodford and Vangent, 1960). Straight chained, saturated FAME are used as the reference series, and the reference equals the length of the fatty acid carbon chain. The principle is explained in figure 12, with compounds eluting between two trailing FAME, e.g. 16:0 and 17:0 are given retention indices between 16 and 17. The conversion from RT to ECL can be performed using equation 8. Fractional chain lengths (FCL) values are also a handy way to present retention. It is calculated using equation 9 (Stransky et al., 1997). As long at the stationary phase remains the same, retention indices will also remain approximately the same (Ettre, 1993) (Stransky et al., 1997).

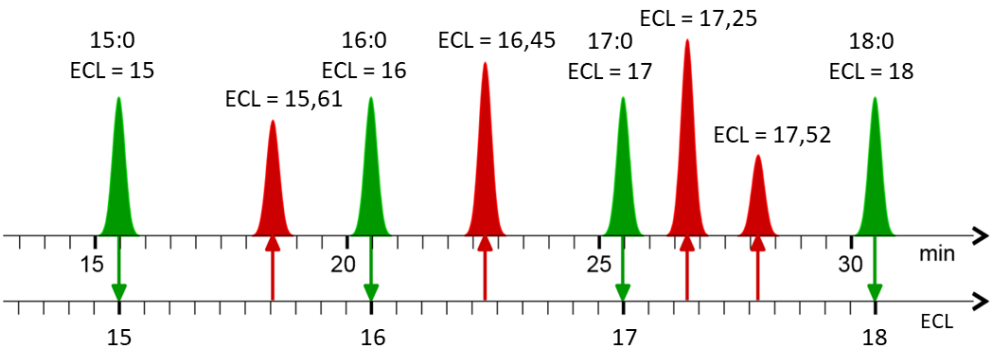

Figure 12: Converting retention times to ECL values by using straight chained saturated FAME (green) as references. Modified from lecture by Svein A. Mjøs, University of Bergen.

$$ECL_{(i)} = \frac{t_{R(i)} - t_{R(z)}}{t_{R(z+1)} - t_{R(z)}} + z$$ Equation 8

$$FCL_{(i)} = ECL_{(i)} - n_{C(i)}$$ Equation 9

2.1.2. Gas chromatography

Gas chromatography (GC) is a chromatographic technique where the mobile phase is a gas. It is the premier technique for the separation and analysis of volatile compounds, often preferred because it is fast, simple, cheap and sensitive, thus small amounts of sample is required (Miller, 2005). It separate species primary based on differences in boiling point/vapor pressure and polarity (Stauffer, 2008).

GC is normally a suitable choice for volatiles up to 350°C with an upper molecular weight of 600 Da (Miller, 2005). Thermally unstable compounds must be derivatised prior to analysis due to the high operation temperatures. The distribution ratio between the mobile and stationary phase in GC is dependent on the vapour pressure (Braithwaite, 1996). If the sample include compounds with a wide range of molecular weights, a temperature programme is normally used. The separation process starts at low temperature and increase gradually until the last compound has eluted. Chromatographic efficiency is normally given by the separation number (SN) in temperature programmed GC. SN is calculated by using equation 10.

$$SN = \frac{t_{R(z+1)} - t_{R(z)}}{w_{h(z)} + w_{h(z+1)}}$$ Equation 10

The resolution between two peaks in temperature programmed GC of FAME can be calculated using equation 11.

$$R_s \approx 1.177 \cdot \Delta ECL \cdot (SN + 1)$$ Equation 11

2.1.3. High performance liquid chromatography

High performance liquid chromatography (HPLC) is a chromatographic technique where the mobile phase is a liquid, and the separation is performed in capillary columns. It is the preferred technique for the separation and analysis when samples are less volatile or lack thermal stability, such as polymers and polar, ionic or thermally unstable compounds. A range of sorption processes can be used to achieve separation (Braithwaite, 1996).

2.1.4. Thin layer chromatography

The principle of thin layer chromatography (TLC) is to utilize the capillary action of a volatile solvent in a saturated environment to separate a sample applied to a plate coated with a thin layer of adsorbent (Braithwaite, 1996). Then, the separated components may be visualised by staining or charring, and the results may be used both qualitatively and quantitatively (Braithwaite, 1996).

2.2. Detectors

2.2.1. Mass spectrometry

Mass spectrometry (MS) is a technique studying the masses of atoms, molecules or fragments of molecules. Mass spectras are obtained by ionizing gaseous species, and then separate them according to their mass-to-charge ratio (*m/z*) by an acceleration through an electric field. Ions are then detected, and results presented as a mass spectrum (Harris, 2010). Ionized molecules are unstable and may fragment based on its structure. The molecular mass of the compound is often given by the highest present *m/z* value, the molecular ion (M^+) (de Hoffman, 2007). The fragmentation and relative abundance of fragments depend on how the molecule can achieve the lowest possible energy. The most likely fragmentation results in a peak with 100% relative abundance, called the base peak (de Hoffman, 2007).

2.2.1.1. MS identification of fatty acid methyl esters

Spectra's of unknown FAME may be identified by comparison to mass spectrums of a reference substance. Often, reference substances are not available because of commercial secrecy. Identification based on comparison of these compounds thus get hard. Mass spectrums can be manually interpreted to get structural information if reference structures for certain compounds are not available. The natural starting point would be to consider the strongest signal and the highest mass in the spectrum. The strongest signal, called the base peak, gives information about the dominating fragmenting point in the structure. This gives a strong indication of the main part of the molecule. The highest mass in the spectrum often indicates the mass of the molecular ion (M^+).

Fragmentation of saturated FAME

The most important ions in saturated FAME are m/z 74, 87 and 143. The McLafferty ion is usually the base peak. In most cases, this gives a base peak with m/z 74 (Christie, 2019). Branched FAME with a methyl group in position 2 from the carboxyl group are the exceptions, with a base peak at m/z 88 (Apon and Nicolaides, 1975). Whether the FAME is branched or not can easily be determined by looking at the ECL values described in section 2.1.1.3, if coupled with a GC. Determination of the branching point is described under the section about double bonds and branching points. Usually, the molecular ion is clearly visible, and the molecular mass can easily be determined. Amongst the higher masses, the most prominent ions are the M-43, M-31 and M-29.

Fragmentation of mono-unsaturated FAME

Series separated by 14 mass units is a strong indicator for mono-unsaturated FAME. The most important ions are m/z 55, 69 and 83. The closer the double bond is to the carboxyl group, the weaker these ions are relative to other ions such as m/z 74 and 96 (Christie, 2019). Usually, the molecular ion is clearly visible. Additionally, M-32 is prominent. Independent of the chain length, other prominent ions in the higher masses are m/z 152 and 194 in most FAME.

Fragmentation of di-unsaturated FAME

The most important ions in saturated FAME are m/z 67, 81 and 95. The base peak is usually m/z 67, but m/z 81 may also occur. Amongst the higher masses the molecular ion and M-31 are usually amongst the prominent ions (Christie, 2019).

Fragmentation of poly-unsaturated FAME

Poly-unsaturated FAME include all FAME with more than 2 double bonds. Important ions from poly-unsaturated FAME are m/z 79 and 91. m/z 79 ($C_6H_7^+$) is usually the base peak. m/z 91, part of the series $(C_nH_{2n-7})^+$ tend to increase with an increasing number of double bonds (Hallgren et al., 1959). The presence and intensity of the molecular ion is also an indication of the number of double bonds. FAME with 3, and sometimes 4 double bonds give MS spectrums with significant molecular ions, while these may be invisible in more unsaturated compounds.

Position of double bonds and branching points

Certain diagnostic ions can be used to determine the position of double bonds in unsaturated FAME. The position of the first double bond counted from the methyl end can be determined by a series of ions (ω-ions) with the molecular formula $(C_nH_{2n-4})^{+\cdot}$. Diagnostic ω-ions for n-3, n-4 and n-6 FAME are m/z 108, 122 and 150, respectively (Brauner, 1982). ω-ions cannot be used to determine n-1 or n-2, since these ions are abundant inn all FAME spectrums. A similar series of ions (α-ion) with the molecular formula $(C_nH_{2n-6})^{+\cdot}$ indicate the position of the first double bond counted from the carboxyl end. Δ6 and Δ9 positions give ions of m/z 194 and 236 respectively (Brauner, 1982). Ions indicating the different positions of the double bond are separated by 14 mass units in both series (Christie, 2019).

Apon and Nicolaides (1975) neatly describes the fragmentation (and the mechanisms giving those fragments) of all the branching points of the 18:0 FAME, giving an “a” and a “b” ion as shown in figure 13. The above mentioned saturated 2Me-FAME gives the m/z 88 McLafferty ion as the base peak. Every other cases of branching of saturated FAME usually give very similar mass spectrums, with small differences in the fingerprint area. Different branching points give different prominent ions in the higher masses (Apon and Nicolaides, 1975).

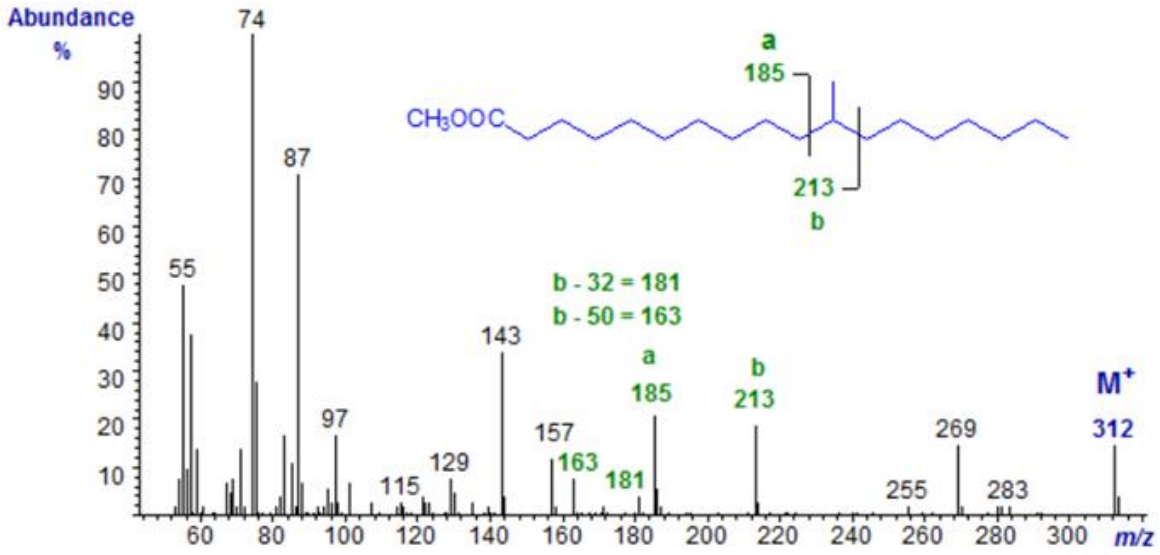

Figure 13: The branching of saturated FAME gives rise to two identifying molecules, “a” and “b”, respectively giving m/z 185 and m/z 213 for Br 18:0, 11Me. (Christie, 2019).

2.2.2. Flame ionization detection

The flame ionization detector (FID) is used for quantification of volatile organic compounds. Organic compounds are burned in a small oxygen-hydrogen flame, and chemical ionization following the general ionization reaction $CH + O \rightarrow CHO^+ + e^-$ occurs. The ions constitute an ion current proportional to the number of carbon atoms (Zimmermann et al., 2002). The current gets amplified and sent to the data system. FID is a good choice for quantitative analysis of organic compounds and is a good choice for organic analysis because of its sensitivity, stability and linearity (Miller, 2005).

2.3. Fluorescence microscopy of PAHs

The emission of photons by atoms or molecules whose electrons are transiently stimulated to a higher excitation state by radiant energy from an outside source is called fluorescence (Murphy, 2001). According to their aromatic structures the delocalized electrons in the PAH structures are easily exited, thus fluorescent when exposed to light in certain ranges (Rivera-Figueroa et al., 2004). During fluorescence, the absorption and emission of photons occur almost simultaneously. As soon as the light disappears, so does the fluorescent effect (Murphy, 2001). To further examine the fluorescent effect, the object must be photographed or filmed. Different species fluorescent from light of different wavelengths. Filters are often used let light of only certain wavelengths specified for the species of interest through.

3. Material and methods

3.1. Collection of sponge specimen

In March 2017, several large individuals of *G. barretti* were collected within Langenuen fjord, Norway. Explants were cultivated at a depth of 170 m following the procedure described by Kutti

et.al. (2015) (Kutti et al., 2015). 80 explants of similar size (wet weight averaging 32 g (Stevenne, 2018)) were harvested in January 2018 and transported to IMRs deep-sea laboratory in Austevoll, Norway. They were transferred to 16 50L mesocosms (5 per tank) and left to acclimatize to the research facility conditions 5 days prior to the experiments. The mesocosms were supplied with sand filtered seawater pumped from a depth of 160 m. Additional feeding of the sponges was not necessary as the seawater naturally contain particles the sponges consume as food (Strand et al., 2017).

3.2. Experimental design

Following the DWH oil spill in the Gulf of Mexico, the properties and behaviour of the released oil in seawater were characterized. Oil has lower density than seawater, hence larger oil droplets tend to rise to the surface. However, oil microdroplets with diameters less than 70 µm are neutrally buoyant and remain in the water column (Beyer et al., 2016). In the months following the DWH oil spill, the total hydrocarbon concentration ranged from 7.5 µg/L to 100 µg/L (Murawski et al., 2016) but in certain locations, hydrocarbon concentrations can potentially reach much higher concentration (Beyer et al., 2016). The experimental setup aimed at reproducing conditions similar to those experienced by deep-water communities after the DWH oil spill, with high concentrations simulating the concentration close to the spill and the low concentrations simulating a much larger area further away from the spill.

The oil used in the experiment was a weathered blend crude oil from the Troll oil field of the Norwegian Sea. This mix is representative of oil types found in the Lofoten area (Sorhus et al., 2015). The most volatile compounds in an oil blend tend to evaporate within a few days after an oil spill at sea (Nordtug et al., 2011a).To take account for the fast evaporation, the oil was artificially weathered through a one-step evaporation at 200°C, leaving behind residues corresponding to the remains after a few days at 10°C at the sea surface (Sorensen et al., 2017).The oil was pumped in a dispersion system by a HPLC pump (Shimadzu, LC-20AD Liquid Chromatograph Pump) with a flow of 5 µL/min together with a flow of seawater of 180 mL/min (Sorhus et al., 2015). To generate oil dispersion with oil droplets of defined sizes (range 12-16 µm), the system described by Nordtug et. al. was used with a load of 26 mg/L (stock solution). It is designed to maintain a continuous and stable production of dispersed oil droplets in the abovementioned size range (Nordtug et al., 2011a). This system includes 3-way magnetic valves, which are mixing units allowing a precise dilution of the oil from the stock solution in clean seawater. A computer-controlled relay (Sorhus et al., 2015) performed timing of the relative sampling from oil stock solution and seawater to obtain different solutions. An illustration of the experimental gear and tank setup is provided in Appendix A.

In order to simulate the conditions that benthic organisms may experience after an oil spill and to observe the sponges' responses over time, the sponge explants were exposed to different concentrations of dispersed oil for a time range of 1-8 days. The experimental oil exposure setup consisted of three treatments and one control, each with 4 replicate mesocosms. The oil doses were determined by opening the magnetic valves in cycles, with different opening intervals depending on the treatment. Table 1 show the details of each treatment.

Table 1: The aimed oil concentrations in each treatment and the time interval of the magnetic valve required to achieve the aimed concentration.

Treatment	Replicates	Oil concentration (µg/L)	Time interval (s/min)
Control	C1, C2, C3, C4	0	0
Low	L1, L2, L3, L4	33	1.1
Medium	P1, P2, P3, P4	100	3.4
High	H1, H2, H3, H4	300	10.1

During the experimental period, the oil pump stopped working twice. The first occasion was noticed on the morning of the 09/02 (day 4 of treatment for replicates 2 and 4, and day 5 of treatment for replicates 1 and 3), and the pump was estimated to have stopped 7,5 hours before it was restarted. The same occurred on the morning of 12/02 (day 7 of treatment for replicates 2 and 4, and day 8 of treatment for replicates 1 and 3).

Five sponge explants (n=5) were placed into each of the 16 mesocosms (4 per treatment) and exposed to the different experiment treatments for a period of 8 days. At each sampling point (24h, 48h, 4 days and 8 days of exposure to oil), one explant per tank were sacrificed for tissue sampling. On day 9, the remaining sponges (n=1/tank) were moved to mesocosms free of oil contamination for a recovery period of 30 days. Transferring the remaining sponges from oil contaminated mesocosms required dilution of the water in which the sponges were kept. To keep the sponges underwater at all time, each sponge was retrieved from its tank in an open plastic container and consecutively plunged into three 1 litre beakers containing clean seawater. In this way, the water in which the sponge was immersed was sequentially diluted. Finally, each sponge was transferred to 50L recovery mesocosms identical to the treatment mesocosms. After 30 days spent in the recovery tanks (day 38 of the experiment), samples were taken. A complete schedule of the experimental setup is shown in Appendix A, and figure 14 show the timeline and mesocosm design.

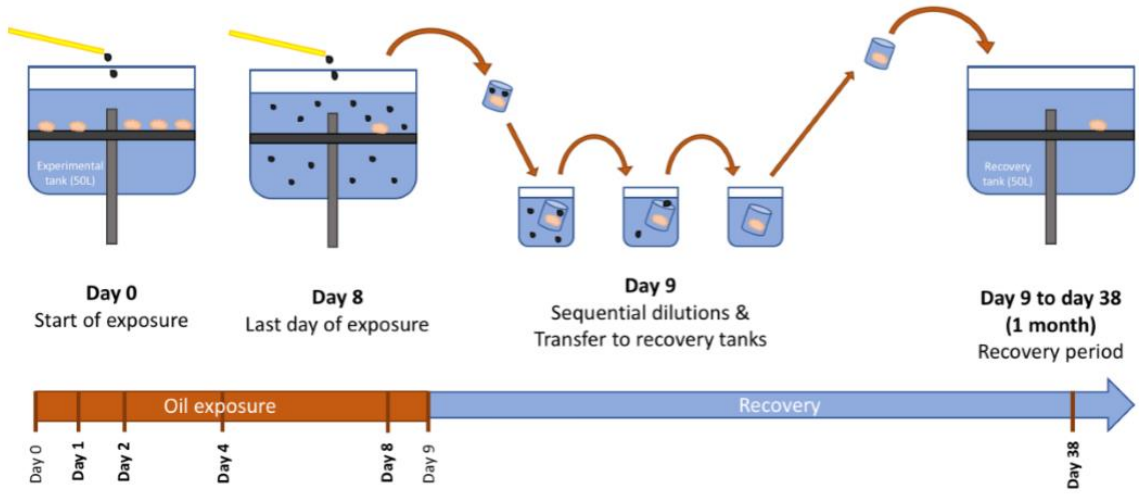

Figure 14: Timeline and setup of the experiment. *Day 0* - Representation of one experimental tank on the first day of exposure to oil: 5 sponge explants are set on a PVC false bottom in 50 L of seawater and micro-droplets of oil are dispensed to the tank. *Day 8* – Representation of one experimental tank on the last day of exposure to oil: one explant remains in the water (the other 4 have been sampled during time points day 1, 2, 4 and 8), oil is present in suspension in the water. *Day 9* – Representation of the sequential dilutions during the transfer of the remaining sponge explant from the exposure mesocosm to the recovery mesocosm: the sponge is placed in a small open plastic container and is sequentially immersed in 3 beakers containing oil-free seawater. *Day 9 to day 38* – After the sequential dilutions, the explant is transferred to a new tank for recovery over a period of 30 days. The last sampling point occurs on day 38. *Timeline* – The days marked in bold (day 1, 2, 4, 8 and 38) are the time points during which respiration measurements and sampling were performed. (Stevenne, 2018).

Water samples from the experimental mesocosms were taken throughout the first 8 days of the experimental setup (marked as brown in the timeline in figure 14). This was to ensure a stable exposure to dispersed oil, and to know whether the oil dispersion system succeeded on the aimed concentration or not.

The experimental work was performed in cooperation with master student Chloé Stévenne. Her work focused on the physiological effects on the oil exposed sponge and included measuring respiration rates and looking at cellular stress by studying the lysosomal membrane stability (LMS) and the bacterial communities in the *G. barretti*. A summary of her results will be presented and discussed in section 4 and 5.

3.3. Sample collection

About 1000 mL of water was sampled from the experimental mesocosms using from the experimental mesocosms were transferred to 1 L glass containers using a teflon tube. The water samples were added 100 µL internal standard (0,01 µg/mL d-PAH) and conserved by adding 1 ml of concentrated HCl and 30 ml of dichloromethane (DCM) stored dark and cold (4 °C) until sample preparation and analysis (Sorensen et al., 2017).

The sponge explants were transferred to the laboratory in a sealed plastic beaker filled with oil exposed seawater from their associated experimental tank. They were stored in a fridge at 4°C prior to cutting. Tissue samples taken for lipid chemistry purpose were cut into small pieces at the laboratory using a scalpel and watch glass and placed in 16 mL glass vials. Lipids tend to oxidize quickly when not in solution, and the lipid oxidation decrease with decreasing storage temperature (Aydin and Gokoglu, 2014). To minimize these events, liquid nitrogen was used for flash freezing and the samples were then stored at -80°C prior to sample preparation and analysis. During transportation they were kept in containers with dry ice. Cross sections with a thickness of 1-3 mm of the same sponge explants were transported in plastic beakers filled with water to the microscopy laboratory. They were stored partly outdoor (1-4°C) and partly indoor (15-20°C) for a couple of hours during photographing with UV/visible light. Then, they were sampled and stored as mentioned for the lipid samples and used for PAH chemistry purpose.

3.4. UV microscopy of sponge cross sections

As explained in section 1.2.2., PAHs are considered the main class of oil-related compounds responsible for toxic effects in marine organisms (Sorensen et al., 2017). When exposed to light in a certain range, the accumulated PAHs in oil droplets will appear as fluorescent, bright spots. To support the chemical analyses on PAH accumulation in sponge specimen, cross sections of all sponges were photographed using fluorescent microscopy. Photographs were obtained using a Nikon AZ100 microscope with fluorescence (Intensilight C-1 HGFI). A DAPI filter was used to irradiate the tissue with UV light at around 358 nm. When radiated lights of this wavelength, PAH transmits light of a slightly longer wavelength (around 461 nm), and this light was captured using a SPOT RT sCMOS camera. The exposure time was 180 ms, the photosensitivity was set to 4 and the photo resolution was set to 2224 · 1024 pixels. The light source was used on the maximum setting, and the object was enlarged 4 times (2 · objective and 2 · zoom). Cross sections were put in a glass petri dish filled with water photographed using both visible and fluorescent light. An over-view image of the cross section (both visible and fluorescent light), and close-up photos of a cross-over of the cross section was taken. For the close-up photos, all photos were taken using fluorescent light, but the first image was also captured using visible light.

The aim was to use software to analyse the amount of light on each image. However, the sponge itself had some background radiation that would make the radiation from the bright, but very small

spots from PAH insignificant. Therefore, the spots were counted instead. The average of the number of spots per close-up photo was used for comparison to the data from the chemical analyses of PAH accumulation.

3.5. Sample preparation and analysis of water samples

A total of 33 water samples was taken and worked up for PAH analysis. Prior to analysis, the PAH had to be extracted from the water phase to an organic solvent. The water was transferred to a separation funnel, and 30 mL DCM. The funnel was shaken for 2 minutes and then left untouched for some time so the organic phase and the water phase could separate. The organic phase was transferred to a glass container before the extraction process was repeated another time, adding up to a total of 60 mL DCM. A rotavapor was used to evaporate the solvent. When about 1 mL of the DCM was left, some n-hexane was added and evaporated to 1 mL. This step was repeated two times for solvent exchanges (Sorensen et al., 2016b). The extract (now solved in n-hexane) was transferred to GC-vials and run on an Agilent 6890 GC coupled with an Agilent 5973 quadrupole MS fitted with and electron ionization (EI) source operated in SIM mode was used for the chemical analysis. The GC columns was an Agilent J&W DB-5MS UI (30 m · 0.25 mm · 0.25 µm) and the carrier gas was helium at constant flow rate 1 mL/min. 1 µL samples were injected at 300°C splitless. The oven temperature was held at 40°C for 1 min, then ramped to 315°C at 6°C/min and held at this temperature for 5 min. The transfer line temperature was 300°C, the ion source temperature was 230°C and the quadrupole temperatures were 150°C. The EI source was operated at 70 eV (Sorensen et al., 2016a). Integration was performed in MassHunter and further data handling was performed in MS Excel as described in the following section.

3.6. Sample preparation and analysis of PAH body burden

A total of 79 samples were prepared for PAH body burden analysis. In addition, the preparation of 6 laboratory blanks and 7 spiked were done, one or more per day of work-up. Sørensen et. al.'s method for extraction of PAH from cod/haddock eggs (Sorensen et al., 2016b) were used as a base for the method, but some changes had to be made in the homogenizing step due to structural differences between sample types. Sponge samples were found to contain about 75% water. To avoid the formation of emulsion, but still retain sensitivity even at low exposure levels, different amounts of sample was tested. A sponge WW of about 200 mg satisfied both demands.

Sponge samples (including the cortex) were placed on watch glass and homogenized using a scalpel. About 200 mg were transferred to a 12 mL tube. 4 mL 50% DCM in hexane, 100 µL internal standard (0,01 µg/mL d-PAH) and ~0,2g $NaSO_4$ were added. The samples were oscillated for 30 seconds, then centrifuged at 2000 rpm for 2 minutes. The extraction process was repeated two times with 3 mL solvent, and after each extraction the organic phase was transferred to a new tube, adding up to a total of 10 mL.

Each sample were evaporated to 1 mL extracts prior to solid phase extraction (SPE) into a clean 16 mL tube. 3 mL Chrombond SiOH columns and vacuum were used for this purpose. The columns (one per sample) were rinsed with 6 mL hexane. Each sample was transferred to the column, and the old tube was rinsed 2-3 times with hexane. Then, the column was rinsed with 6 mL 10% DCM in hexane, adding up to 8-10 mL of clean extract in the new tube. The extracts were evaporated and transferred to 250 µL GC vials.

An Agilent 6890 GC coupled with an Agilent 5973 quadrupole MS fitted with and electron ionization (EI) source operated in SIM mode was used for the chemical analysis. The GC columns was an Agilent J&W DB-5MS UI (30 m · 0.25 mm · 0.25 µm) and the carrier gas was helium at constant flow rate 1 mL/min. 1 µL samples were injected at 300°C splitless. The oven temperature was held at 40°C for 1

min, then ramped to 315°C at 6°C/min and held at this temperature for 5 min. The transfer line temperature was 300°C, the ion source temperature was 230°C and the quadrupole temperatures were 150°C. The EI source was operated at 70 eV (Sorensen et al., 2016a). Each sample were run 3 times. One run to identify single compounds, and two runs to identify clusters of compounds.

Integration/quantification was performed using MassHunter. In the single compound run, quantification was performed directly in the program. For the cluster runs, however, the integration would be performed in the program, but the quantification in terms of concentration would be performed in MS Excel. The two cluster programs, NDP (naphthalenes, dibenzothiophenes and phenanthrenes) and BFPC (benzothiophenes, fluorenes, pyrenes and chrysenes) would include some of the single compounds. In the calculation of total PAH, these single compounds would be excluded.

3.7. Sample preparation and analysis of lipids

3.7.1. Folch's method and thin layer chromatography.

Folch's method for lipid extraction is a method for extracting total lipids from animal tissues (Folch et al., 1957). The advantage of extracting lipids in their original form is that the lipid classes can be separated based on polarity, e.g. by TLC (Olsen and Henderson, 1989). Hence, the presence and content of the various lipid classes can be studied individually. Folch's extraction procedure were performed on 4 replicate sponge tissue samples from the groups d0c, d4c, d8c and d8h. Some of the steps, such as the homogenizing step were customized to fit sponge characteristics. 800mg of sponge where chopped into small pieces using a scalpel and watch glass and transferred to a 25 mL tube. 20 mL 2:1 $CHCl_3$: MeOH were added, and so was 4 mL 0,88% KCl(aq). Next, the tube was oscillated for 30 seconds, then centrifuged at 2000 rpm for 5 minutes. This caused the methanol to change phase, from the organic phase to the water phase. The water/methanol phase was removed, and the organic phase was dried using Na_2SO_4(s) and filtered by vacuum filtration into pre-weighed tubes. Extracts were evaporated until dry, the amount of lipids were weighed and then solved to a concentration of 10 mg/mL in $CHCl_3$. Equal amounts of the 4 replicates were mixed and separated using thin layer chromatography. Groups d0c, d8c and d8h were separated using 2D TLC, and d4c was separated using 1D TLC.

The aim of using TLC, whether it is 1D or 2D TLC is to separate lipids based on their polarity. The difference is that 2D TLC usually gives a better resolution than 1D TLC. In both cases, the polar lipids are separated first by using polar solvents, then the non-polar lipids are separated by using a non-polar solvent. The order of the solvents used in this separation are shown in figure 14, and the solvent contents are listed in table 2.

To prevent pollution, all TLC plates (10·10 cm glass plates with a stationary phase of silica gel) were rinsed with 1:1 diethyl ether: n-hexane prior to lipid class separation (Olsen and Henderson, 1989). For the 2D TLC (Figure 15a)), 20 µL of the combined extracts was placed dropwise at the same spot in the bottom left corner of the plate. The plate was placed in a saturated TLC-chamber and eluted with polar solvent 1 followed by 45 minutes in a vacuum exicator. The plate was rotated 90° to the left, and the procedure was repeated with polar solvent 2. Last, the plate was rotated 180° before eluting with the non-polar solvent. All elution's were terminated 1 cm before the solvent front reached the top of the plate. For the 1D TLC (Figure 15b)), the combined extract was placed dropwise along a line giving a concentration of about 50 µg/cm. 10 µL were used for both illustration pictures and GC analyses, and 45 µL was used for LC analyses. The plate was placed in a saturated TLC-chamber and eluted with polar solvent 1 until 3,5 cm before the solvent front reached the top of the plate. Then, 45 minutes in a vacuum exicator. The procedure was repeated with the non-polar solvent, but this time the elution was terminated 1 cm before the solvent front reached the top of the plate.

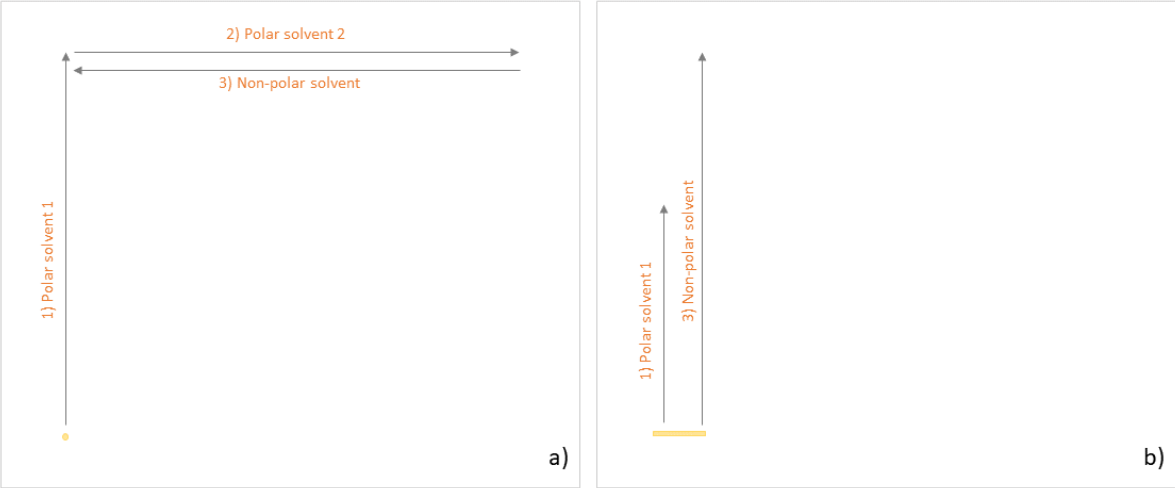

Figure 15: a) 2D TLC: The lipid extract is placed dropwise in the bottom left corner and eluted by the three different solvents in the order given in the figure. Between every elution, the plate was turned so that the arrow would always point upwards. b) 1D TLC: The lipid extract is placed dropwise with a concentration of 50µg/cm along a line 1 cm from the bottom of the plate. Elution by 2 different solutions in the order given by the figure.

Table 2: List of solvents used for TLC-purposes.

Solvent:	**Content:**
Polar solvent 1	methyl acetate: iso-propanol: CH_3Cl: MeOH: 0,25%KCl (25:25:25:10:9)
Polar solvent 2	$CHCl_3$: MeOH: acetic acid: H_2O (55:37.5:3:2)
Non-polar solvent	n-hexane: diethyl ether: acetic acid (80:20:2)

Four different standards were also eluted using 1D TLC. The contents in these standards are listed in table 3.

Table 3: Content of the standards used in 1D TLC.

Standard:	**Content:**
TLC *(TLC18-4, Nu-Chek Prep Inc., Minnesota, USA)*	C – Cholesterol FFA – Free fatty acid TAG – Triacylglycerol FAME – Fatty acid methyl ester
Std 1 (PL-std)	PC – Phosphatidyl choline, 16:0-22:6 *(Avanti Polar Lipids, Inc., Alabama, USA)* PE – Phosphatidylethanolamine, 18:0-20:5 (*Avanti Polar Lipids, Inc., Alabama, USA)* PS – Phosphatidyl serine, porcine brain *(Sigma-Aldrich Inc., Darmstadt, Germany)* PI –Phosphatidylinositol, bovine brain *(Sigma-Aldrich Inc., Darmstadt, Germany)* CL – Cardiolipin, bovine heart *(Sigma-Aldrich Inc., Darmstadt, Germany)* SM – Sphingomyelin porcine brain *(Sigma-Aldrich Inc., Darmstadt, Germany)*
Std A	PA – Phosphatidic acid 840101 *(Avanti Polar Lipids, Inc., Alabama, USA)*
Std B	PG – Phosphatidylglycerol 841138 *(Avanti Polar Lipids, Inc., Alabama, USA)*

One set of plates were sprayed with 3% $Cu(CH_3COO)_2$ in 8% phosphoric acid and burned at 160°C for 20 minutes to visualize the lipid fractions. The two other set were sprayed with 2',7'-dochlorofluorescein solved in MeOH. When dry, the plates were placed under UV-light. The UV-visible fractions were circled using a pencil and scraped off into a tube.

The set going to LC analysis for determination of lipid classes was solved in 1 mL 2:1 $CHCl_3$:MeOH and stored at -20°C overnight. The lipids solve easily in the solvent, but the silica from the TLC-plate does not, hence it had to be removed by filtration. Several methods were attempted. The fractions from 2D TLC were filtrated using filters made by plastic. However, these samples got destroyed by pollution. Glass wool was used to filter the fractions from 1D TLC, but this only removed the coarse particles. Some fractions (1, 2, 3 and blank) were attempted filtrated using micro glass filter papers, but this method was liquidated due to the risk of losing material. Also, a lot of fine particles remained in the extract after using this method. Last, all fractions were filtered by vacuum filtration, but it did not remove all fine particles. The extracts were evaporated and transferred to small GC-vials. There, they were evaporated until dry, and the GC-vials were refilled with 50-250 µL 2:1 $CHCl_3$: MeOH based on the assumed amount of lipids in each fraction. Samples were infused by a HPLC system using methanol at flow rate 0.3 mL/Min as spraying reagent. They were analysed on an AccuTOFTM JMS-T100LC MS operated with an orthogonal electrospray ionization (ESI) source with positive mode, an orthogonal accelerated time of flight (TOF). Ion source temperature was set to 200°C and the needle voltage was set to 2500 V. The desolvation gas flow was 2.0 L/min and the nebulising gas flow was 1.0 L/min.

Due to solvent shortage, the fractions from 1D TLC were stored dry at -80°C overnight. The following day, the FA and sterols were extracted as FAME from the fractions as described in section 3.7.2. Lipid fraction extracts were stored at -20°C until analysis.

3.7.2. Direct methanolysis and total fatty acids

As described in section 1.4.1., fatty acids and the change of the fatty acid profile are good indicators of an organism's response to changes (Denich et al., 2003). Direct methanolysis was used to liberate FA from the larger lipid molecules and to esterify FA to FAME prior to GC analysis, as to increase their volatility and thermal stability (Akoh, 2002). In this reaction, free or esterified FA are converted to their corresponding FAME using an acidic catalysator and a large surplus of methanol (Mjos, 2006). The methanolysis reagent used for this reaction is 2 M dry HCl in MeOH. Sterols with hydroxy groups may also react to form methyl esters.

The methanolysis and extraction method of Meier et. al. was used as a base for this procedure (Meier et al., 2006), but a larger amount of starting material was used due to the low lipid content of sponge WW. 100 µL internal standard 19:0 was added to all tubes and the solvent evaporated. 300 mg sponge was weighed in to 16 mL tubes. 1 mL methanolysis reagent was added, and the tube was heated at 100°C for 2 hours. After heating, half of the sample was evaporated to get rid of the hydrochloric acid. 0,5 mL H_2O and 2 mL n-hexane were added before the sample was oscillated for 30 seconds and centrifuged at 2000 rpm for 5 minutes. The organic phase was transferred to a new tube, whereas the water phase was extracted with n-hexane yet another time. The extract was evaporated to 1 mL and transferred to GC vials, then stored at -20°C until analysis. The analysis total FA was performed on an Agilent 6890N GC with FID detection. The GC column was an Agilent 122-5062 DB-5 (60 m · 0.25 mm · 0.25 µm) and the carrier gas was helium at a constant flow rate of 1 mL/min. 10 µL samples were injected at 280°C splitless. The oven temperature was held at 60°C and ramped to 130°C at a rate of 60°C/min, then ramped to 325°C at 1°C/min rate and held at this temperature for 7 min. The detector temperature was 300°C. The TLC fractions were analysed on an Agilent 7890A GC with FID detection. An automatic liquid sampler was used to inject 5-12.5 µL samples (depending on lipid content). Besides this, TLC fractions were analysed using the same column and the same method specifications as given for the total FA.

Prior to quantification, a qualitative analysis was performed on one sample of total FA. Two different columns (the above-mentioned DB-5 column and a polar CP-WAX column) and 2 different temperature were used. Satisfactory chromatographic resolution had to be obtained, and the

different FA hade to be identified using MS detection. The chosen column and temperature programme were the above-mentioned DB-5 column and 1°C/min programme. The GC was coupled to an Agilent 5973 quadrupole MS with an EI source. The ion source temperature was 230-250 °C and the quadrupole temperatures were 150-200 °C.

3.8. Normalization of results

Some results were normalized from sponge WW to dry ash free (DAF) sponge. This gives a more accurate image of the results than using the wet weight, as the amount of water in the sponge specimen varied. Also, the ash weight (AW) varies, as the structure of the sponge tissue varied.

300 mg sponge were weighed and placed in pre-weighed alumina containers. Sponges were dried for 24 hours at 110 °C to obtain the dry weight (DW). The samples cooled down for a couple of minutes to reach room temperature before weighing, since the temperature affect the analytical balance. After a couple of minutes, the samples were weighed consecutively, as moisture tend to accumulate on dry samples at room temperature. The samples were given individual caps made by loosely fitted and perforated alumina foil and burned at 450 °C for 6 hours to obtain the AW. After burning, ash was the only thing left. Samples were taken out of the oven at around 100 °C and placed consecutively in an exicator to avoid moisture from sticking to the samples. Then the samples were weighed, and the results were normalised to DAF using equation 12 and 13.

$$DAF = \frac{Sponge\ DW(g) - Sponge\ AW(g)}{Sponge\ WW(g)} \quad \text{Equation 12}$$

$$Sponge\ DAF\ (g) = Sponge\ WW(g) \cdot DAF \quad \text{Equation 13}$$

3.9. Data analysis and statistics

A calibration curve of 11 points were used to calculate the concentration of PAH in both water samples and tissue samples. The correlation coefficient (r), calculated from equation 9 was 0.9987 or higher for all compounds. All values considering sponge accumulation of PAH and the change of lipid composition are reported as averages of 3 or 4 replicates. For some groups lack of material caused only 3 replicates to be analysed. The mean value ($\bar{x}$) and standard deviation (S) are calculated using equation 14 and 15, respectively. Along with the mean value, the variance was used for all significance calculations. Variance is given by S^2.

$$\bar{x} = \frac{1}{n}\sum_{i=1}^{n} x_i = \frac{1}{n}(x_1 + x_2 + \cdots + x_n) \quad \text{Equation 14}$$

$$S = \sqrt{\frac{\sum_{i=1}^{n}(x_i - \bar{x})^2}{n-1}} \quad \text{Equation 15}$$

Accumulation of PAH in sponge tissue are reported as significant different to control levels with 95% confidence level (two-way t-test, p≤0,05).

Values considering total FA of *G. barretti* are reported as averages and standard deviations calculated using equation 14 and 15. Results are normalized and weighted. Principal component analysis (PCA) was performed on the total FA results.

4. Results

4.1. Water samples

Figure 16 show the concentration of PAH in the water in the experimental mesocosms. As expected, the results show a trend of increasing concentration from control to high treatments. Also, the

results show that the concentration remained stable throughout the experiment, from day 1 through day 8 for all treatments except for the medium treatment.

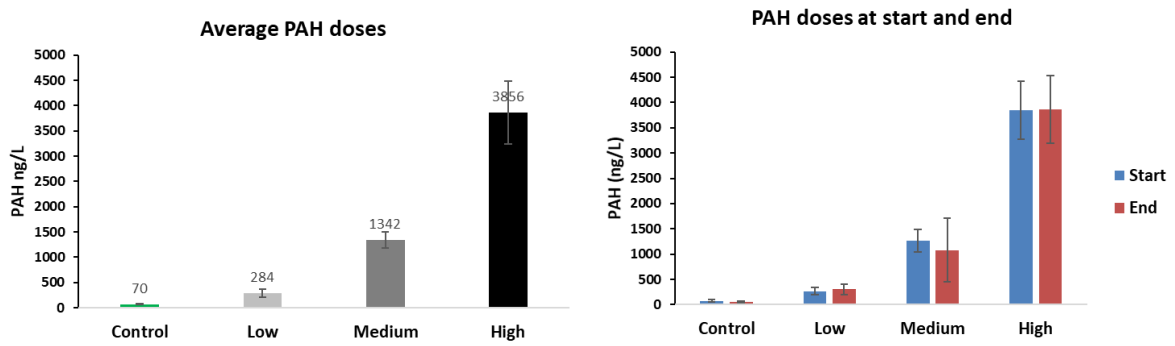

Figure 16: Average and start/end levels of PAH in the water in the experimental setup.

The Troll crude oil consist of 1.3 % PAH. The measured concentration of PAH in the water is very close to the estimated PAH concentration calculated from the PAH contents in the Troll crude oil and the nominal doses of dispersed oil in the water (Table 4).

Table 4: Comparison between the nominal concentration of dispersed oil in water to the estimated and measured PAH concentrations.

Treatment:	Nominal oil concentration (µg/L):	Estimated PAH concentration (µg/L):	Measured PAH concentration (µg/L):
Control	0	0	0.07 ± 0.01
Low	33	0.43	0.28 ± 0.08
Medium	100	1.30	1.34 ± 0.16
High	300	3.90	3.86 ± 0.62

4.2. PAH body burden

As shown in figure 17, PAH accumulated in sponge specimen with a dose-related response. Sponge explants exposed to the low concentration of PAH did not show significantly elevated amounts of PAH (two-way t-test, $p \leq 0.05$). Compared to the control samples, sponge explants exposed to the high and medium doses of PAH showed significantly elevated amounts of PAH after 1 and 2 days of exposure respectively. For the medium and high doses, results show a clear gradient with increased PAH accumulation following increasing exposure, time and concentration both considered. However, d8h breaks with this trend, as the levels of total PAH flattens out at this sampling point. After an 8-day exposure to oil followed by a 30-day recovery, the PAH levels dropped significantly. Explants exposed to the medium concentration of oil dropped to close to control values, and explants exposed to the high concentration dropped to values clearly below the levels after only one day of exposure.

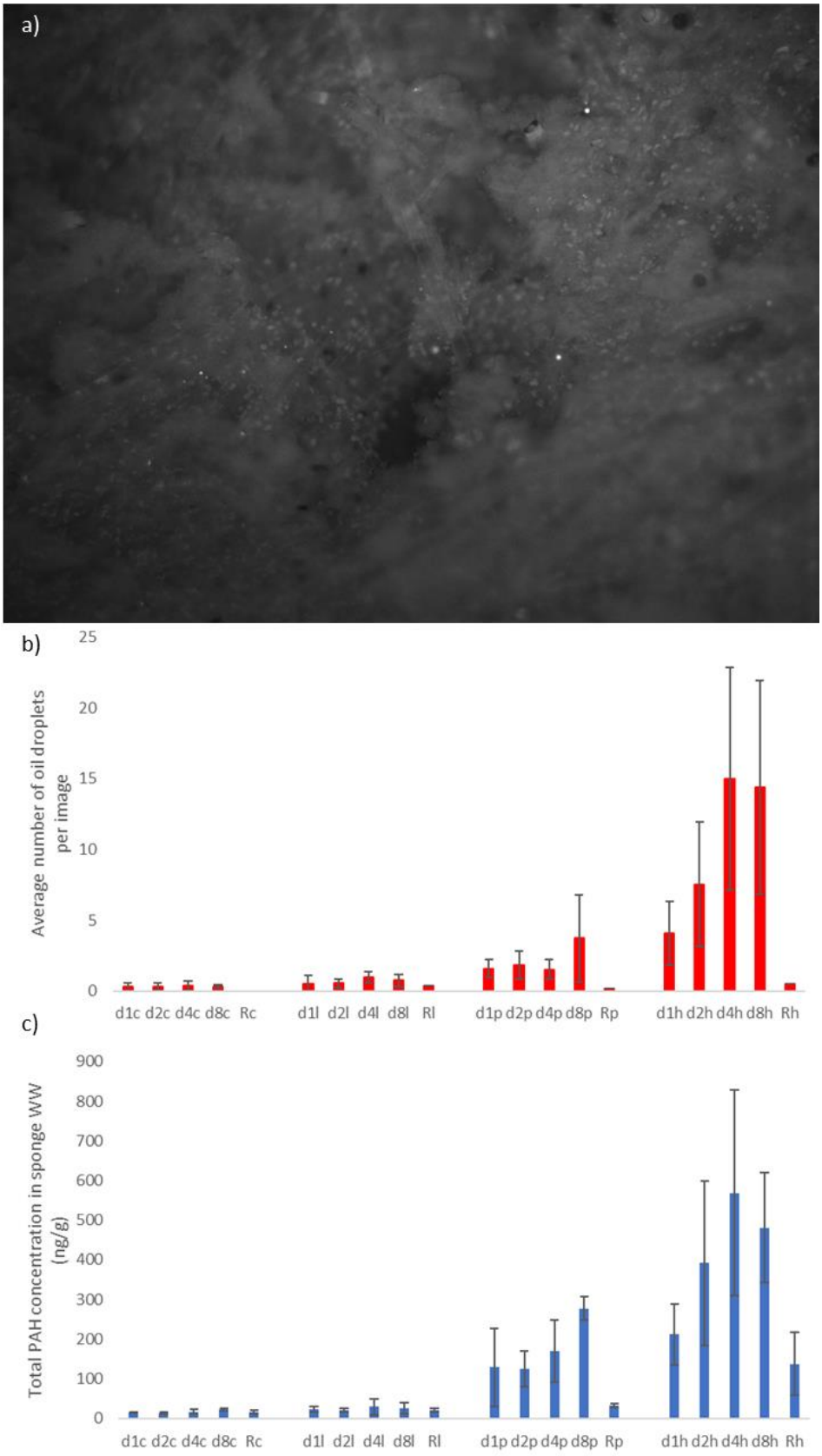

Figure 17: The accumulation of total PAH in sponge specimen. (a) show the accumulation of PAH as droplets in a sponge explant exposed to the high concentration of oil for 8 days. (b) and (c) show the number of oil droplets and the total PAH concentration in the *G. barretti* tissue (WW) respectively. Both (b) and (c) show control to the left, with an increasing exposure moving to the right.

There is correlation between the counted number of oil droplets and the PAH body burden. This correlation is shown in figure 18. Oil droplets in this experiment is assumed to have a size range of 5-20 µm (Sorhus et al., 2015), and as a result of that the volume of the oil droplets also varies. When counted, all oil droplets were counted as equivalently big.

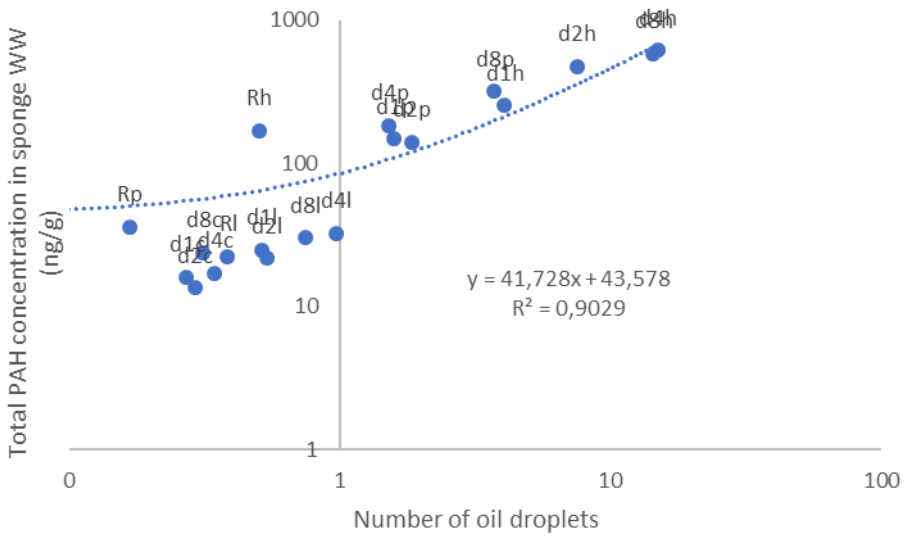

Figure 18: Correlation between the number of oil droplets per section and the total PAH accumulation, logarithmic scale.

The oil profile of the crude oil used in the experimental setup is shown in figure 19a). Figure 19 also gives the oil profile in sponges after 8 days of treatment ac different exposure levels. As the exposure level increases, the closer the oil profile gets to the profile of crude oil from the Troll field.

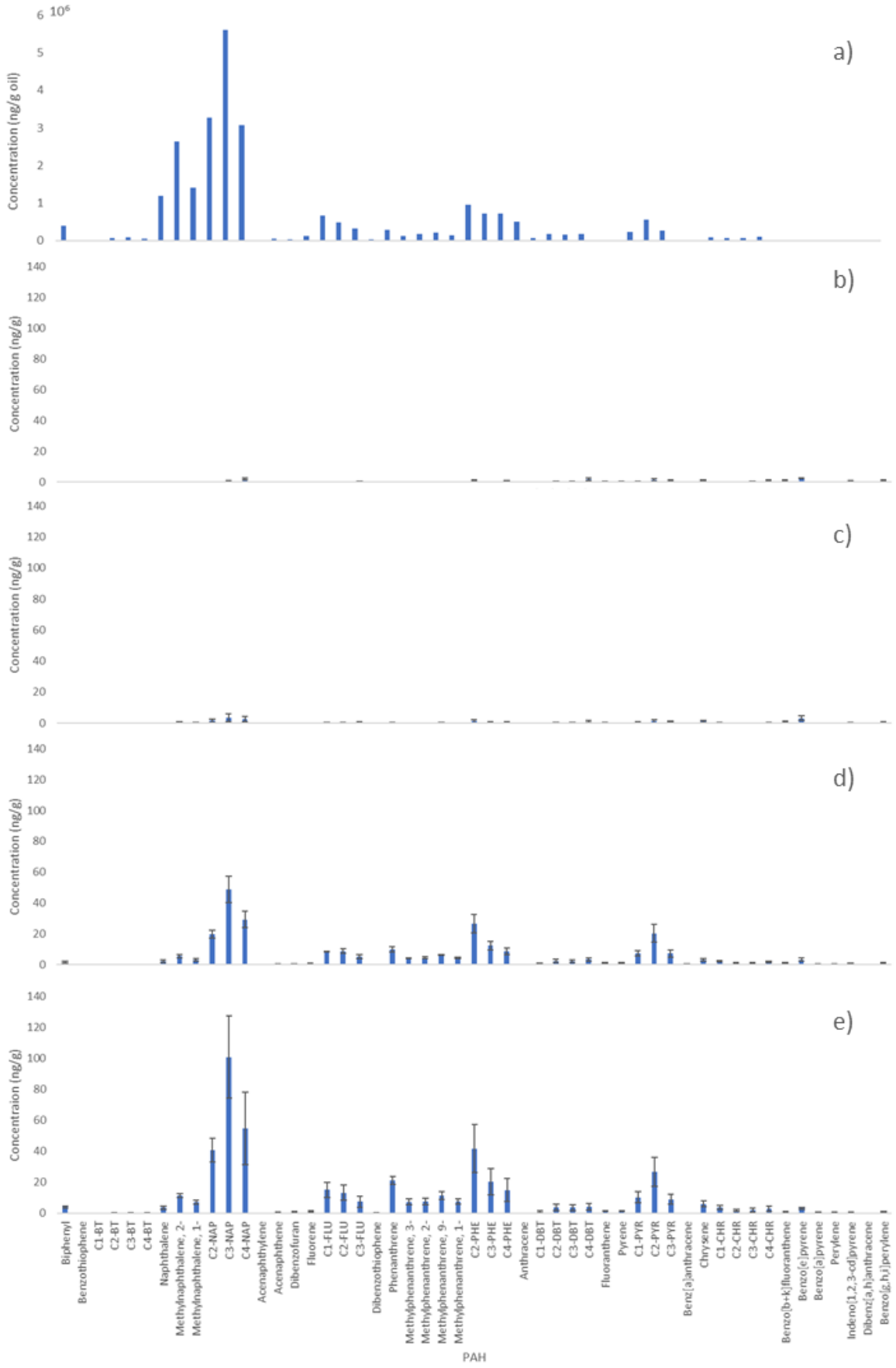

Figure 19: Oil profile in crude oil from the Troll Field (a), and in sponges after 8 days of exposure where (b) is control, (c) is low, (d) is medium and € is high concentration of oil. (b) to (e) is drawn with the same concentration scale.

4.3. Physiological effects on oil exposed sponges

Oil exposure did not result in increased mortality, as none of the sponge specimen showed visual signs of death or compromised health during the 38-day experimental period. Nor did it affect the sponge respiration rates (rates in which they consume oxygen) in any significant manner (Figure 20 a)) (Stevenne, 2018). LMS is a general stress biomarker that has been recommended in cases of chemical pollution, as lysosomes accumulate contaminants and quickly show destabilisation in organisms exposed to pollutants (Martínez-Gómez, 2015). Sponge specimen showed an increased lysosomal destabilisation following exposure to increased concentrations of dispersed oil, but the duration of the exposure did not affect the destabilisation significantly. The levels returned to control levels after a 30-day recovery as shown in figure 20 b) (Stevenne, 2018).

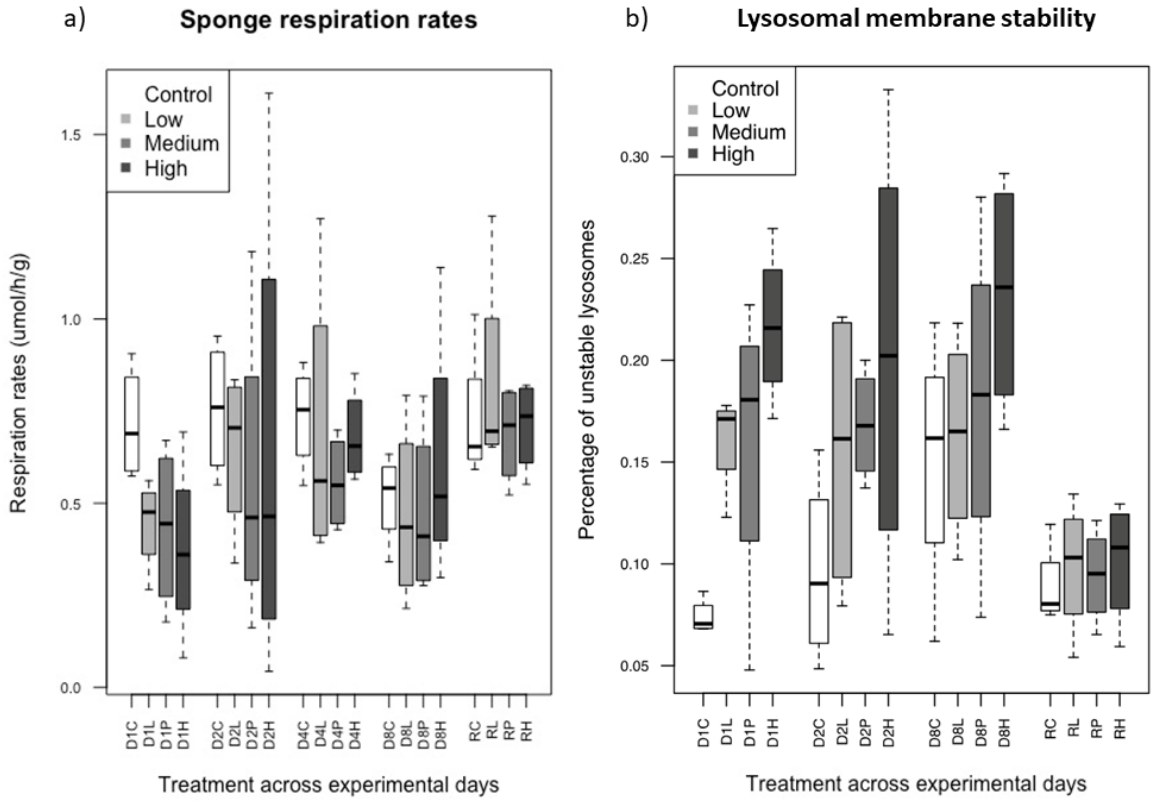

Figure 20: The effect of oil treatment on a) respiration rates and b) lysosomal membrane stability. (Stevenne, 2018).

Sponges harboured a microbiome that differed from the surrounding water in the experimental mesocosms (Figure 21), and the bacterial communities did not seem to be affected by the different oil treatments (Stevenne, 2018).

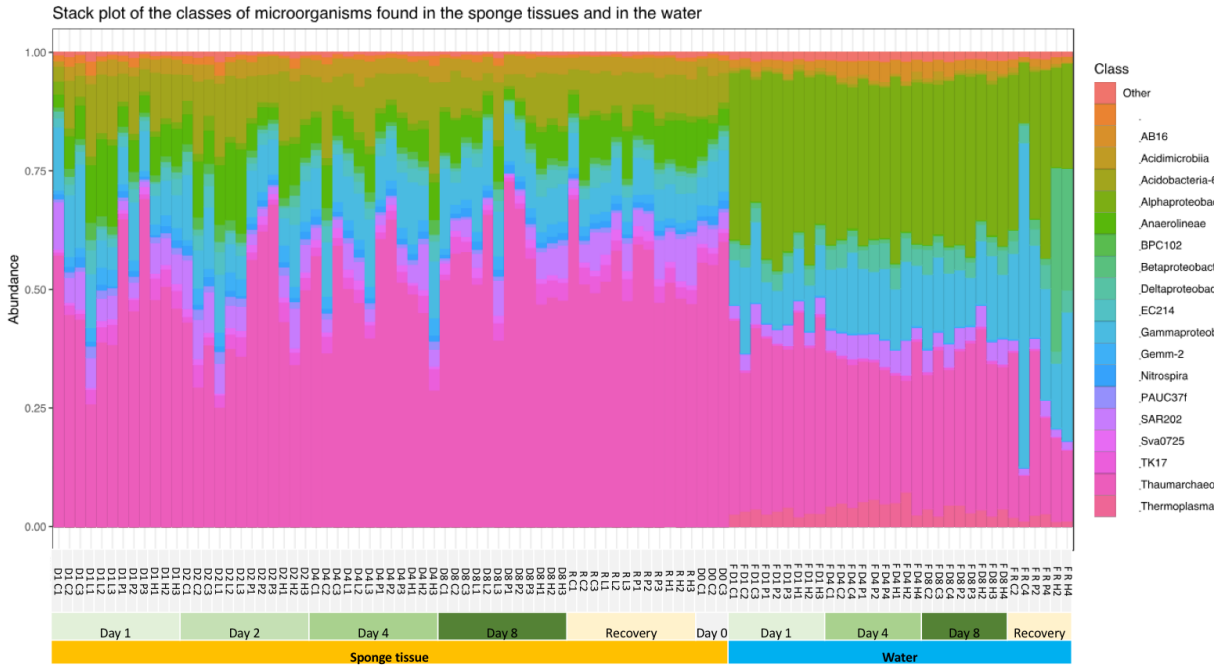

Figure 21: The microbial community in sponge specimen and the surrounding water in the experimental mesocosms. (Stevenne, 2018).

The physiological effects and the identification of the microbial community was measured by Chloè Stevenne, a master student from Université de Liége, Belgium. Chloè Stevenne and I work together on the exposure study of the sponges at Austevoll research station. Figure 20 and 21 are taken from her master thesis.

4.4. Method development and FA identification

As there are no prior publications on the complete FA profile of *G. barretti*, a big part of this thesis was to develop a suitable method for separation and identification. Many marine organisms, e.g. salmon and trout have a fatty acid profile dominated by unsaturated fatty acids (Blanchet et al., 2005), and so have other marine species such as algae (Volkman et al., 1989). Polar columns are usually a good choice for separation of such FAME because saturated and unsaturated FAME are separated, as well as different isomers of unsaturated fatty acids (Mjos and Grahl-Nielsen, 2006). However, a large number of saturated and branched saturated FA have previously been observed in bacteria (O'Leary, 1962), and sponges have been proved to be a rich source of unusual FA (Berge and Barnathan, 2005). One polar column (CP-WAX), one non-polar column (DB-5) and two different temperature programmes (1°C/min and 2°C/min) were tested for this purpose.

The fatty acid profile of *G. barretti* was found be highly complex with 177 known compounds and several unknowns. It was found to contain large amounts of saturated FA, of which a vast amount was branched. Mono- and di-unsaturated FA were also abundant, but only small amounts of poly-unsaturated fatty acids were found. This caused the non-polar DB-5 column to be chosen as the most suitable, as it provides better general separation because of higher chromatographic efficiency than polar columns (Waktola and Mjos, 2018). Since so many different branched SFA were found, and the complexity of the samples were so high, the 1°C/min programme that had the highest efficiency was chosen, as the chromatographic efficiency increases when the temperature rate decreases (Mjos and Waktola, 2015). The complexity of the sample and the differences between the two columns are shown in appendix B.

Wasta and Mjøs describes how Chrombox utilizes databases of spectra's and retention indexes (Chrombox, 2019) and use both to identify FAME (Wasta and Mjos, 2013). The databases contain a limited selection of branched FAME, including only the most common iso and ante-iso FAME. No retention indexes for columns equivalent to the DB-5 column has been published, but retention indexes from an unpublished database on algae was available. However, algae contain mostly PUFA, the most common SFA, MUFA and PUFA, and a very limited selection of branched FAME. Hence, identification largely had to be performed manually by using the spectra's. Every species in the databases has a code, a short name and a long name. When identifying new species, they had to be given names and individual temporary codes.

Table 5 gives the identity of the FA found in *G. barretti*. Appendix B gives a comparison of the two columns at the 1°C/min temperature programme, and it also includes some compounds that remained unidentified but were given an EOX-code. Most of these are assumed to be some kind of unsaturated ethers (Weijers et al., 2006) or sterols. The spectra's and structure of all species are given in Appendix C. When applying the method for quantification on GC-FID, some compounds that were not present during the identification in Chrombox appeared. These compounds are not mentioned in Appendix B nor C, but some of them will be mentioned in section 4.4 and 4.5.

Table 5: The identity and code of the FA present in *G. baretti*, their identifying ions and retention time (t_R) in minutes and equivalent chain values (ECL) in the DB-5 column at 1°C/min. The base peak is denoted as "bp".

Code	Identity:	Ions (m/z):	t_R	ECL
EOX-031		55, 74, 87bp, 113, 129, 157	13.0271	10.2350
EOX-032		67, 79bp, 93, 108, 150, 182	14.1134	10.4089
EOS-001	Br 10:0 (xMe)	55, 74bp, 87, 143, 157, 186	14.5282	10.4748
EOS-002	Br 11:0 (4,8 DiMe)	71, 74, 87bp, 127, 143, 169, 171	16.6614	10.8101
EOS-003	Br 11:0 (xMe)	55, 74bp, 87, 143, 157, 169, 200	17.1157	10.8806
EOX-033		59, 101, 143bp, 175, 185	21.0661	11.4814
EOS-004	i-12:0	55, 74bp, 87, 143, 171, 183, 214	22.3104	11.6660
SAN-003	12:0	55, 74bp, 87, 129, 143, 171, 183, 214	24.5424	11.9914
EOS-005	i-13:0	55, 74bp, 87, 143, 185, 228	28.8681	12.6016
EOS-006	ai-13:0	55, 74bp, 87, 143, 185, 199, 228	29.4211	12.6777
EOS-007	i-14:0	55, 74bp, 87, 143, 199, 242	36.5515	13.6186
EOM-001	14:1 n-x	55, 74bp, 84, 98, 110, 124, 137, 151, 164, 180, 240	37.7728	13.7728
SAN-005	14:0	55, 74bp, 87, 143, 199, 242	39.5933	13.9976
EOM-002	14:1 n-5, 13Me	69, 74bp, 81, 84, 97, 109, 124, 180, 199, 222	42.5166	14.3460
EOS-008	Br 15:0 (3Me)	55, 74bp, 101, 225, 256	42.7733	14.3759
EOS-009	Br 15:0 (6Me)	55, 74bp, 87, 115, 143, 180, 225, M+ =?	43.2474	14.4309
EOS-010	Br 15:0 (8Me)	55, 74, 87, 143bp, 171, 256	43.4054	14.4491
EOS-011	Br 15:0 (9Me)	57, 74bp, 87, 143, 157, 185, 213, 256	43.6424	14.4764
EOS-012		70bp/74bp, 83, 96/97, 109, 123, 153, 180, 185, 222, 225	43.7807	14.4923
EOS-013	Br 15:0 (10Me)	55, 74bp, 87, 143, 199, 213, 256	43.9782	14.5150
SAB-078	i-15:0	55, 74bp, 87, 143, 213, 256	45.0053	14.6326
SAB-077	ai-15:0	55, 74bp, 87, 143, 199, 213, 227, 256	45.6769	14.7092
SAN-006	15:0	55, 74bp, 87, 143, 213, 256	48.1853	14.9954
EOS-014	Br 16:0 (3,x DiMe)	55, 74, 101bp, 213, 256, 270	48.2051	14.9977
EOS-015	Br 16:0 (x,x DiMe/x Et)	57, 74bp, 87, 143, 171, 227, 270	48.6791	15.0520
EOS-016	Br 16:0 (x,x DiMe/x Et)	57, 74bp, 87, 143, 199, 227, 270	48.9359	15.0814
EOM-003	16:1 n-x	55, 74bp, 81, 96/97, 101, 152, 194, 213, 236, 268	51.1679	15.3354
EOS-017	Br 16:0 (3Me)	74, 101bp, 157, 239, 270	51.4641	15.3689

EOS-018	Br 16:0 (6Me)	55, 74bp, 87, 143, 194, 270	51.8789	15.4159
EOS-019	Br 16:0 (8Me)	57, 74bp, 87, 143, 171, 227, 270	52.0962	15.4405
EOS-020	Br 16:0 (10Me)	57, 74bp, 87, 143, 199, 227, 270	52.3332	15.4673
EOS-021	Br 16:0 (11Me)	55, 74bp, 87, 143, 185, 213, 227, 270	52.7085	15.5097
DIU-494	16:2 n-6	67, 81bp, 95, 109, 150, 217, 266	53.5776	15.6078
SAB-072	i-16:0	55, 74bp, 143, 227, 270	53.7356	15.6256
EOS-022	ai-16:0	55, 74bp, 87/84/81, 97/96, 110, 152, 194, 236, 270/268	54.4664	15.7080
MOU-275	16:1 n-9	55bp, 74, 84, 87, 98/96, 110, 123, 152, 194, 236, 269	54.6442	15.7281
MOU-021	16:1 n-7	55bp, 69, 83, 87, 97, 110, 123, 152, 194, 236, 269	55.0985	15.7793
MOU-255	16:1 n-5	55bp, 74, 87, 97, 110 ,152, 194, 236, 269	55.9281	15.8729
SAN-007	16:0	55, 74bp, 87, 143, 227, 270	57.0539	16.0000
EOS-023	Br 17:0 (x,x DiMe/x Et)	55, 74bp, 87, 143, 171, 284	57.3897	16.0379
EOS-024	Br 17:0 (x,x DiMe/x Et)	55, 74bp, 87, 143, 185, 241, 284	57.4687	16.0468
EOM-004	17:1 n-x	69bp, 83, 143, 251, 282, 284	57.7255	16.0758
EOM-005		57, 74bp, 81, 83, 97/96, 111, 126, 138, 157, 180, 233, 251, 282	58.3378	16.1448
EOM-006	16:1 n-x, 3Me	55bp, 69, 74, 83, 101, 111, 152, 207, 250	59.1674	16.2382
EOM-007	16:1 n-x, xMe	55, 69, 81, 97, 138bp, 167, 251, 282	59.3846	16.2626
EOM-008		55, 74bp, 84, 97, 110, 152, 194, 227, 250, 282	60.0562	16.3382
MOU-022	Br 17:1 n-7	69bp, 74, 83, 97, 111, 152, 194, 227, 250, 282	60.3525	16.3715
EOS-025	Br 17:0 (8Me)	55, 74bp, 87, 143, 171, 284	60.6882	16.4092
EOS-026	Br 17:0 (9Me)	55, 74bp, 87, 143, 185, 241, 284	60.7870	16.4203
EOS-027	Br 17:0 (10Me)	57, 74bp, 87, 143, 199, 241, 284	60.9450	16.4381
EOS-028	Br 17:0 (11Me)	55, 74, 87, 143, 185, 213, 241, 284	61.2018	16.4669
MOB-286	16:1 n-10, 7Me	55, 69, 83, 97, 115,138bp, 167, 251, 282	61.8339	16.5380
EOS-029		57, 74, 87, 143bp, 241, 284, 298	62.5252	16.6158
SAB-074	i-17:0	55, 74bp, 87, 143, 241, 284	62.6900	16.6269
SAB-073	ai-17:0	57, 74bp, 87, 143, 185, 199, 241, 284	63.3745	16.7115
MOU-436	17:1 n-8	55bp, 74, 87, 97, 110, 152, 250, 282, 298	63.6708	16.7449
EOD-001	18:2 n-x	67, 81, 95bp, 109, 180, 207, 239, 266, 298	65.3299	16.9326
SAN-008	17:0	55, 74bp, 87, 143, 241, 284	65.8632	16.9932
EOS-030	Br 18:0 (x,x DiMe/x Et)	55, 74bp, 87, 111, 115, 143, 222, 248, 298	66.1793	17.0292
EOS-031	Br 18:0 (x,x DiMe/x Et)	55, 74bp, 87, 143, 187, 222, 255, 298	66.2188	17.0337
EOS-032	Br 18:0 (x,x DiMe/x Et)	57, 74bp, 87, 143, 199, 255, 298	66.5743	17.0742
EOS-033	Br 18:0 (x,x DiMe/x Et)	55, 74bp, 87, 115, 143, 222, 248, 298	66.8903	17.1102
EOS-034	Br 18:0 (8Me)	55, 74bp, 87, 143bp, 185, 215, 298	69.3198	17.3874
EOS-035	Br 18:0 (10Me)	55, 74bp, 87, 143, 199, 255, 298	69.4976	17.4077
EOS-036	Br 18:0 (12Me)	57, 74bp, 87, 143, 199, 255, 298	69.9519	17.4598
SOH-769	16:0-3OH	71bp, 74, 82, 97, 113, 152, 194, 237, 298	70.4801	17.4801
DIU-027	18:2 n-6	67, 81, 95, 109, 123, 150, 164, 220, 294	70.4457	17.5164
EOS-037	i-18:0	55, 74bp, 87, 143, 199, 255, 298	71.3937	17.6252
EOS-038	ai-18:0	67, 74bp, 81, 97, 110, 180, 222, 264, 298	72.1246	17.7094
MOU-023	18:1 n-9	55bp, 69, 83, 87, 97, 111, 123, 125, 152, 280, 222, 264, 296	72.1838	17.7162
EOS-039		55, 69, 97, 129bp, 137, 201bp, 283, 296	72.4998	17.7527
MOU-079	18:1 n-7	55bp, 74, 83, 97, 110, 123, 152, 180, 194, 222, 264, 296	72.7171	17.7778
EOM-009	19:1 n-x, xMe	55bp, 69, 83, 97, 111, 125, 140, 152, 171, 194, 222, 264, 279, 310	73.0332	17.8143
MOU-258	18:1 n-5	55bp, 69, 74, 83, 97, 110, 152, 180, 222, 264, 296	73.6060	17.8807
SAN-009	18:0	55, 74, 87, 43, 199, 255, 298	74.6330	18.0000
EOS-040		55bp, 74, 83, 87, 97, 126, 153, 185, 236, 279, 310	74.9886	18.0414

EOM-010	18:1 n-6, 11Me	69bp, 83, 97, 125, 140, 152, 171, 194, 279, 310	75.1466	18.0598
EOM-011	19:1 n-x	55, 74bp, 81, 97, 111, 125, 140, 152, 171, 194, 236, 278, 310	75.4231	18.0921
EOD-002	19:2 n-x	67, 81bp, 95, 109, 123, 150, 164, 308	75.5614	18.1082
UNK-288	UNK-288	67, 81, 95, 109, 150, 185bp, 187bp, 299, 308	75.6404	18.1174
EOM-012	19:1 n-x	55bp, 69, 83, 97, 111, 125, 140, 152, 171, 194, 211, 278, 310	75.8379	18.1405
EOM-013	19:1 n-x	57bp, 69, 83, 97, 111, 125, 139, 157, 180, 194, 261, 278, 310	75.9367	18.1521
EOM-014	19:1 n-x	57, 74bp, 85, 97, 111, 125, 140, 152, 171, 194, 211, 236, 278, 310	76.1934	18.1821
EOS-041	Br 19:0 (10Me)	57, 74bp, 87, 143, 199, 269, 312	78.0501	18.3999
EOS-042	Br 19:0 (11Me)	57, 74bp, 87, 143, 185, 213, 269, 312	78.2081	18.4185
EOS-045		55, 74bp, 87, 97, 143, 236/238, 297, 312, 326	79.5710	18.5793
EOS-046		55, 74bp, 87, 143, 236/238, 283, 297, 326	79.6303	18.5863
EOS-043	i-19:0	55, 74bp, 87, 143, 269, 312	79.9660	18.6260
EOS-044	ai-19:0	5, 74bp, 87, 143, 255, 269, 312	80.7166	18.7150
POU-035	20:4 n-6	67, 79bp, 91, 93, 106, 120, 150, 175, 318	85.4176	19.2775
POU-036	20:5 n-3	67, 79bp, 91, 93, 105, 108, 117, 131,180, 201, 312	85.8916	19.3346
DIU-028	20:2 n-6	55, 67, 81bp, 95, 109, 123, 150, 322	87.3730	19.5138
EOS-047	Br 20:0 (xMe)	55bp, 74, 83, 87, 97, 129, 141, 163, 229, 250, 292, 320, 326	89.1506	19.7303
EOS-048		55, 69, 81, 97, 129bp, 157, 229bp, 279, 311	89.1704	19.7328
SAN-011	20:0	55, 74bp, 87, 143, 283, 326	91.3036	19.9951
EOD-024		55, 67/74, 81/83, 95/97, 171bp, 229bp, 326	92.1134	20.0954
EOD-025		55, 69, 97, 157bp, 243bp, 306	92.2912	20.1175
EOS-049	Br 21:0 (10Me)	55, 74bp, 87, 97, 143, 199, 257, 297, 340	94.3454	20.3739
SAN-012	21:0	55, 74bp, 87, 143, 297, 340	99.2438	20.9949
EOS-050	Br 21:0 (x,x DiMe/x Et)	57, 74bp, 87, 143, 311, 354	99.7772	21.0634
EOS-051	Br 21:0 (x,x DiMe/x Et)	55, 74bp, 87, 97, 141, 169, 184, 199, 278, 322, 354	99.8364	21.0710
POU-066	22:5 n-6	67, 79bp, 91, 105, 117, 131, 150	100.0734	21.1015
POU-039	22:6 n-3	67, 79bp, 91, 93, 119, 131, 145, 273	100.6265	21.1727
POU-038	22:5 n-3	67, 79bp, 91, 93, 105, 108, 117, 131, 145, 328	101.7326	21.3158
SAN-013	22:0	55, 74bp, 87, 143, 311, 354	106.9668	22.0026
EOS-052	Br 23:0 (xMe)	57, 74bp, 87, 143, 199, 255, 325, 368	109.7321	22.3719
EOS-053	Br 23:0 (xMe)	57, 74bp, 87, 143, 199, 255, 325, 368	110.0679	22.4170
EOS-054	i-23:0	57, 74bp, 87, 143, 199, 269, 325, 368	111.6875	22.6356
EOS-055	ai-23:0	57, 74bp, 87, 143, 283, 325, 368	112.3591	22.7267
SAN-014	23:0	57, 74bp, 87, 143, 325, 368	114.3343	22.9963
EOS-056	Br 24:0 (x,x DiMe/x Et)	57, 74bp, 87, 97, 143, 199, 339, 382	114.8281	23.0641
EOS-057	Br 24:0 (17Me)	57, 74bp, 87, 97, 143, 255, 283, 339, 382	117.1588	23.3862
EOS-058	ai-24:0	57, 74bp, 87, 97, 143, 339, 382	119.5685	23.7233
MOU-571	24:1 n-x	55bp, 69, 83, 97, 111, 125, 152, 194, 264, 306, 348bp, 380	120.2006	23.8124
EOM-015	24:1 n-x	55bp, 69, 83, 97, 111, 125, 152,194, 264, 306, 348, 380	120.9906	23.9242
SAN-015	24:0	57, 74bp, 87, 143, 199, 283, 339, 382	121.5239	24.0000
EOD-003	25:2 n-x	55, 67, 81bp, 95, 109, 136, 142, 150, 250, 360, 382	122.6300	24.1577
EOS-059	Br 25:0 (xMe)	57, 74bp, 87, 97, 143, 199, 297, 353, 396	124.2497	24.3902
EOM-016	25:1 n-x	69, 83, 97, 111, 125, 143, 278, 307, 319, 339, 362bp, 394, 396	124.4077	24.4129
EOD-004	25:2 n-x, xMe	55, 57, 69, 81bp, 109, 141, 150, 410	125.2965	24.5414
EOS-060		57bp, 74, 87, 97, 143, 199, 255, 325, 367, 410	125.3953	24.5557
EOS-061	i-25:0	74bp, 87, 143, 199, 297, 353, 396	125.8891	24.6273
EOS-062	ai-25:0	57, 74bp, 87, 143, 353, 396	126.5804	24.7279
EOD-005		55, 69, 81, 255, 366bp, 396	128.4963	25.0087

EOD-006	(Br) 26:2 n-x	67, 81bp, 95, 109, 121, 141, 150, 380, 406	128.7531	25.0465
EOD-007	(Br) 26:2 n-x	67, 81bp, 95, 109, 121, 136, 141, 150, 264, 366, 406	129.6024	25.1721
EOD-008		55, 67, 81, 95, 109, 247, 353, 368bp, 410	131.0048	25.3807
EOD-009	(Br) 26:2 n-x	55bp, 69, 81, 95, 109, 123, 137, 150, 194, 375, 406	131.9134	25.5167
EOD-010	(Br) 26:2 n-x	67, 81bp, 95, 109, 136, 141, 150, 264, 374, 406	132.2492	25.5670
EOD-024		69bp, 83, 97, 111, 145, 159, 213, 255, 292, 376, 380, 410	134.0663	25.8411
EOD-011	(Br) 27:2 n-x	57, 67, 81bp, 95, 109, 141, 150, 278, 371, 388, 420	134.7577	25.9459
EOD-012	(Br) 27:2 n-x	67, 81bp, 95, 109, 141, 149, 420	135.0342	25.9880
EOD-013	(Br) 27:2 n-x	57, 67, 81bp, 95, 109, 136, 141, 150, 181, 278, 388, 420	135.2515	26.0210
EOD-014	(Br) 27:2 n-x	55bp, 69, 81, 95, 109, 123, 150, 389, 420	135.8440	26.1113
EOD-015	(Br) 27:2 n-x	67, 81bp, 95, 109, 136, 141, 150, 278, 388, 420	136.3576	26.1898
EOD-016		55, 57, 81, 95, 109, 145, 213, 283, 365, 380bp, 388, 420	137.0686	26.2988
EOD-017		55, 81, 145, 159, 161, 259, 283, 356, 380bp	137.2661	26.3291
EOD-018		55, 81, 145, 159, 283, 365, 380bp	137.5822	26.3777
EOD-019	(Br) 27:2 n-x	67, 81bp, 109, 136, 141, 150, 420	138.8463	26.5727
EOD-020	(Br) 27:2 n-x	67, 81bp, 109, 141, 150, 420	139.2018	26.6277
EOD-021		55bp, 69, 81, 95, 109 123, 402, 413	144.8113	27.5076
EOD-022		67, 81bp, 95, 109, 141, 150, 207, 306, 416	147.6359	27.9587
EOD-023		55, 69, 81bp, 95, 109, 159, 285, 412	147.7346	27.9746

Kubinéc et. al. determined the ECL values of all C4-C23 saturated monomethyl branched FAME , and the determination of the branching point position was done by comparison to the *m/z* column in table 1 in this article (Kubinec et al., 2011). As mentioned in section 2.2.1.1., the position of the branching point causes the formation of two diagnostic ions a and b. In Appendix C, these ions are highlighted. For some compounds the b-ion is missing, especially for the FA with iso branching. The reason for this is the formation of the energetically less favourable methyl radical by cleavage at the b position. Additionally, the ECL values were compared to the corresponding ECL values (Kubinec et al., 2011) and to the ECL values in table 1 in Apon and Nicolaides regarding the same subject (Apon and Nicolaides, 1975).

Counted from the methyl end of the chain, each group of branching points (e.g. all iso FA) has a linear correlation between the ECL/FCL values and the number of carbons. Such plots provide a visual aid to identify FA structure and has previously been performed to identify e.g. unsaturated FA (Wotherspoon et al., 2018). The correlation for the iso and ante-iso FA are clear, but the further into the carbon chain the branching point is located, the closer the ECL/FCL values get. This method can be used as an affirmation for the branching position in iso and ante-iso FA. Figure 22 show the linear correlation between the FCL values and the number of carbons in mono-branched saturated FAME.

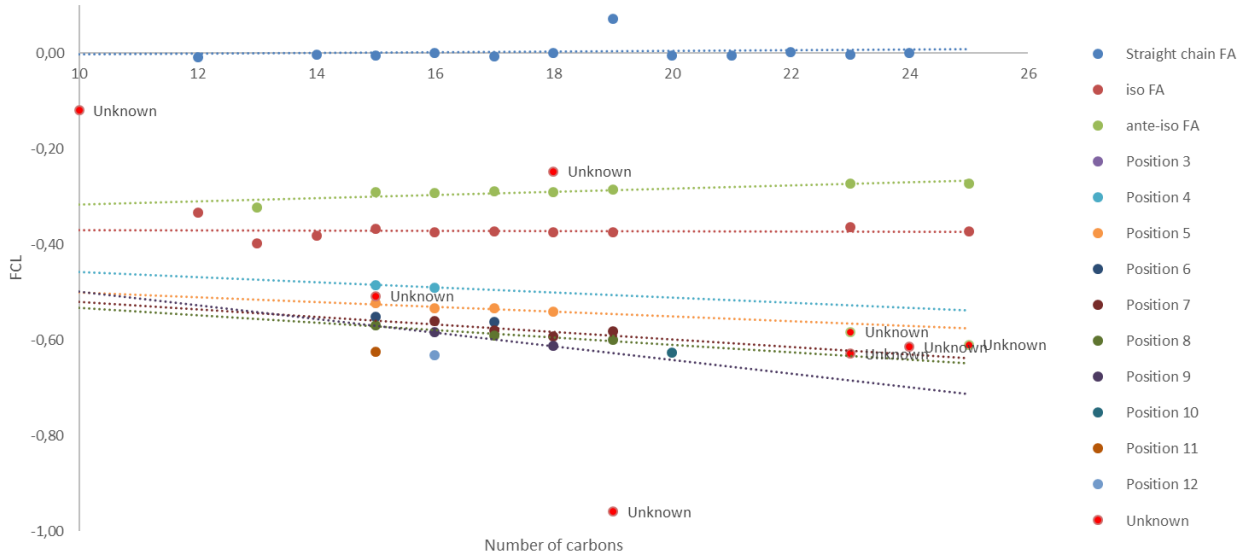

Figure 22: Correlation between FCL values and number of carbons in mono branched saturated FAME.

4.5. Total FA and change in FA profile

The absolute FA content remained stable throughout the experiment, with an average of 204 ± 31 mg FA per g organic material (DAF). This equals a lipid% of 1.87 ± 0.28% of sponge WW. When looking at the different FA classes individually, some differences appear, as some groups have significantly different levels compared to the control levels (two-way t-test, $p \leq 0.05$). The concerned groups (two from the low exposure and four from the high exposure) are listed in table 6.

Table 6: Summary of groups that were significantly different to control levels (two-way t-test, p≤0,05).

Group	∑org.mat.	∑FA	∑SFA	∑MUFA	∑DUFA	∑PUFA
d1l		higher	higher			
d4l		higher	higher	higher		
d1h			higher	higher		
d2h			higher			
d8h		higher	higher	higher		
Rh		higher	higher	higher		lower

The numbers were normalized, and control sponges were compared to the sponges exposed to high doses og PAH (Figure 23). Some differences do appear, but only the differences in MUFA and PUFA are significant (two-way t-test, $p \leq 0.05$). Figure 23 also show the relative abundance of each group, with large amounts of SFA, DUFA and others (e.g. sterols), and less of MUFA. PUFA is almost absent.

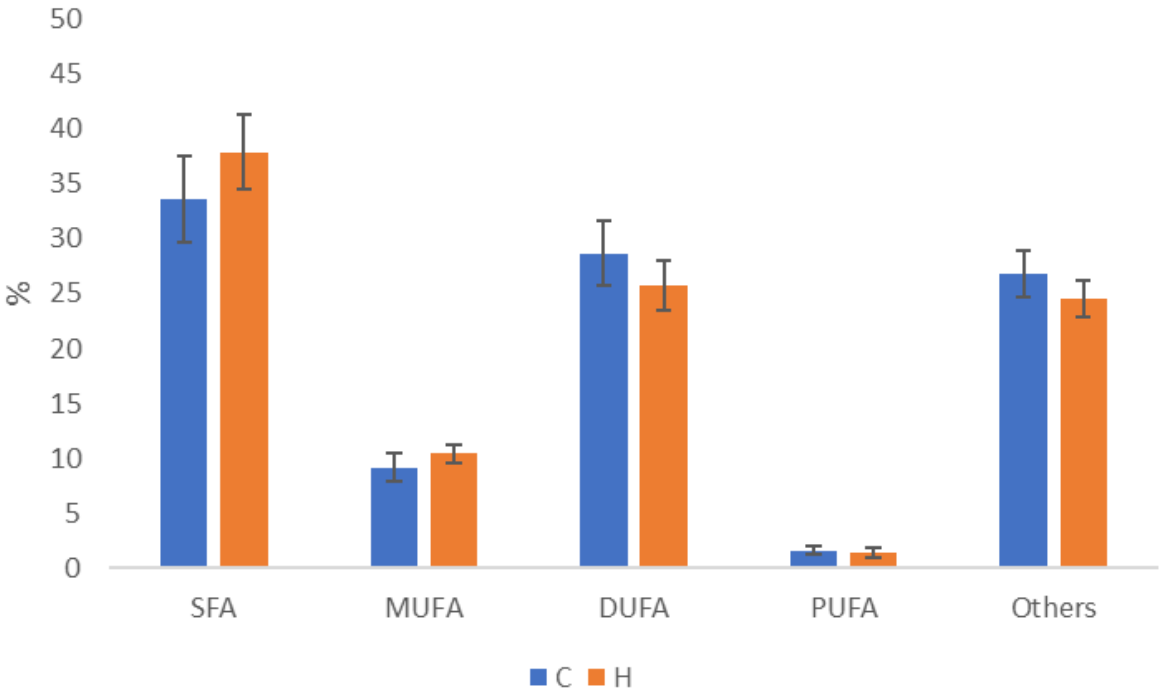

Figure 23: The average percentage of the different FA classes in control sponges (n=20) compared to sponges exposed to high doses of PAH (n=19). The amount of MUFA and PUFA are significantly different between the treatments.

A PCA was performed on the dataset to investigate whether the different treatments lead to differences for any specific FA, and if the increase of one FA lead to the decrease of another one. The FA in the dataset were normalized to 100% and divided by the mean value. By weighing the results by the mean value, the FA with the highest RSD get a higher importance in the PCA. The RSD caused by natural variation is assumed to be similar for all FA, and the variation caused by biological activity stands out. To decrease the noise only FA accounting for more than 1% of the total were included. The original PCA of >1% FA revealed three outliers, Br 19:0 (11Me), i-19:0 and 22:5 n-6, which was removed. The outlier had an RSD in the range of 50-141% and there was no systematic change with respect to the treatments. Especially Br 19:0 (11Me) was hard to integrate as it had poor resolution from the surrounding peaks. It was decided to exclude the mentioned FA rather than the affected objects as every group contained only 4 replicates. Normalization and standardization of the new data set was performed prior to a new PCA. The score plot of all samples sorted by the intensity of the treatment (control-high) is presented in figure 24. Each treatment consists of sponges from all sampling points (day 1, day 2, day 4, day 8 and after a 30-day recovery). Smaller score and loading plots presenting each day and each treatment are shown in Appendix D.

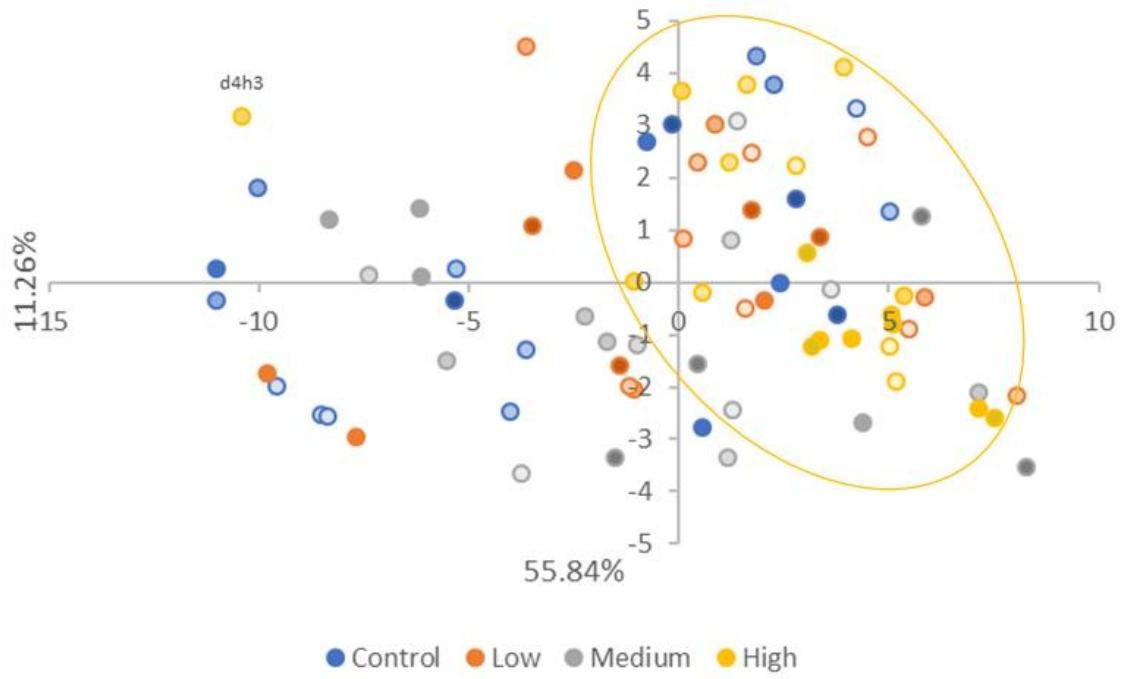

Figure 24: Score plot of all samples in the dataset sorted by the intensity of the oil exposure (control-high). Each group have a colour scale going from fair to strong, indicating the duration of the treatment from day 1 through recovery. The high group is circled, and a possible outlier, d4h3 from the high group is labelled.

Samples from the control and medium treatment are evenly distributed in the score plot. Except one outlier, the sponges exposed to the high dose of PAH are concentrated slightly further to the left compared to the others. The sponges exposed to the low concentration of PAH experience slight clustering, but to a smaller degree than the high ones. The individual days and treatments are giving similar loading plots, even at the control treatment (Appendix D).

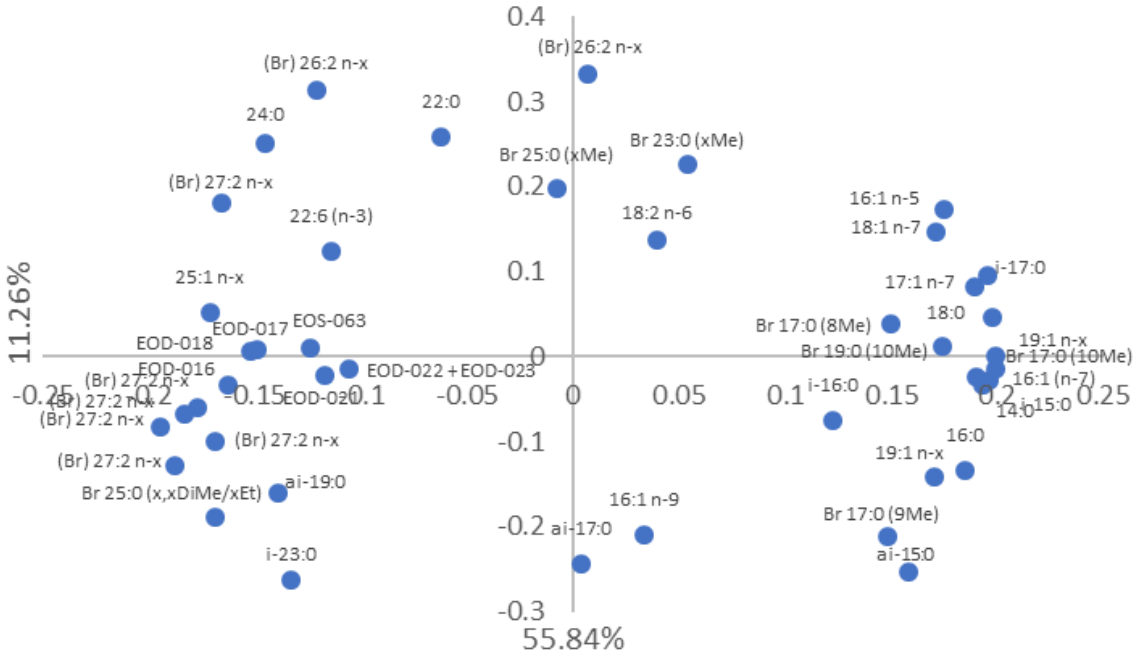

Figure 25: Loading plot of all >1% FA (except the three outliers Br 19:0 (11Me), i-19:0 and 22:5 n-6).

None of the FA in figure 25 stands out to affect the results in any direction. However, the shorter chained (>20C) SFA and MUFA are concentrated on the right, whereas the longer chained and less saturated FA are concentrated further to the left. Figure 26 presents a comparison of the FA in control sponges and sponges exposed to high concentration of PAH.

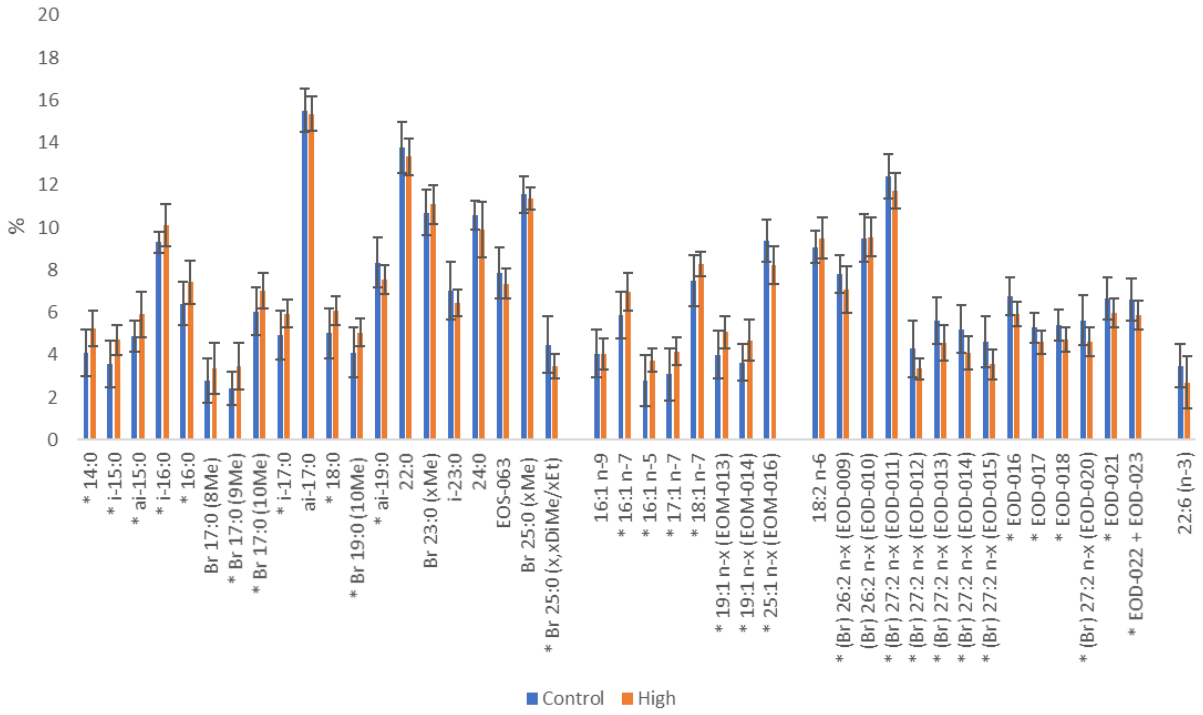

Figure 26: Box plot of the >1% FA contributing to the PCA analysis, comparing the control sponges (n=20) to the sponges exposed to the high concentration of PAH (n=19). FA that differ significantly between the treatments are marked with *.

Generally, the sponges exposed to the high concentration of PAH contain more short chain (<20C) FA and MUFA than the control sponges, and less long chain (>20C) FA and DUFA/PUFA. These differences are thoroughly presented in Appendix E.

4.6. Lipid classes and distribution of FA amongst lipid classes

Figure 27a) present the visualisation of a 1D TLC separation of lipid classes within *G. barretti*. Four different standards (Table 3) were also eluted on the same plate for comparison between the sample and the four standards. Figure 27b) presents the 1D TLC plated that were visualised using 2',7'-dichlorofluorescein solved in MeOH, scraped off and analysed with LC-MS (identification of lipid classes) and GC-FID (FAME present within lipid classes).

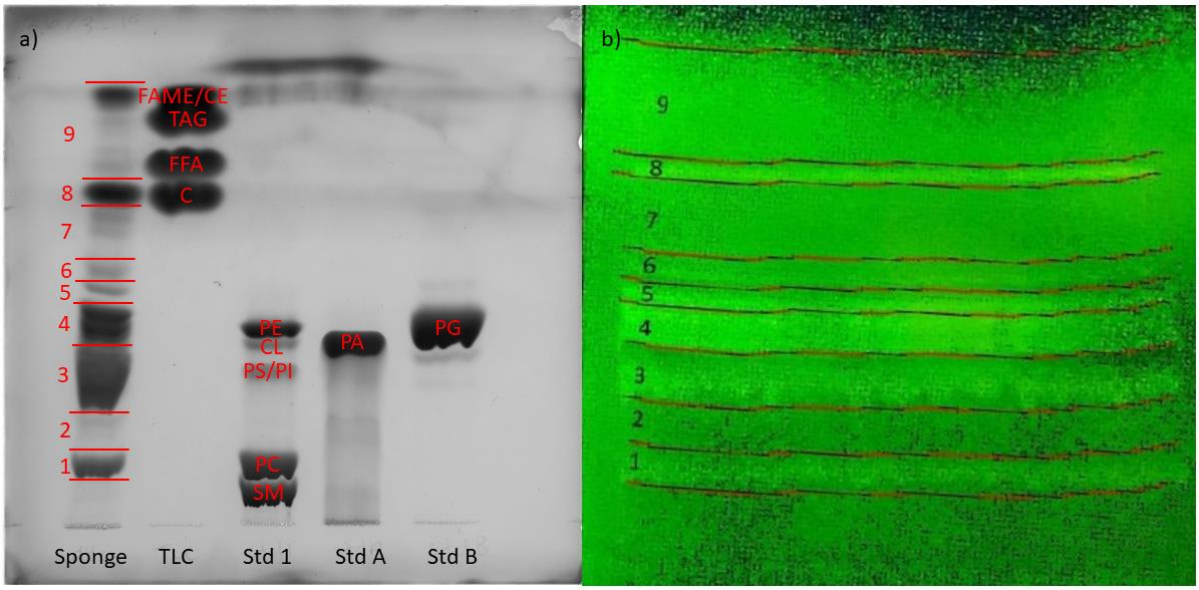

Figure 27: a) 1D TLC plate showing the separation of a control sponge extract, along with the elution of the contents of four different standards. b) 1D TLC plate showing the fractions that were scraped off for LC-MS/GC-FID analysis.

The results from the GC-FID analysis and the 1D TLC plate presented in figure 23a) are combined and presented in table 7. When summarised, the 9 fractions analysed for FA and sterols (GC-FID analyses) only accounted for 70,24% of the corresponding analysis on the total lipids. The numbers presented in column 3 are these numbers normalized to 100%. The numbers presented in column 5 are the % presence of each FA/sterol accounting for more than 2% of the total within each lipid class. Appendix F show the chromatogram of the total FA extract and the chromatogram of each fraction. Conclusions cannot be drawn from the results of the LC-MS analyses as there were to much noise from the staining agent, hence they are not presented.

Table 7: Lipid class and most abundant FA/sterols (>2%) in each fraction.

Fraction:	Lipid class:	Amount (%):	Most abundant FA:	Amount (%):
1	PC	6.90	18:2 n-6	18.32
			18:0	7.12
			EOU-005	5.18
			22:6 n-3	5.01
			18:1 n-7	4.62
			Br 19:0 (10Me)	3.33
			Br 17:0 (10Me)	3.20
			20:5 n-3	3.17
			17:1 n-7	3.11
			16:1 n-7	2.98
			ai-19:0	2.82
			16:0	2.07
2		0.95	16:0	19.49
			18:0	17.49
			EOU-036	8.00
			ai-19:0	5.65
			Br 15:0 (10Me)	3.93
			21:0	3.33
			20:5 n-3	3.07
			19:1 n-x (EOM-009)	2.05
3	PS/PI/PA/CL	14.93	Br 26:2 n-x (EOD-010)	9.15
			22:0	7.29
			i-23:0	7.03
			Br 27:2 n-x (EOD-013)	6.35
			25:1 n-x (EOM-016)	5.65
			24:0	4.67
			Br 26:2 n-x (EOD-009)	4.58
			Br 19:0 (10Me)	2.78
			Br 23:0 (xMe) (EOS-052)	2.75

			Br 27:2 n-x (EOD-014) Br 27:2 n-x (EOD-012) EOU-022 Br 27:2 n-x (EOD-015) EOS-063	2.73 2.54 2.54 2.37 2.21
4	PE/PA/PG/CL	17.33	Br 19:0 (11Me) Br 19:0 (10Me) Br 26:2 n-x (EOD-010) i-15:0 ai-15:0 Br 27:2 n-x (EOD-013) 18:0 16:1 n-7 Br 26:2 n-x (EOD-009) 16:0 Br 17:0 (10Me) 17:1 n-7 Br 27:2 n-x (EOD-014)	9.21 4.68 4.55 4.54 4.24 4.02 3.92 3.72 3.44 3.21 2.60 2.35 2.12
5		16.37	Br 27:2 n-x (EOD-013) EOX-010 EOX-011 16:0 16:1 n-7 EOX-013 Br 19:0 (10Me) Br 24:0 (17Me) Br 27:2 n-x (EOD-011) Br 17:0 (10Me) 17:1 n-7 19:1 n-x (EOM-013)	8.80 8.54 7.33 4.60 4.44 4.20 3.97 3.97 2.56 2.55 2.48 2.11
6		1.68	Br 19:0 (11Me) Br 19:0 (10 Me) 16:0 Br 17:0 (8Me) 18:0 ai-17:0 Br 15:0 (10Me) Br 17:0 (9Me) EOU-036 Br 17:0 (10Me) 19:1 n-x (EOM-014) i-17:0	19.25 11.88 8.15 6.79 6.16 3.48 3.31 2.74 2.65 2.64 2.52 2.24
7		2.76	ai-17:0 ai-19:0 Br 17:0 (10Me) 16:0 EOU-036 Br 19:0 (10Me) i-17:0 14:0 Br 17:0 (9Me) 20:5 n-3 Br 16:0 (8Me) Br 15:0 (10Me) Br 26:2 n-x (EOD-007) i-16:0	21.25 12.85 8.89 8.04 7.25 3.38 3.07 2.92 2.75 2.52 2.35 2.14 2.14 2.02
8	C	29.78	EOD-021 EOD-022+EOD-023 Sterol (EOX-17) EOD-018 EOD-017 EOU-027 Sterol (EOX-018) Sterol (EOX-016) EOU-028 EOU-023 Sterol (EOX-021) EOU-029 Br 26:2 n-x (EOD-009)	10.17 9.82 8.80 7.43 5.75 4.86 3.75 3.11 2.75 2.59 2.43 2.33 2.17
9	FAME/CE	9.39	ai-19:0 Br 25:0 (xMe) (EOS-059)	14.68 3.49

			Br 17:0 (10Me)	3.39
			12:0	3.04
			ai-17:0	2.90
			EOU-036	2.78
			Br 27:2 n-x (EOD-013)	2.69
			Br 19:0 (10Me)	2.59
			16:0	2.42
			Br 19:0 (11Me)	2.08
			18:0	2.08
			EOU-011	2.03

5. Discussion

5.1. Water samples

The nominal levels of PAH in the treatment water are levels one would expect in the surrounding waters after an accidental oil spill, and the high levels demonstrate levels higher than previously observed following accidental large-scale oil spills. PAH levels up to 100 µg/L were registered following the DWH blowout. However, most levels within the contaminated areas were in the range of 0.1-10 µg/L (Boehm et al., 2016). Most measurements following the Exxon Valdez accident were within the same range, with maximum levels of 42 µg/L (Boehm et al., 2007). The measured levels of PAH in the treatment water (Table 4) are shown to be very close to the nominal levels, hence the experiment has been performed with ecologically relevant levels of PAH. Most treatments had a constant concentration throughout the experiment. However, one group in the medium concentration (P2) had an outlier with 1506 ng/L at the start and 162 ng/L at the end. This can be seen in figure 15, as the average end concentrations are a bit lower than the average start concentrations. When looking at the body burden results, there are no obvious explanation for this. At day 1, the body burden is clearly higher than the other groups, and at day 2 it is clearly lower. But, at day 4 and 8 there are no significant difference between P2 and the other groups. If the system at some point did get clogged for the P2 exposure, one would expect the body burden significant lower at the last samplings (day 8, and maybe day 4 and 2, depending on when the clogging happened). One likely explanation would be that something went wrong during the sampling or work up of this sample.

5.2. PAH body burden

The results show a clear trend of PAH accumulation following the treatment. This is as expected, as sponges are filter feeders and have been proven to accumulate PAH in previous studies (Batista et al., 2013). Figure 17a) show how PAH is accumulated as dispersed oil droplets in the sponge tissue, and figure 17b) and c) shows how the accumulation of total PAH is both time and dose related for the medium and high concentrations, while not significantly elevated for the low concentration. The high and medium concentrations, typically present close to the locations of an accidental release of HC are accumulated (Boehm et al., 2007) (Boehm et al., 2016). However, the low concentration which is typically spread over larger areas and persists for a longer time does not accumulate. Figure 18 show that the PAH profile of the oil accumulated in *G. barretti* is getting more and more similar to the oil profile of the crude oil used in the experiment. Therefore, the accumulated PAH most certainly originate from the crude oil from the Troll field.

Results for both total PAH concentration and oil profile show large variation, especially in the higher concentrations. The correlation between the average number of oil droplets and the total PAH concentration (Figure 17 b) and c), and Figure 18) show that this must originate from the exposure and not from the work up, as both the trends and variation is similar for both. As the sponge explants are individual organisms, large variation in the results are expected. One hypothesis for this is that

sponge specimen are individuals that may accumulate PAH differently because of differences in structure. The average sponge contains 75,4 ± 3,0% water, 13,8 ± 3,0% ash and 11,0 ± 1,1% organic material, and the structure may vary a lot (Figure 28). Oil droplets may stick easier to sponges with a rougher structure on the cortex and/or inside. Sørensen et. al. has previously suggested that the stickiness of fish eggs may affect the oil droplet fouling on their exterior, and something similar might have happened here (Sorensen et al., 2017). Differences in canal/pore size may also affect the accumulation of oil droplets. A second hypothesis might be, that the bacterial culture in sponges vary (Figure 21) and may process PAH differently.

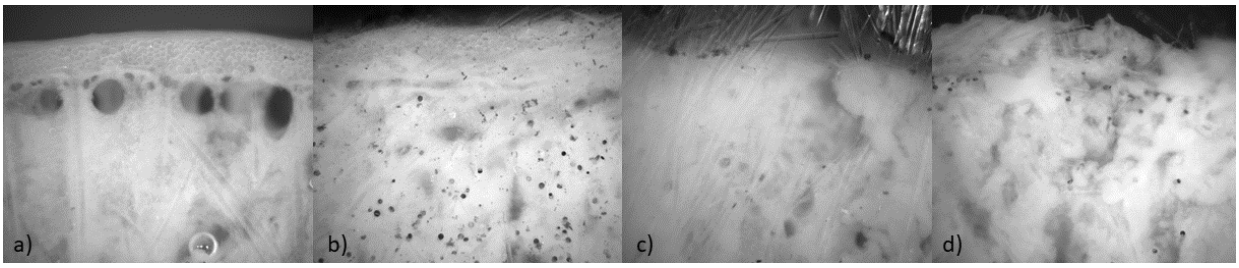

Figure 28: Example of structural differences in sponge specimen. Some sponges had a rather smooth internal structure and a smooth surface with a clear cortex (a). Moving to the right, (b) trough (d), the structure gets "stickier", both regarding the internal structure but also the cortex, as e.g. (c) has a lot of spicules on its cortex.

The variation seen in some of the groups are higher than one would expect. It is hard to believe that an RSD of up to 70 % of the total PAH concentration is caused by natural variation alone. Some single compounds/clusters, especially the ones present in small concentrations even presents an RSD of more than 100%. This may suggest that there are some outliers in the dataset. However, when looking at the data, it is hard to define any values as outliers. Typically, for the total PAH concentration, there are two high and two low values, or four values evenly distributed in the range high to low. Removing an outlier largely impact the results from a data set, especially when each group only have 3 to 4 replicates. As all samples have been treated equally during workup and analysis, it was decided to not remove any samples from the data set.

When looking at figure 16, the results from d8h stands out by breaking the trend of an increased PAH accumulation following the exposure time. Small amounts of oil degrading bacteria have been identified in *G. barretti* (Stevenne, 2018), but this should not only affect this one group.

During the extraction and SPE clean up, samples were not randomized but sorted in by increased oil exposure in order to avoid any accidental PAH transfer from high doses to low. Prior to homogenizing, the samples were put on watch glasses. 9 samples (8 samples and 1 blank or spike) were prepared in a time range of about 70-75 minutes. As water accounts for about 75% of this sponge's WW, some of it evaporated during this period. High exposure samples would lose more water before weighing than the low exposure samples. To correct this, the evaporation rate of four different sponge specimen of similar size as the samples were measured. Figure 29 shows the rate of evaporation of *G. barretti*. After 72 minutes the evaporation had caused a decrease of 26,2% of the original WW measured at time 0. The standard deviation is increasing with the time, and the variation may derive from e.g. different size of the samples, different amount of water originally in the sponge specimen or differences in the structure. Hence, the exact value of sponge WW for the PAH body burden is hard to recover.

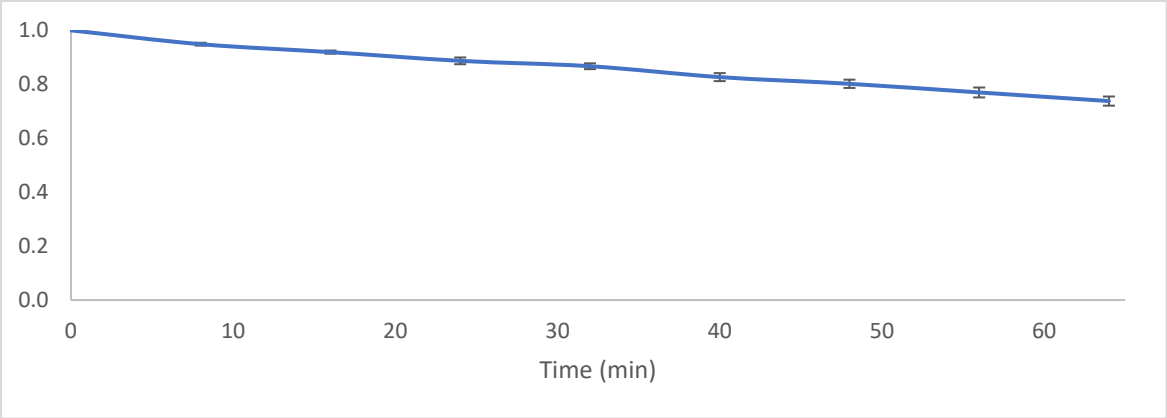

Figure 29: Average evaporation rate of H_2O from four different sponge specimen of *G. barretti*. The samples were of similar size as the samples that were measured for PAH body burden. Samples were weighed every 8th minute over a period of 72 minutes.

5.3. Physiological effects on the oil exposed sponges

Following the DWH blowout, the surrounding coral reefs up to 109 km from the spill site experienced severe effects to the exposure of a hydrocarbon and dispersant combination. 38-50% of the corals showed signs of damage after the accident, compared to the previously observed 4-9% (Beyer et al., 2016). A literature study summarizing effects on corals after both accidental spills and in laboratory studies. Conclusions were that the physical, chemical and biological differences were too big to make a general conclusion about the overall effects.

Throughout the experimental period, sponge *G. barretti* showed no signs of sub-lethal effects, and all effects during the oil exposure returned to control levels after a 30-day recovery. Stressed sponges have been afflicted by a disease-like syndrome leading to discoloration, tissue disintegration and fouling (Luter et al., 2017). No such visual signs of death or compromised health were observed during the experimental period. Other kinds of stress such as increased temperatures have demonstrated mass mortality in field observations on the NCS (Guihen et al., 2012). No significant effect on the sponges' respiration rates were detected due to high variation (Stevenne, 2018). When exposed to various stresses such as mine tailings and drill cuttings (Kutti et al., 2015) and thermal stress (Strand et al., 2017), *G. barretti* has shown both decreased and increased respiration rates. Control sponges showed a proportion of destabilised lysosomes (10.25 ± 1.68%) within the range that has previously been found in healthy sponges (Edge et al., 2016) (Strand et al., 2017). Even though the sponges exposed to the highest treatment presented a count of 23.24 ± 4.19% destabilised lysosomes on day 8 (Stevenne, 2018), G. barrette have displayed much larger proportions when exposed to thermal stress (Strand et al., 2017) and drilling muds (Edge et al., 2016). Also, the levels of destabilised lysosomes returned to control levels after a 30-day recovery (Stevenne, 2018), unlike the thermally stressed sponges, who presented a greater number of destabilised lysosomes even after 65 days of recovery (Strand et al., 2017). *G. barretti's* associated microbiome demonstrated stability across all treatments. Bacterial communities did show slight fluctuation but did not cluster into separate groups associated with treatment (Stevenne, 2018). Nor did the treatment correlate to the community richness. These results indicate that exposure to dispersed oil droplets did not drive clear changes in the structure of *G. barretti's* associated microbiome nor community richness.

G. barretti and its associated microbiome could be naturally exposed to hydrocarbons in the marine environment. The largest source of hydrocarbons in marine ecosystems is natural seeps (Transportation Research Board and National Research Council, 2003).

Numerous oil and gas fields has been identified in the Northern Atlantic, and mapping of clustered oil-slick data indicates the possibility of natural oil seeps at several locations on the NCS (Vis, 2017). A comparison of the distribution of observed sponge grounds and the locations of possible natural oil seeps suggests a vicinity of sponge grounds to natural oil seeps (Figure 30) similar to corals (Cordes et al., 2016). The dominating deep-sea coral in Norwegian waters has been observed to colonize around offshore petroleum platforms, indicating it to be tolerant to hydrocarbons (Gass and Roberts, 2006). As small amounts of oil degrading bacteria have been observed in *G. barretti (*Stevenne*,* 2018*)*, it suggests that the sponge and its associated microbiome might have adapted to a natural exposure to hydrocarbons originating from the sea floor. Other deep-sea sponges have been identified to fuel on methane from natural seeps (Rubin-Blum et al., 2019).

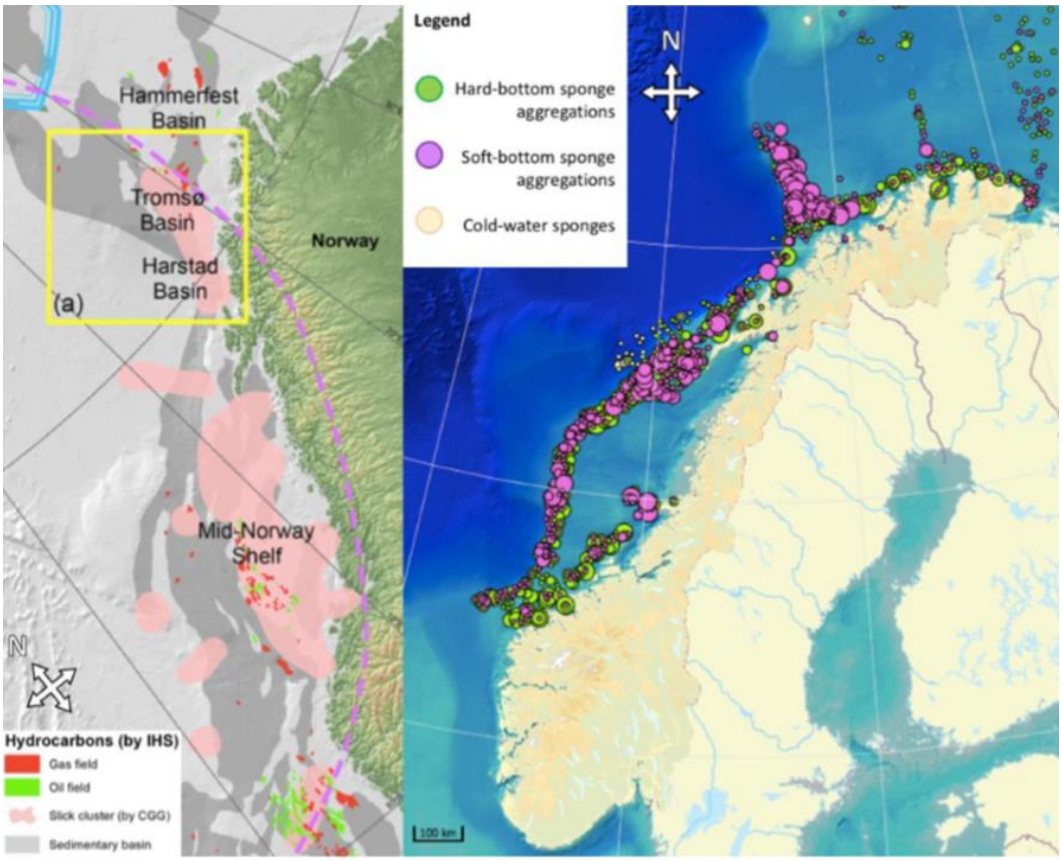

Figure 30: Distribution of oil sources and of sponge aggregations along the NCS. Left: Distribution of oil and gas fields and mapping of clustered oil-slick data(pink) which indicate possible active natural oil seeps. The map is tilted so the north-east is on the top (see compass for orientation). Right – Distribution of observed sponge grounds along the Mid- and North-Norwegian Continental Shelf. (Stevenne, 2018).

However, the duration of the exposure and/or the oil doses might not have been sufficient to induce strong physiological effects on the sponge. Several weeks of exposure to oil contaminated sediments have previously been necessary to induce significant changes in bacterial communities. Also, much higher concentrations were observed a few hundred meters above the sea floor following the DWH blowout (Diercks et al., 2010), and oil sedimentation on corals have caused serious damage (Beyer et al., 2016). Future prospects might include mesocosm studies on the sponge's responses to long term exposure and/or to higher concentration of oil.

5.4. Method development and FA identification

177 different species including 142 different FA were identified using a non-polar DB-5 column with a 1°C/min temperature programme. As the sample showed such a complexity, the method could be

further optimized for better separation by using a lower temperature rate (Mjos and Waktola, 2015). Some of the large clusters containing branched 19:0 and 26:2/27:2 FA could benefit from better separation, and better separation would probably make it possible to identify several additional compounds, as some of these peaks probably contain more than one compound. Of course, this compromises the amount of time used on each sample.

Sponges has previously been proved to be a rich source of unusual FA, or to have unusual amounts of common FA (Berge and Barnathan, 2005). A vast amount of the 142 FA in table 4 is odd-numbered, branched or very long (>24C), none of which is designated as "normal". However, it was no surprise to find these kinds of FA in *G. barretti*. Typical bacterial biomarkers include both odd-numbered and iso/ante-iso FA (Dalsgaard et al., 2003), and large amounts of branched FA has previously been found in sponges (Berge and Barnathan, 2005). This includes several of the branched FA observed in *G. barretti* such as 16:0, 10Me and 18:0 10Me (Berge and Barnathan, 2005), some 3Me FA and di-branched FA (Nechev et al., 2002). Another study has also showed that *G. barretti* contain large amounts of complex isomeric mixtures of mid-chain branched FA in the C15-C25 range, along with the VLC-FA 26:2 and 27:2. These VLC-FA with double bonds in position 5 and 9 are classically considered unique for Demospongiae (Thiel et al., 2002), and is biosynthesized within the sponge from precursors e.g. 14:0, 16:0 and 18:0 (Hahn et al., 1988). Similar results were discovered for other sponges (Thiel et al., 2002). The presence of VLC-FA and saturated FA is also expected as sponges are deep-sea organisms and hydrostatic pressure is known to decrease membrane fluidity by increased proportions of long chained FA and saturated FA (Montagne et al., 2014).

Figure 19 shows the linear relationship within the branching point groups, and one can clearly see that the unbranched FA, iso and ante-iso FA are in different groups. One value in the unbranched group stands out, the 19:0 FA. This is a non-existing natural FA that has been used as internal standard. It is added in excessively, and the strange value is caused by chromatographic drifting, as this peak is much larger than the others. In the iso group, i-12:0 stands out. When looking at figure 19, it is natural to think that it should rather belong to the ante-iso group. However, it is provisional identified as i-12:0 based on the fragmentation in the MS spectra (Appendix D). 8 branched FA with unknown position of the branching point is included in the figure. The unknown branched 10:0, 18:0 and 19:0 FA are not mono-methyl branched FA, as they do not fit to any of the groups, nor to any of Kubinéc et. al.'s ECL values (Kubinec et al., 2011). The unknown branched 15:0 FA might be the result of an accidental peak split, as it has very similar values to 15:0, 9Me (position 5), but may also be in a group that is not represented in the figure. The unknown branched 23:0, 24:0 and 25:0 FA is probably possible to place in some of the existing groups, but since the FCL values for FA with branching in position 3-12 is so similar, it is not enough for certain identification.

Further work should include a certain determination of branching point/double bonds of the partly identified FA. Literature suggests that some of the VLC-FA have double bonds at the Δ5,9 position (position 5 and 9 counted from the carboxyl end) (Thiel et al., 2002), but others must be present too, as several peaks have appeaser in the chromatogram. Identification of sterols and the unknown species assumed to be unsaturated ether should also be performed.

5.5. Total FA and change in FA composition

Fluidity is a property of membranes that is related to the ability of molecules to move inside the membranes and is typically adversely affected by environmental changes (Siliakus et al., 2017). To maintain physiological homeostasis when exposed to changes, membrane fluidity is secured by a mechanism called "homeoviscous adaption" based on changing the chemical composition of the membrane. These modifications often cause shifts in ratios of lipid types and/or their FA moieties,

rather than complete replacement of certain species (Siliakus et al., 2017). Generally, shorter FA and higher degree of unsaturation increases membrane fluidity and vice versa.

Figure 24 suggests that there are some differences between the FA in sponges exposed to high concentrations of oil compared to the rest of the treatments, as the high treatment presents a slight clustering in contrast to the others. However, this cluster is completely overlapped by samples from the other treatments and certain conclusions cannot be drawn that there are differences between the groups based on this. None of the FA stand out to affect the result in any particular direction, but figure 25 shows that there might a shift in ratio of FA towards shorter and less saturated FA. This is supported by this section's remaining figures. The statistical basis (n=4/group) to conclude whether the effects persists after a 30-day recovery is too thin.

The change in FA composition towards shorter chained and less saturated FA suggest that the sponge and its associated microbiome might have decreased the fluidity of their cell membrane. Some of the underlying mechanisms might be explained by Hahn et.al. (1998) as a "reversed" synthesis of demospongic acids (Hahn et al., 1988). Decreased saturation has previously been experienced when exposing bacteria to PAHs (Certik et al., 2003). Bacteria have been shown to survive despite being exposed to toxic aromatic compounds (including PAHs) by modifying their FA composition, hence changing their membrane fluidity (Sikkema et al., 1995).

5.6. Lipid classes and distribution of FA amongst lipid classes

Figure 27 reveals that a large share of the total lipids of *G. barretti* are phospholipids, and the FA in the PL fractions (fraction 1-4) accounts for about 40% of the total FA. The PL fraction of sponges vary a lot amongst sponge species, but these numbers correspond with the total PL fraction previously found for another sponge of the *Geodia* family (Genin et al., 2008). From the total PL of this sponge, PC, PI and PG constitutes 19.2%, 52.9% ang 27.9% respectively. PC accounts for 17.2% of the FA in the PL fractions. One of the dominating FA in this fraction is 22:6 n-3, has previously been observed for other sponges (Dasgupta et al., 1986). The remaining fractions may contain PI and PG, but with no supplementary results it is hard to decide whether other PL classes such as PS, CL, PE and PA are present, and to what degree. PE has been found to usually be predominant in a range of sponge species (Genin et al., 2008), but at the same time the presence of occurrence of bacteria are often accompanied by huge levels of PI and PG (Hahn et al., 1988).The PL fractions of *G. barretti* contain several branched FA and 26:2/27:2 FA, supporting the presence of bacteria (Genin et al., 2008) (Hahn et al., 1988). The 26:2/27:2 FA are concentrated in fraction 3 and 4, which is similar to previous findings in the PE, PG and PS fraction of sponge *P. psila* (Dasgupta et al., 1986).

A large proportion of the lipids of *G. barretti* are also neutral lipids, including sterols (fraction 8 in figure 27). Table 7 confirms that fraction 8 contain sterols, and that this fraction accounts for about 30% of the total lipids. Previously, sponges of the *Cinachyrella* family has demonstrated sterol contents of 17-27% (Barnathan et al., 2003). The number of sterols in sponges vary greatly amongst the different species but are generally limited to between seven and ten (Bergquist et al., 1986). Fewer sterols have also been observed, suggesting that they might have unique biological roles (Djerassi, 1981). Almost all sponge sterols originate from its diet and may be transformed in order to fit the cell membrane requirements of the sponge (De Rosa et al., 2006).

Figure 27 show that fraction 9 must contain FAME and/or sterol esters (CE), and table 7 reveals that this fraction accounts for more than 9% of the total FA. These results are unusual, as FAME in large proportions are not common in cell membranes. However, no sterols are dominating this fraction, so it is very unlikely that this fraction is dominated by CE.

LC-MS analyses of the did not give any results that could give supplemental information about the lipid classes, and results are not presented in this thesis. A prospect for further work would be to improve the method for lipid class work-up. This could include 1) better separation by TLC, 2) other ways of fractionating the total lipid extract to avoid residues of 2',7'-dichlorofluorescein in the fraction and 3) develop a better LC-MS method. It has previously been demonstrated that polar head groups can play a significant role in the maintenance of membrane fluidity (Siliakus et al., 2017). Therefore, further work could also include investigating if oil treatment cause effects on the lipid class distribution. Fraction 5 in figure 27 is accounting for more than 16% of the total FA, but none of the lipid classes from the standards are corresponding to the retention of this fraction. The determination of this lipid class may also be an object for further investigation.

6. Conclusion

Sponges are key organisms in benthic deep-sea systems and support vital processes such as contributing to benthic-pelagic coupling and providing habitat for other deep-sea organisms. Understanding how hydrocarbon exposure impact their functioning will give useful information for managing risks associated with oil and gas exploration.

This co-operational mesocosm study with master student Chloé Stévenne, where the deep-sea sponge *Geodia barretti* was exposed to three ecologically relevant doses of PAH reveal the first evidence that *G. barretti* and its associated microbiome is resilient to a simulated short-term oil exposure. Results provide evidence that the deep-sea sponge does accumulate PAH, but the studies of physiological responses support the conclusion that the sponge does not show strong sub-lethal responses to oil treatment. The changes in lysosomal membrane destabilization and increased variation in respiration rates suggest that the sponges experienced slight changes in their functioning, but as the levels returned to control levels after a 30-day recovery these effects did not persist once the exposure ended. The balance of fatty acids altered slightly towards shorter and less saturated FA, suggesting that cells have decreased their membrane fluidity as a response to oil exposure. Further work could include exposure to more extreme concentrations of PAH and/or studying the effects of long-term exposure.

During the work on this thesis, 104 FA were fully or partly identified along with several unidentified sterols and unknowns. A vast amount of them were branched, saturated FA and VLC-FA known to be unique for sponges and bacteria. *G. barretti* were proved to have a similar lipid class structure as other sponges. Further work could include improving the chromatographic separation and identification of the unknowns and the partly identified FA. It should also include a further look at the lipid classes.

References

The cell [Online]. Spain: Faculcy of Biology, University of Vigo. Available: https://mmegias.webs.uvigo.es/02-english/5-celulas/3-propiedades1.php [Accessed May 14 2019].

ACHTEN, C. & ANDERSSON, J. T. 2015. Overview of Polycyclic Aromatic Compounds (PAC). *Polycyclic Aromatic Compounds,* 35**,** 177-186.

ADAMS, J., BORNSTEIN, J. M., MUNNO, K., HOLLEBONE, B., KING, T., BROWN, R. S. & HODSON, P. V. 2014. Identification of compounds in heavy fuel oil that are chronically toxic to rainbow trout embryos by effects-driven chemical fractionation. *Environmental Toxicology and Chemistry,* 33**,** 825-835.

AKOH, C. C. M., D. B. 2002. *Food Lipids - Chemistry, Nutrition, and Biotechnology,* New York, Marcel Dekker Inc.

ANDERSON, J. L. B., A.; ESTÉVEZ, V. P.; STALCUP, A. M. 2015. *Analytical Separation Science*, Wiley.

APON, J. M. B. & NICOLAIDES, N. 1975. DETERMINATION OF POSITION ISOMERS OF METHYL BRANCHED FATTY-ACID METHYL-ESTERS BY CAPILLARY GC-MS. *Journal of Chromatographic Science,* 13**,** 467-473.

APPEA. 2019. Available: https://www.appea.com.au/oil-gas-explained/production/uses-of-oil/ [Accessed April 11 2019].

AYDIN, I. & GOKOGLU, N. 2014. Effects of temperature and time of freezing on lipid oxidation in anchovy (Engraulis encrasicholus) during frozen storage. *European Journal of Lipid Science and Technology,* 116**,** 996-1001.

BARNATHAN, G., GENIN, E., VELOSAOTSY, N. E., KORNPROBST, J. M., AL-LIHAIBI, S., AL-SOFYANI, A. & NONGONIERMA, R. 2003. Phospholipid fatty acids and sterols of two Cinachyrella sponges from the Saudi Arabian Red Sea: comparison with Cinachyrella species from other origins. *Comparative Biochemistry and Physiology B-Biochemistry & Molecular Biology,* 135**,** 297-308.

BATISTA, D., TELLINI, K., NUDI, A. H., MASSONE, T. P., SCOFIELD, A. D. & WAGENER, A. D. R. 2013. Marine sponges as bioindicators of oil and combustion derived PAH in coastal waters. *Marine Environmental Research,* 92**,** 234-243.

BELL, J. J. & CARBALLO, J. L. 2008. Patterns of sponge biodiversity and abundance across different biogeographic regions. *Marine Biology,* 155**,** 563-570.

BELL, J. J., MCGRATH, E., BIGGERSTAFF, A., BATES, T., CARDENAS, C. A. & BENNETT, H. 2015. Global conservation status of sponges. *Conservation Biology,* 29**,** 42-53.

BENNEAR, L. S. 2015. Offshore Oil and Gas Drilling: A Review of Regulatory Regimes in the United States, United Kingdom, and Norway. *Review of Environmental Economics and Policy,* 9**,** 2-22.

BERGE, J. P. & BARNATHAN, G. 2005. Fatty acids from lipids of marine organisms: Molecular biodiversity, roles as biomarkers, biologically active compounds, and economical aspects. *In:* GAL, Y. L. & ULBER, R. (eds.) *Marine Biotechnology I.*

BERGQUIST, P. R., LAVIS, A. & CAMBIE, R. C. 1986. Sterol composition and classification of the porifera. *Biochemical Systematics and Ecology,* 14**,** 105-112.

BEYER, J., TRANNUM, H. C., BAKKE, T., HODSON, P. V. & COLLIER, T. K. 2016. Environmental effects of the Deepwater Horizon oil spill: A review. *Marine Pollution Bulletin,* 110**,** 28-51.

BLANCHARD, A., HAUGE, K. H., ANDERSEN, G., FOSSA, J. H., GROSVIK, B. E., HANDEGARD, N. O., KAISER, M., MEIER, S., OLSEN, E. & VIKEBO, F. 2014. Harmful routines? Uncertainty in science and conflicting views on routine petroleum operations in Norway. *Marine Policy,* 43**,** 313-320.

BLANCHET, C., LUCAS, M., JULIEN, P., MORIN, R., GINGRAS, S. & DEWAILLY, E. 2005. Fatty acid composition of wild and farmed Atlantic salmon (Salmo salar) and rainbow trout (Oncorhynchus mykiss). *Lipids,* 40**,** 529-531.

BOEHM, P. D., MURRAY, K. J. & COOK, L. L. 2016. Distribution and Attenuation of Polycyclic Aromatic Hydrocarbons in Gulf of Mexico Seawater from the Deepwater Horizon Oil Accident. *Environmental Science & Technology,* 50**,** 584-592.

BOEHM, P. D., NEFF, J. M. & PAGE, D. S. 2007. Assessment of polycyclic aromatic hydrocarbon exposure in the waters of Prince William Sound after the Exxon Valdez oil spill: 1989-2005. *Marine Pollution Bulletin,* 54**,** 339-356.

BOND, C. 1992. CONTINUOUS CELL MOVEMENTS REARRANGE ANATOMICAL STRUCTURES IN INTACT SPONGES. *Journal of Experimental Zoology,* 263**,** 284-302.

BRAITHWAITE, A. S., F. J. 1996. *Chromatographic methods,* Suffolk, Chapman & Hall.

BRAUNER, A. B., H.; BOLAND, W. 1982. Studies in chemical ionization mass spectrometry. *Organic Mass Spectrometry.*

CARBALLO, J. L. & BELL, J. 2017. Climate Change and Sponges: An Introduction.

CARDENAS, P., RAPP, H. T., KLITGAARD, A. B., BEST, M., THOLLESSON, M. & TENDAL, O. S. 2013. Taxonomy, biogeography and DNA barcodes of Geodia species (Porifera, Demospongiae, Tetractinellida) in the Atlantic boreo-arctic region. *Zoological Journal of the Linnean Society,* 169**,** 251-311.

CARLS, M. G., HOLLAND, L., LARSEN, M., COLLIER, T. K., SCHOLZ, N. L. & INCARDONA, J. P. 2008. Fish embryos are damaged by dissolved PAHs, not oil particles. *Aquatic Toxicology,* 88**,** 121-127.

CERTIK, M., DERCOVA, K., SEJAKOVA, Z., FINDOVA, M. & JAKUBIK, T. 2003. Effect of polyaromatic hydrocarbons (PAHs) on the membrane lipids of bacterial cell. *Biologia,* 58**,** 1111-1117.

CHRISTIE, W. W. 2019. *The Lipid Web* [Online]. Available: http://www.lipidhome.co.uk/ms/methylesters.htm [Accessed April 16 2019].

CHROMBOX. 2019. *Chrombox* [Online]. Available: https://www.chrombox.org/data/fame/register.html [Accessed April 25 2019].

OSPAR COMMISSION. 2010. Background Document for Deep-sea sponge aggregations. OSPAR Commission.

CORDES, E. E., AUSCAVITCH, S., BAUMS, I. B., FISHER, C. R., GIRARD, F., GOMEZ, C., MCCLAIN-COUNTS, J., MENDLOVITZ, H. P., MILES, SMITH, S., VOHSEN, S. & WEINHEIMER, A. 2016. ECOGIG: Oil Spill Effects on Deep-Sea Corals Through the Lenses of Natural Hydrocarbon Seeps and Long Time Series. *Oceanography,* 29**,** 28-29.

TRANSPORTATION RESEARCH BOARD AND NATIONAL RESEARCH COUNCIL. 2003. Oil in the Sea III: Inputs, Fates and Effects. Washington DC: Transportation Research Board and National Research Council.

DALSGAARD, J., ST JOHN, M., KATTNER, G., MULLER-NAVARRA, D. & HAGEN, W. 2003. Fatty acid trophic markers in the pelagic marine environment. *In:* SOUTHWARDS, A. J., TYLER, P. A., YOUNG, C. M. & FUIMAN, L. A. (eds.) *Advances in Marine Biology, Vol 46.*

DASGUPTA, A., AYANOGLU, E., WEGMANNSZENTE, A., TOMER, K. B. & DJERASSI, C. 1986. PHOSPHOLIPID STUDIES OF MARINE ORGANISMS .12. MASS-SPECTRAL BEHAVIOR AND HPLC OF SOME UNUSUAL MOLECULAR PHOSPHOLIPID SPECIES. *Chemistry and Physics of Lipids,* 41**,** 335-347.

DE HOFFMAN, E. S., V 2007. *Mass Spectrometry - Principles and Applications* Wiley.

DE ROSA, S., SEIZOVA, K., KAMENARSKA, Z., PETROVA, A., IODICE, C., STEFANOV, K. & POPOV, S. 2006. Sterol and lipid composition of three Adriatic Sea sponges. *Zeitschrift Fur Naturforschung C-a Journal of Biosciences,* 61**,** 129-134.

DENICH, T. J., BEAUDETTE, L. A., LEE, H. & TREVORS, J. T. 2003. Effect of selected environmental and physico-chemical factors on bacterial cytoplasmic membranes. *Journal of Microbiological Methods,* 52**,** 149-182.

DIERCKS, A. R., HIGHSMITH, R. C., ASPER, V. L., JOUNG, D. J., ZHOU, Z. Z., GUO, L. D., SHILLER, A. M., JOYE, S. B., TESKE, A. P., GUINASSO, N., WADE, T. L. & LOHRENZ, S. E. 2010. Characterization of subsurface polycyclic aromatic hydrocarbons at the Deepwater Horizon site. *Geophysical Research Letters,* 37.

NORWEGIAN PETROLEUM DIRECTORATE. 2019. norskpetroleum.no. Available: https://www.norskpetroleum.no/en/exploration/licensing-position-for-the-norwegian-continental-shelf/ [Accessed April 11 2019].
DJERASSI, C. 1981. RECENT STUDIES IN THE MARINE STEROL FIELD. *Pure and Applied Chemistry,* 53**,** 873-890.
EDGE, K. J., JOHNSTON, E. L., DAFFORN, K. A., SIMPSON, S. L., KUTTI, T. & BANNISTER, R. J. 2016. Sub-lethal effects of water-based drilling muds on the deep-water sponge Geodia barretti. *Environmental Pollution,* 212**,** 525-534.
EIA. 2019. Available: https://www.eia.gov/beta/international/ [Accessed April 11 2019].
MINISTRY OF PETROLEUM AND ENERGY. 2019. Government.no. Available: https://www.regjeringen.no/no/tema/energi/olje-og-gass/id1003/ [Accessed April 11 2019].
ETTRE, L. S. 1993. NOMENCLATURE FOR CHROMATOGRAPHY. *Pure and Applied Chemistry,* 65**,** 819-872.
FANG, J. K. H., ROOKS, C. A., KROGNESS, C. M., KUTTI, T., HOFFMANN, F. & BANNISTER, R. J. 2018. Impact of particulate sediment, bentonite and barite (oil-drilling waste) on net fluxes of oxygen and nitrogen in Arctic-boreal sponges. *Environmental Pollution,* 238**,** 948-958.
FISHER, C. R., MONTAGNA, P. A. & SUTTON, T. T. 2016. How Did the Deepwater Horizon Oil Spill Impact Deep-Sea Ecosystems? *Oceanography,* 29**,** 182-195.
FOLCH, J., LEES, M. & STANLEY, G. H. S. 1957. A SIMPLE METHOD FOR THE ISOLATION AND PURIFICATION OF TOTAL LIPIDES FROM ANIMAL TISSUES. *Journal of Biological Chemistry,* 226**,** 497-509.
FORSGREN, E. C.-D., S.; FAUCHALD, P.; JÄRNEGREN, J.; NÆSJE, T. F. 2009. Norwegian marine ecosystems - are northern ones more vulnerable to pollution from oil than southern ones? Trondheim: NINA.
GASS, S. E. & ROBERTS, J. M. 2006. The occurrence of the cold-water coral Lophelia pertusa (Scleractinia) on oil and gas platforms in the North Sea: Colony growth, recruitment and environmental controls on distribution. *Marine Pollution Bulletin,* 52**,** 549-559.
GENIN, E., WIELGOSZ-COLLIN, G., NJINKOUE, J. M., VELOSAOTSY, N. E., KORNPROBST, J. M., GOUYGOU, J. P., VACELET, J. & BARNATHAN, G. 2008. New trends in phospholipid class composition of marine sponges. *Comparative Biochemistry and Physiology B-Biochemistry & Molecular Biology,* 150**,** 427-431.
GONZALEZ-DONCEL, M., GONZALEZ, L., FERNANDEZ-TORIJA, C., NAVAS, J. M. & TARAZONA, J. V. 2008. Toxic effects of an oil spill on fish early life stages may not be exclusively associated to PAHs: Studies with Prestige oil and medaka (Oryzias latipes). *Aquatic Toxicology,* 87**,** 280-288.
GUIHEN, D., WHITE, M. & LUNDÄLV, T. 2012. Temperature shocks and ecological implications at a cold-water coral reef. *Marine Biodiversity Records,* 5**,** e68.
HAHN, S., STOILOV, I. L., HA, T. B. T., RAEDERSTORFF, D., DOSS, G. A., LI, H. T. & DJERASSI, C. 1988. BIOSYNTHETIC-STUDIES OF MARINE LIPIDS .17. THE COURSE OF CHAIN ELONGATION AND DESATURATION IN LONG-CHAIN FATTY-ACIDS OF MARINE SPONGES. *Journal of the American Chemical Society,* 110**,** 8117-8124.
HALLGREN, B., RYHAGE, R. & STENHAGEN, E. 1959. THE MASS SPECTRA OF METHYL OLEATE, METHYL LINOLEATE, AND METHYL LINOLENATE. *Acta Chemica Scandinavica,* 13**,** 845-847.
HANSEN, B. H., ALTIN, D., OLSEN, A. J. & NORDTUG, T. 2012. Acute toxicity of naturally and chemically dispersed oil on the filter-feeding copepod Calanus finmarchicus. *Ecotoxicology and Environmental Safety,* 86**,** 38-46.
HARRIS, D. C. 2010. Introduction to Analytical Separations. *Quantitative Chemical Analysis.* Eigth Edition ed. New York: W. H. Freeman and Company.
HODSON, P. V. 2017. The Toxicity to Fish Embryos of PAH in Crude and Refined Oils. *Archives of Environmental Contamination and Toxicology,* 73**,** 12-18.
IUPAC 1993. Nomenclature for chromatography. *Pure Applied Chemistry***,** 819.

KOVATS, E. 1958. GAS-CHROMATOGRAPHISCHE CHARAKTERISIERUNG ORGANISCHER VERBINDUNGEN .1. RETENTIONSINDICES ALIPHATISCHER HALOGENIDE, ALKOHOLE, ALDEHYDE UND KETONE. *Helvetica Chimica Acta,* 41**,** 1915-1932.

KUBINEC, R., BLASKO, J., GOROVA, R., ADDOVA, G., OSTROVSKY, I., AMANN, A. & SOJAK, L. 2011. Equivalent chain lengths of all C4-C23 saturated monomethyl branched fatty acid methyl esters on methylsilicone OV-1 stationary phase. *Journal of Chromatography A,* 1218**,** 1767-1774.

KUTTI, T., BANNISTER, R. J. & FOSSA, J. H. 2013. Community structure and ecological function of deep-water sponge grounds in the Traenadypet MPA-Northern Norwegian continental shelf. *Continental Shelf Research,* 69**,** 21-30.

KUTTI, T., BANNISTER, R. J., FOSSA, J. H., KROGNESS, C. M., TJENSVOLL, I. & SOVIK, G. 2015. Metabolic responses of the deep-water sponge Geodia barretti to suspended bottom sediment, simulated mine tailings and drill cuttings. *Journal of Experimental Marine Biology and Ecology,* 473**,** 64-72.

LUDEMAN, D. A., REIDENBACH, M. A. & LEYS, S. P. 2017. The energetic cost of filtration by demosponges and their behavioural response to ambient currents (vol 220, pg 995, 2017). *Journal of Experimental Biology,* 220**,** 4743-4744.

LUTER, H. M., BANNISTER, R. J., WHALAN, S., KUTTI, T., PINEDA, M. C. & WEBSTER, N. S. 2017. Microbiome analysis of a disease affecting the deep-sea sponge Geodia barretti. *Fems Microbiology Ecology,* 93.

MARTÍNEZ-GÓMEZ, C. B., J.; LOWE, D. 2015. Lysosomal membrane stability in mussels. Copenhagen: ICES.

MEIER, S., MJOS, S. A., JOENSEN, H. & GRAHL-NIELSEN, O. 2006. Validation of a one-step extraction/methylation method for determination of fatty acids and cholesterol in marine tissues. *Journal of Chromatography A,* 1104**,** 291-298.

MILLER, J. M. 2005. Gas Chromatography. *Chromatography, Concepts and Contrasts* Hoboken, New Jersey: John Wiley & Sons, Inc.

MJOS, S. A. 2006. *Interpretation og chromatographic and mass spectrometric data from analyses of fatty acid methyl esters.* PhD PhD, University of Bergen.

MJOS, S. A. & GRAHL-NIELSEN, O. 2006. Prediction of gas chromatographic retention of polyunsaturated fatty acid methyl esters. *Journal of Chromatography A,* 1110**,** 171-180.

MJOS, S. A. & WAKTOLA, H. D. 2015. Optimizing the relationship between chromatographic efficiency and retention times in temperature-programmed gas chromatography. *Journal of Separation Science,* 38**,** 3014-3027.

MONTAGNE, K., UCHIYAMA, H., FURUKAWA, K. S. & USHIDA, T. 2014. Hydrostatic pressure decreases membrane fluidity and lipid desaturase expression in chondrocyte progenitor cells. *Journal of Biomechanics,* 47**,** 354-359.

MUEHLENBACHS, L., COHEN, M. A. & GERARDEN, T. 2013. The impact of water depth on safety and environmental performance in offshore oil and gas production. *Energy Policy,* 55**,** 699-705.

MURAWSKI, S. A., FLEEGER, J. W., PATTERSON, W. F., HU, C. M., DALY, K., ROMERO, I. & TORO-FARMER, G. A. 2016. How Did the Deepwater Horizon Oil Spill Affect Coastal and Continental Shelf Ecosystems of the Gulf of Mexico? *Oceanography,* 29**,** 160-173.

MURPHY, D. B. 2001. Fluorescence Microscopy. *Fundamentals of Light Microscopy and Electron Imaging.* Wiley-Liss, Inc.

NECHEV, J., CHRISTIE, W. W., ROBAINA, R., IVANOVA, A., POPOV, S. & STEFANOV, K. 2002. Chemical composition of the sponge Chondrosia reniformis from the Canary Islands. *Hydrobiologia,* 489**,** 91-98.

NOAA. 2019. Available: https://oceanservice.noaa.gov/facts/light_travel.html [Accessed April 12 2019].

NORDTUG, T., OLSEN, A. J., ALTIN, D., MEIER, S., OVERREIN, I., HANSEN, B. H. & JOHANSEN, O. 2011a. Method for generating parameterized ecotoxicity data of dispersed oil for use in environmental modelling. *Marine Pollution Bulletin,* 62**,** 2106-2113.

NORDTUG, T., OLSEN, A. J., ALTIN, D., OVERREIN, I., STOROY, W., HANSEN, B. H. & DE LAENDER, F. 2011b. Oil droplets do not affect assimilation and survival probability of first feeding larvae of North-East Arctic cod. *Science of the Total Environment,* 412**,** 148-153.
O'LEARY, W. M. 1962. THE FATTY ACIDS OF BACTERIA. *Bacteriological reviews,* 26**,** 421-447.
OLSEN, R. E. & HENDERSON, R. J. 1989. THE RAPID ANALYSIS OF NEUTRAL AND POLAR MARINE LIPIDS USING DOUBLE-DEVELOPMENT HPTLC AND SCANNING DENSITOMETRY. *Journal of Experimental Marine Biology and Ecology,* 129**,** 189-197.
OPEC 2018. 2018 OPEC World Oil Outlook. Organization of the Petroleum Exporting Countries.: OPEC.
RAMIREZ-LLODRA, E., TYLER, P. A., BAKER, M. C., BERGSTAD, O. A., CLARK, M. R., ESCOBAR, E., LEVIN, L. A., MENOT, L., ROWDEN, A. A., SMITH, C. R. & VAN DOVER, C. L. 2011. Man and the Last Great Wilderness: Human Impact on the Deep Sea. *Plos One,* 6.
RIVERA-FIGUEROA, A. M., RAMAZAN, K. A. & FINLAYSON-PITTS, B. J. 2004. Fluorescence, absorption, and excitation spectra of polycyclic aromatic hydrocarbons as a tool for quantitative analysis. *Journal of Chemical Education,* 81**,** 242-245.
RUBIN-BLUM, M., ANTONY, C. P., SAYAVEDRA, L., MARTINEZ-PEREZ, C., BIRGEL, D., PECKMANN, J., WU, Y. C., CARDENAS, P., MACDONALD, I., MARCON, Y., SAHLING, H., HENTSCHEL, U. & DUBILIER, N. 2019. Fueled by methane: deep-sea sponges from asphalt seeps gain their nutrition from methane-oxidizing symbionts. *Isme Journal,* 13**,** 1209-1225.
SCHOTTNER, S., HOFFMANN, F., CARDENAS, P., RAPP, H. T., BOETIUS, A. & RAMETTE, A. 2013. Relationships between Host Phylogeny, Host Type and Bacterial Community Diversity in Cold-Water Coral Reef Sponges. *Plos One,* 8.
SHOBERT, H. 2013. *Chemistry of Fossil Fuels and Biofuels,* Cambridge, Cambridge University Press.
SIKKEMA, J., DEBONT, J. A. M. & POOLMAN, B. 1995. MECHANISMS OF MEMBRANE TOXICITY OF HYDROCARBONS. *Microbiological Reviews,* 59**,** 201-222.
SILIAKUS, M. F., VAN DER OOST, J. & KENGEN, S. W. M. 2017. Adaptations of archaeal and bacterial membranes to variations in temperature, pH and pressure. *Extremophiles,* 21**,** 651-670.
SOETAERT, K. & VAN OEVELEN, D. 2009. Modeling Food Web Interactions in Benthic Deep-Sea Ecosystems A Practical Guide. *Oceanography,* 22**,** 128-143.
SORENSEN, L., MEIER, S. & MJOS, S. A. 2016a. Application of gas chromatography/tandem mass spectrometry to determine a wide range of petrogenic alkylated polycyclic aromatic hydrocarbons in biotic samples. *Rapid Communications in Mass Spectrometry,* 30**,** 2052-2058.
SORENSEN, L., SILVA, M. S., BOOTH, A. M. & MEIER, S. 2016b. Optimization and comparison of miniaturized extraction techniques for PAHs from crude oil exposed Atlantic cod and haddock eggs. *Analytical and Bioanalytical Chemistry,* 408**,** 1023-1032.
SORENSEN, L., SORHUS, E., NORDTUG, T., INCARDONE, J. P., LINBO, T. L., GIOVANETTI, L., KARLSEN, O. & MEIER, S. 2017. Oil droplet fouling and differential toxicokinetics of polycyclic aromatic hydrocarbons in embryos of Atlantic haddock and cod. *Plos One,* 12.
SORHUS, E., EDVARDSEN, R. B., KARLSEN, O., NORDTUG, T., VAN DER MEEREN, T., THORSEN, A., HARMAN, C., JENTOFT, S. & MEIER, S. 2015. Unexpected Interaction with Dispersed Crude Oil Droplets Drives Severe Toxicity in Atlantic Haddock Embryos. *Plos One,* 10.
STATISTA. 2019. Available: https://www.statista.com/statistics/271823/daily-global-crude-oil-demand-since-2006/ [Accessed April 11 2019].
STAUFFER, E. D., J. A.; NEWMAN, R. 2008. Gas Chromatography and Gas Chromatography - Mass Spectometry. *Fire Debris Analysis.* Academic Press.
STEVENNE, C. 2018. *The response of a boreal deep-sea sponge holobiont to an acute crude oil exposure: a mesocosm experiment.* Master Thesis, University of Liège.
STRAND, R., WHALAN, S., WEBSTER, N. S., KUTTI, T., FANG, J. K. H., LUTER, H. M. & BANNISTER, R. J. 2017. The response of a boreal deep-sea sponge holobiont to acute thermal stress. *Scientific Reports,* 7.

STRANSKY, K., JURSIK, T. & VITEK, A. 1997. Standard equivalent chain length values of monoenic and polyenic (methylene interrupted) fatty acids. *Hrc-Journal of High Resolution Chromatography,* 20**,** 143-158.

SUNDBY, S. F., P.; SANDVIK, A.; VIKEBØ, F. B.; ALGEN, A.; BUHL-MORTENSEN, L.; FOLKVORD, A.; BAKKEPLASS, K.; BUHL-MORTENSEN, P.; JOHANNESSEN, M.; JØRGENSEN, M. S.; KRISTIANSEN, T.; LANDA, C. S.; MYKSVOLL, M. S.; NASH, R. 2013. Kunnskapsinnhenting Barentshavet - Lofoten - Vesterålen (KILO). Bergen: Norwegian Institute of Marine Research.

THAKUR, N. & SINGH, A. 2016. Chemical Ecology of Marine Sponges.

THIEL, V., BLUMENBERG, M., HEFTER, J., PAPE, T., POMPONI, S., REED, J., REITNER, J., WORHEIDE, G. & MICHAELIS, W. 2002. A chemical view of the most ancient metazoa - biomarker chemotaxonomy of hexactinellid sponges (vol 89, pg 60, 2002). *Naturwissenschaften,* 89**,** 233-234.

THISTLE, D. 2003. *The deep-sea floor: An overview*.

THURBER, A. R., SWEETMAN, A. K., NARAYANASWAMY, B. E., JONES, D. O. B., INGELS, J. & HANSMAN, R. L. 2014. Ecosystem function and services provided by the deep sea. *Biogeosciences,* 11**,** 3941-3963.

VAN SOEST, R. W. M., BOURY-ESNAULT, N., VACELET, J., DOHRMANN, M., ERPENBECK, D., DE VOOGD, N. J., SANTODOMINGO, N., VANHOORNE, B., KELLY, M. & HOOPER, J. N. A. 2012. Global Diversity of Sponges (Porifera). *Plos One,* 7.

VIS, G.-J. 2017. Geology and Seepage in the NE Atlentic region. *The Geological Society of London***,** 443-455.

VOET, D. V., J. D.; PRATT, C. W. 2013. Lipids and Biological Membranes. *In:* VOET, D. V., J. D.; PRATT, C. W. (ed.) *Fundamentals of Biochemistry - Life at the molecular level.* Fourth Edition ed. Hoboken: John Wiley & Sons, Inc.

VOLKMAN, J. K., JEFFREY, S. W., NICHOLS, P. D., ROGERS, G. I. & GARLAND, C. D. 1989. FATTY-ACID AND LIPID-COMPOSITION OF 10 SPECIES OF MICROALGAE USED IN MARICULTURE. *Journal of Experimental Marine Biology and Ecology,* 128**,** 219-240.

WAKTOLA, H. D. & MJOS, S. A. 2018. Chromatographic efficiency of polar capillary columns applied for the analysis of fatty acid methyl esters by gas chromatography. *Journal of Separation Science,* 41**,** 1582-1592.

WASTA, Z. & MJOS, S. A. 2013. A database of chromatographic properties and mass spectra of fatty acid methyl esters from omega-3 products. *Journal of Chromatography A,* 1299**,** 94-102.

WEBSTER, N. S. & BLACKALL, L. L. 2009. What do we really know about sponge-microbial symbioses? *Isme Journal,* 3**,** 1-3.

WEBSTER, N. S. & TAYLOR, M. W. 2012. Marine sponges and their microbial symbionts: love and other relationships. *Environmental Microbiology,* 14**,** 335-346.

WEIJERS, J. W. H., SCHOUTEN, S., HOPMANS, E. C., GEENEVASEN, J. A. J., DAVID, O. R. P., COLEMAN, J. M., PANCOST, R. D. & DAMSTE, J. S. S. 2006. Membrane lipids of mesophilic anaerobic bacteria thriving in peats have typical archaeal traits. *Environmental Microbiology,* 8**,** 648-657.

WOODFORD, F. P. & VANGENT, C. M. 1960. GAS-LIQUID CHROMATOGRAPHY OF FATTY ACID METHYL ESTERS - THE CARBON-NUMBER AS A PARAMETER FOR COMPARISON OF COLUMNS. *Journal of Lipid Research,* 1**,** 188-190.

WOTHERSPOON, A. T. L., REEVES, K. L. & CRAWFORD, J. 2018. A comparison of structural-functional equation models to identify fatty acids on three common gas chromatography columns. *Analytical Methods,* 10**,** 1747-1759.

WULFF, J. 2010. Regeneration of Sponges in Ecological Context: Is Regeneration an Integral Part of Life History and Morphological Strategies? *Integrative and Comparative Biology,* 50**,** 494-505.

ZIMMERMANN, S., KRIPPNER, P., VOGEL, A. & MULLER, J. 2002. Miniaturized flame ionization detector for gas chromatography. *Sensors and Actuators B-Chemical,* 83**,** 285-289.

Appendix A

Figure A1: The gear used to perform the oil exposure experiment, and the setup of experimental mesocosms.

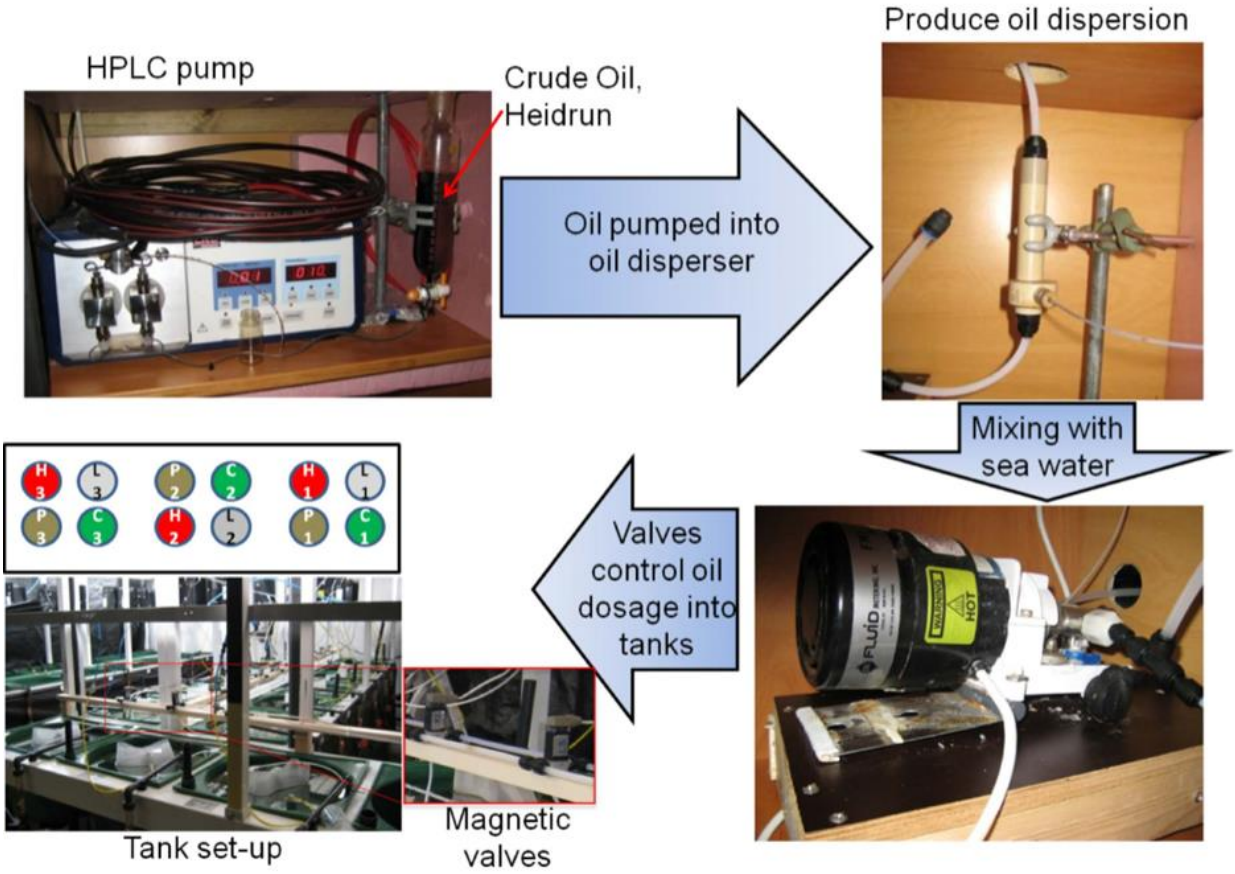

Table A1: Schedule for the experimental setup.

Date	C1-H1	C2-H2	C3-H3	C4-H4
04.02.2018	Day 0	-	Day 0	-
05.02.2018	Day 1	Day 0	Day 1	Day 0
06.02.2018	Day 2	Day 1	Day 2	Day 1
07.02.2018	-	Day 2	-	Day 2
08.02.2018	Day 4	-	Day 4	-
09.02.2018	-	Day 4	-	Day 4
10.02.2018	-	-	-	-
11.02.2018	-	-	-	-
12.02.2018	Day 8	-	Day 8	-
13.02.2018		Day 8		Day 8
14.02.2018	1st day of recovery	1st day of recovery	1st day of recovery	1st day of recovery
…	-	-	-	-
14.03.2018	Last day of recovery	-	Last day of recovery	-
15.03.2018	-	Last day of recovery	-	Last day of recovery

Appendix B

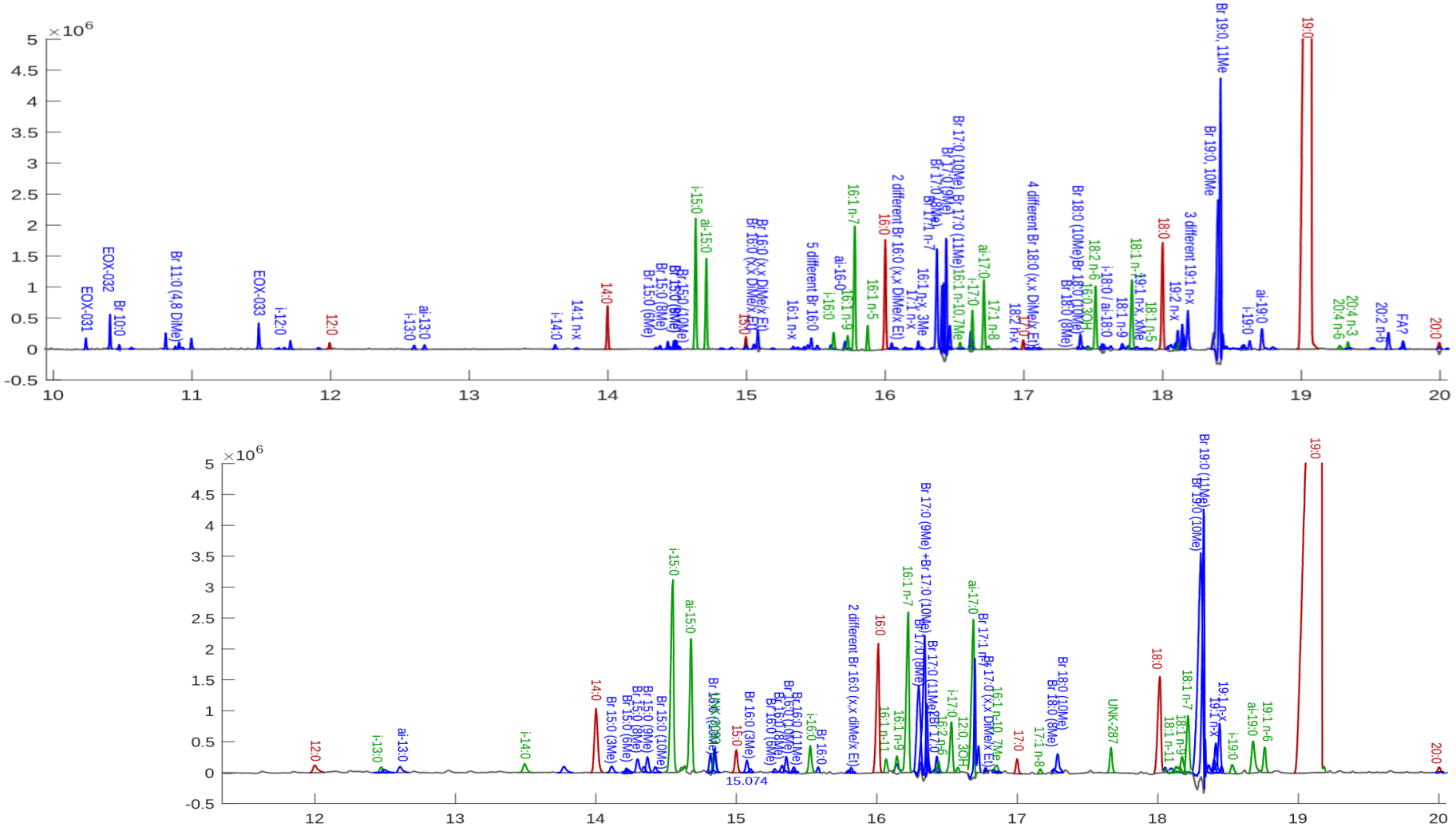

Figure B1: Comparison of the non-polar DB-5 column (top) and polar CB-WAX column (bottom), showing the complexity of the FA profile and the resolution of each column from RT 10-20.

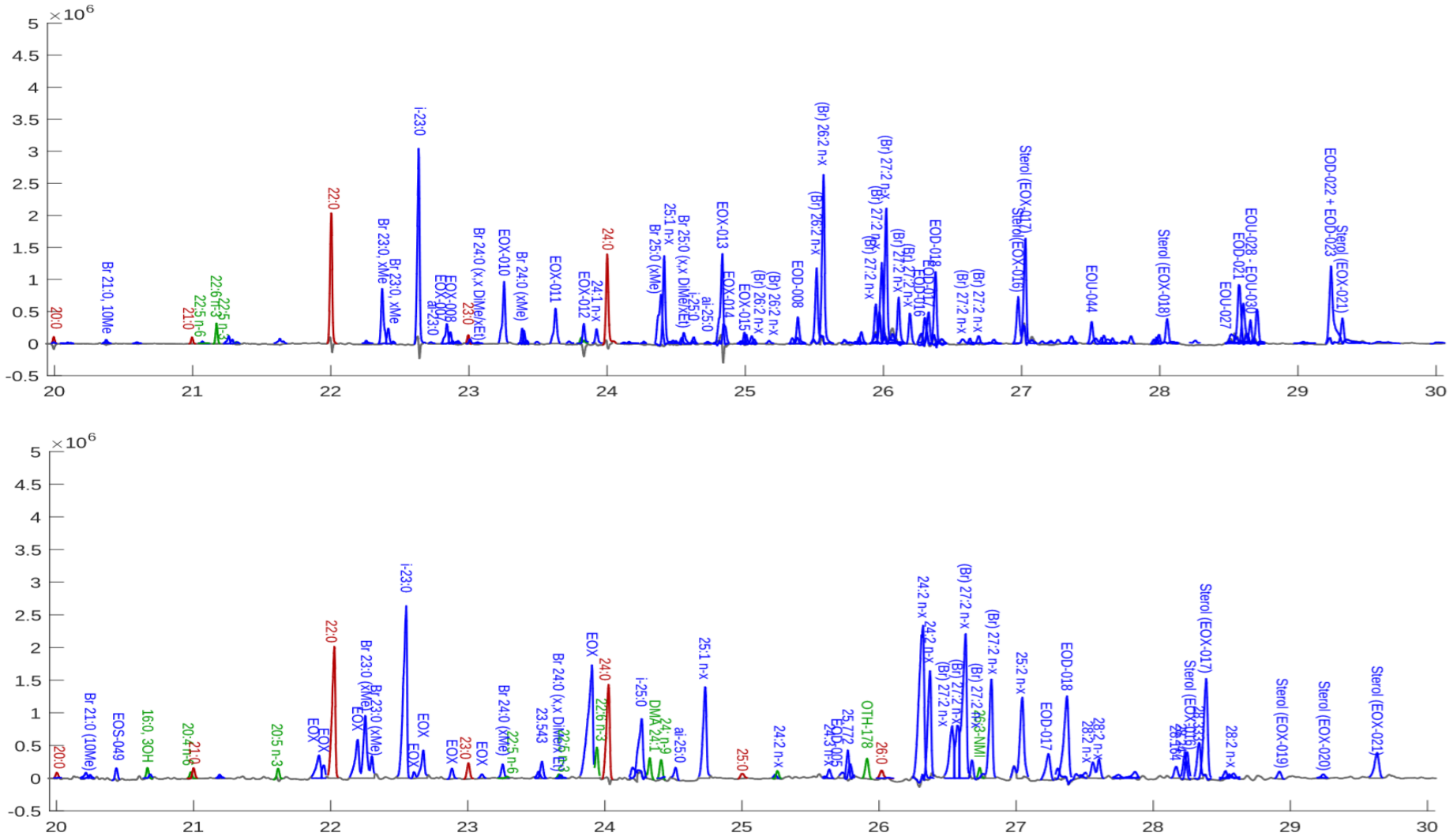

Figure B2: Comparison of the non-polar DB-5 column (top) and polar CB-WAX column (bottom), showing the complexity of the FA profile and the resolution of each column from RT 20-30.

Appendix C

Every species found in the FAME extract oF G. barretti has been given individual codes, and are presented with their respective mass spectras, retention times (RT) end equivalent chain lengths (ECL), only representative for the 60 m DB-5 column at the 1 °C/min temperature programme. Identified or partly identified species are also given a short name and structure. Structures suggested by NIST are marked. Identifying ions for the branching points of branched FAME are highlighted.

Short name:
Code: EOX-031
ECL: 10,2350
RT: 13,0271

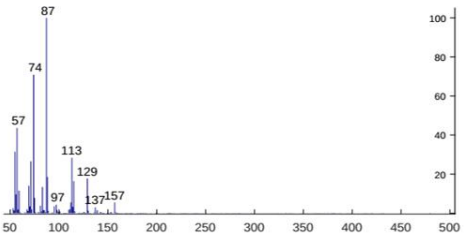

NIST suggestion

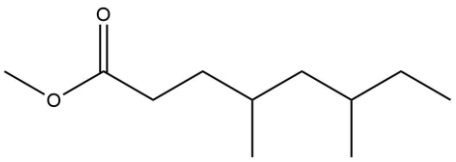

Short name:
Code: EOX-032
ECL: 10,4089
RT: 14,1134

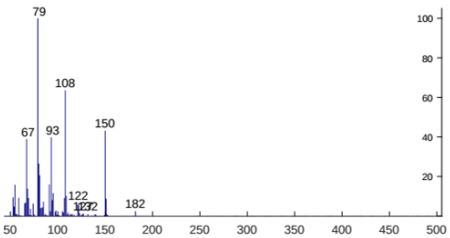

Short name: Br 10:0 (xMe)
Code: EOS-001
ECL:10,4748
RT:14,5282

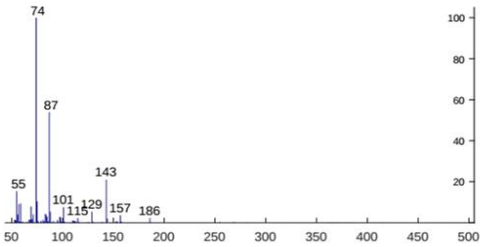

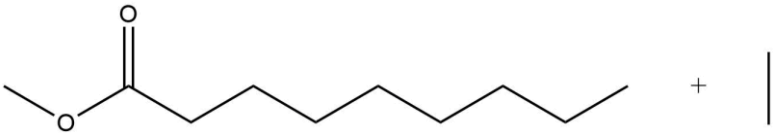

Short name: Br 11:0 (4, 8 DiMe)
Code: EOS-002
ECL: 10,8101
RT:16,6614

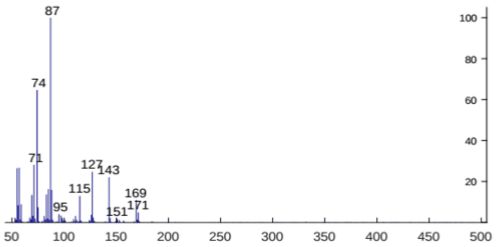

NIST suggestion

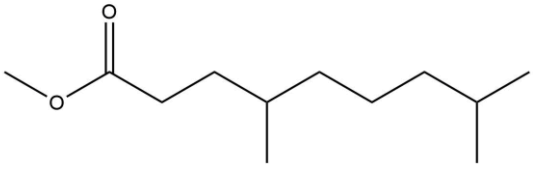

Short name: Br 11:0 (xMe)
Code: EOS-003
ECL: 10,8806
RT: 17,1157

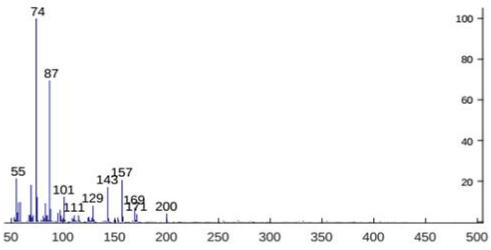

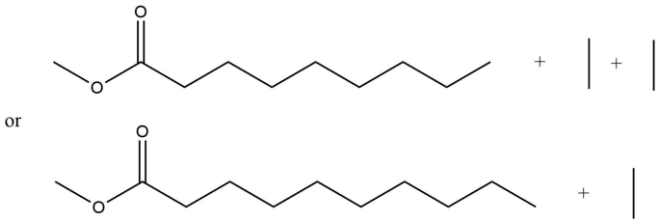

Short name:
Code: EOX-033
ECL: 11,4814
RT: 21,0661

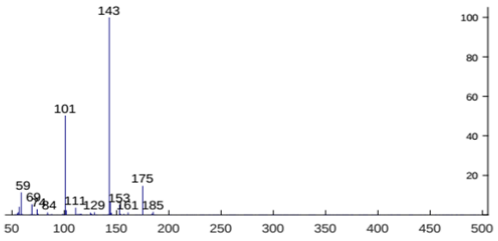

Short name: i-12:0
Code: EOS-004
ECL: 11,6660
RT: 22,3104

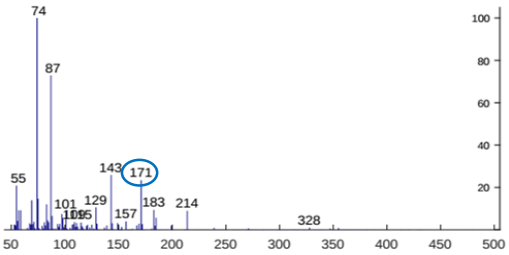

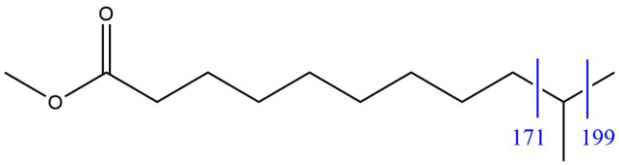

Short name: 12:0
Code: SAN-003
ECL: 11,9914
RT: 24,5424

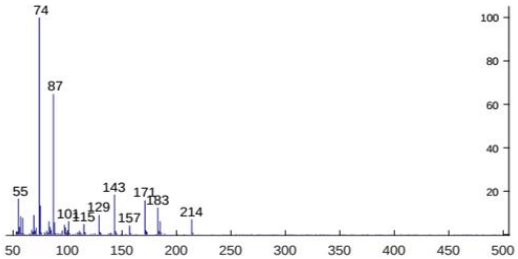

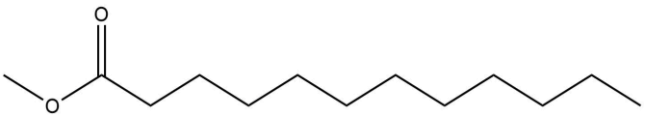

Short name: i-13:0
Code: EOS-005
ECL: 12,6016
RT: 28,8681

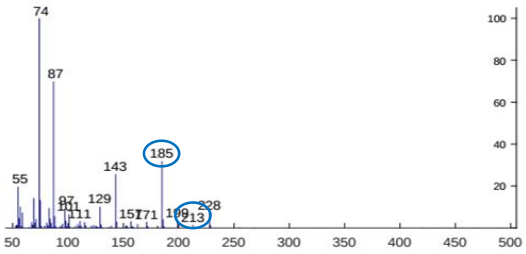

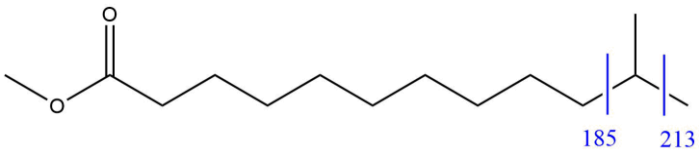

Short name: ai-13:0
Code: EOS-006
ECL: 12,6777
RT: 29,4211

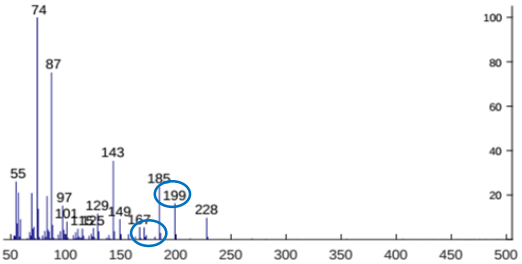

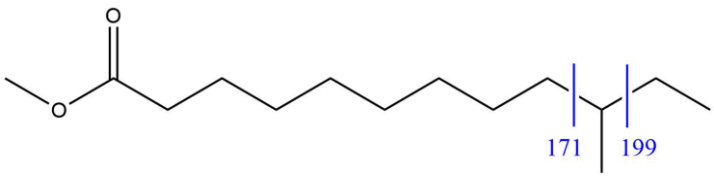

Short name: i-14:0
Code: EOS-007
ECL: 13,6186
RT: 36,5515

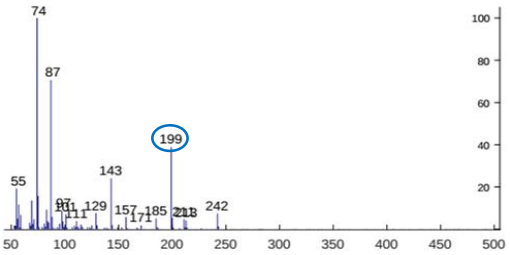

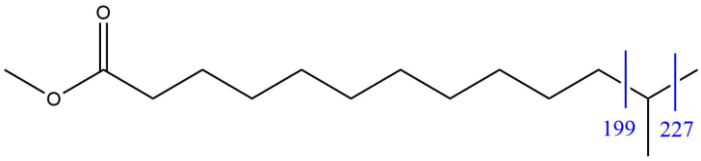

Short name: 14:1 n-x
Code: EOM-001
ECL: 13,7728
RT: 37,7761

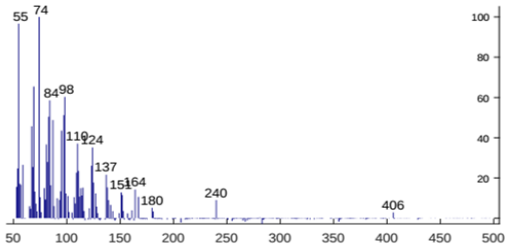

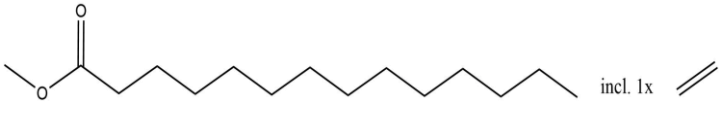

Short name: 14:0
Code: SAN-005
ECL: 13,9976
RT: 39,5933

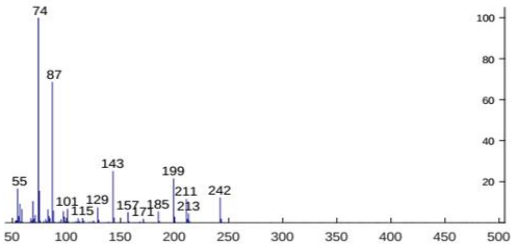

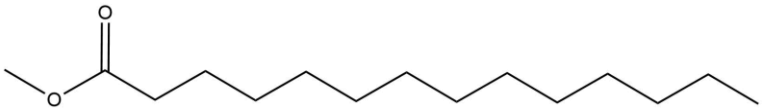

Short name: 14:1 n-5, 13Me
Code: EOM-002
ECL: 14,3460
RT: 42,5166

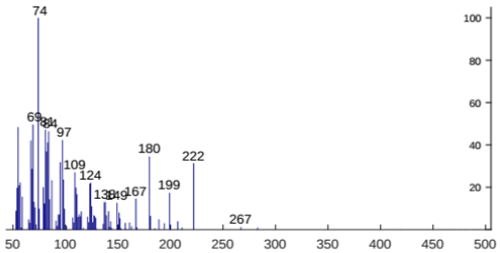

NIST suggestion:

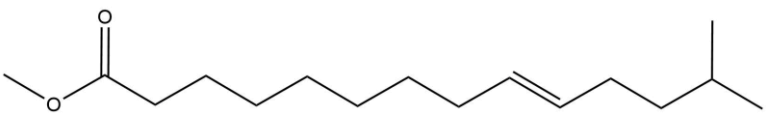

Short name: Br 15:0 (3Me)
Code: EOS-008
ECL: 14,3759
RT: 24,7733

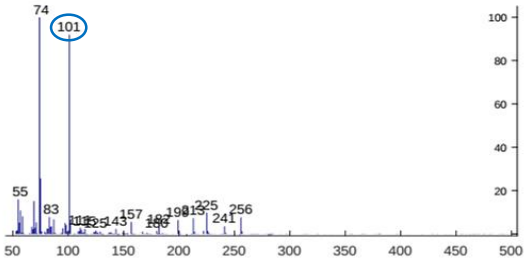

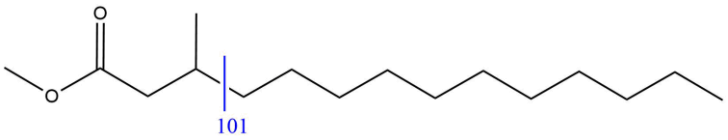

Short name: Br 15:0 (6Me)
Code: EOS-009
ECL: 14,4309
RT: 43,2474

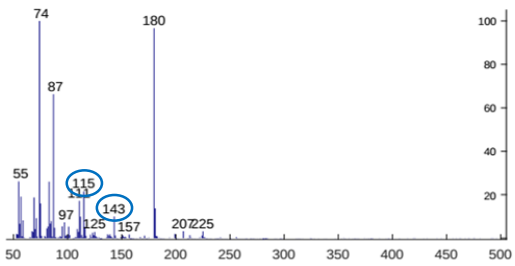

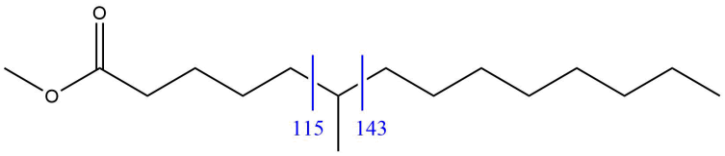

Short name: Br 15:0 (8Me)
Code: EOS-010
ECL: 14,4491
RT: 43,4054

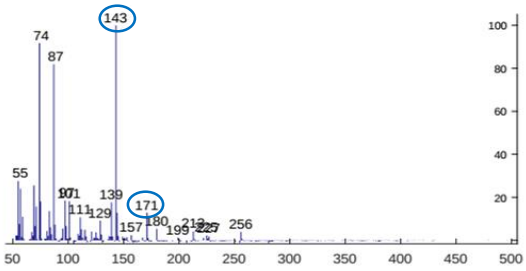

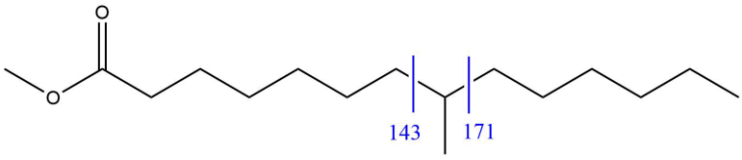

Short name: Br 15:0 (9Me)
Code: EOS-011
ECL: 14,4764
RT: 43,6424

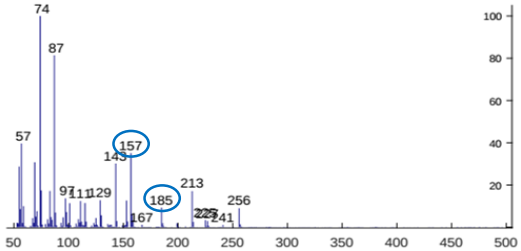

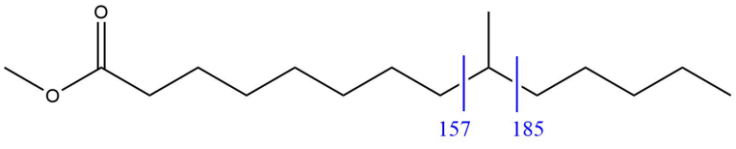

Short name:
Code: EOS-012
ECL: 14,4923
RT: 43,7807

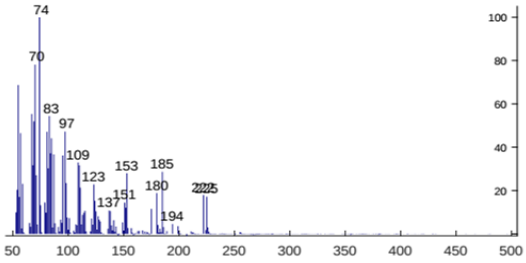

Short name: Br 15:0 (10Me)
Code: EOS-013
ECL: 14,5150
RT: 43,9782

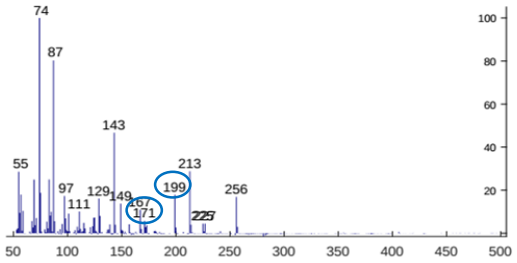

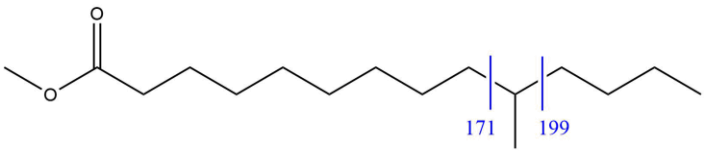

Short name: i-15:0
Code: SAB-078
ECL: 14,6326
RT: 45,0053

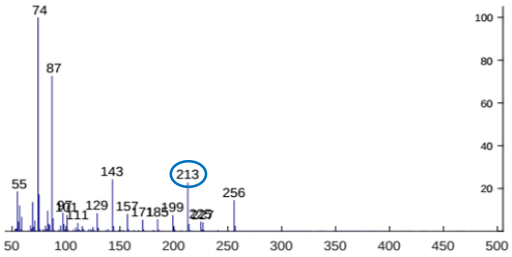

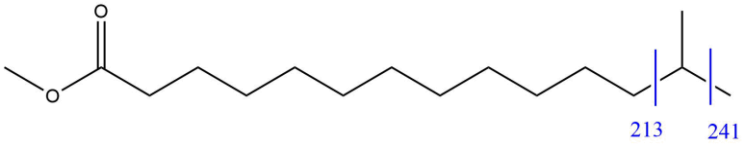

Short name: ai-15:0
Code: SAB-077
ECL: 14,7092
RT: 45,6769

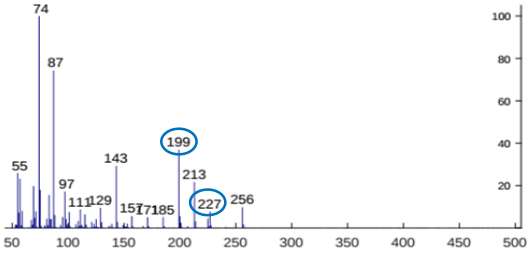

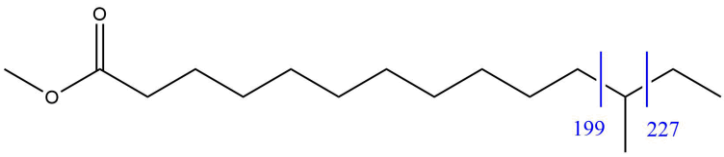

Short name: 15:0
Code: SAN-006
ECL: 14,9954
RT: 48,1853

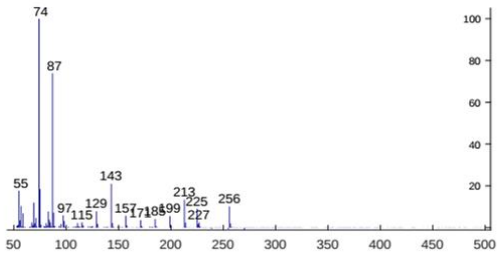

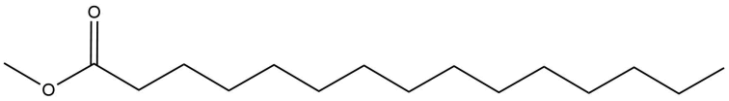

Short name: Br 16:0 (3,x DiMe)
Code: EOS-014
ECL: 14,9977
RT: 48,2051

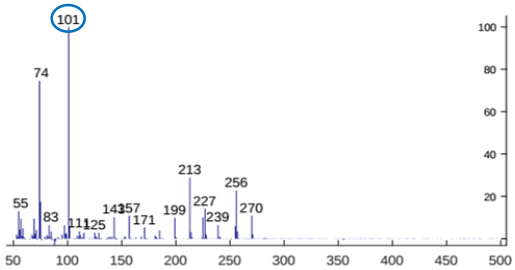

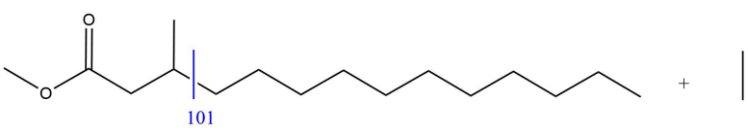

Short name: Br 16:0 (x,x DiMe/x Et)
Code: EOS-015
ECL: 15,0520
RT: 48,6791

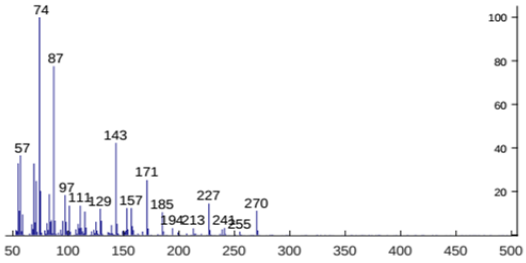

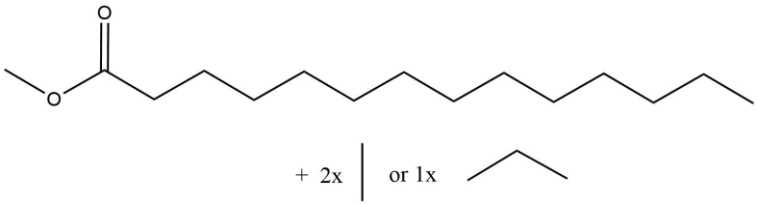

Short name: Br 16:0 (x,x DiMe/x Et)
Code: EOS-016
ECL: 15,0814
RT: 48,9359

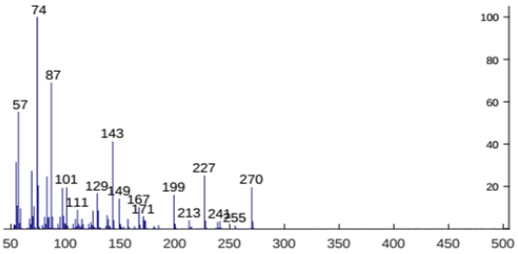

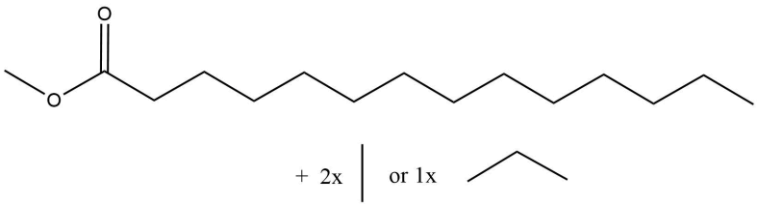

Short name: 16:1 n-x
Code: EOM-003
ECL: 15,3354
RT: 51,1679

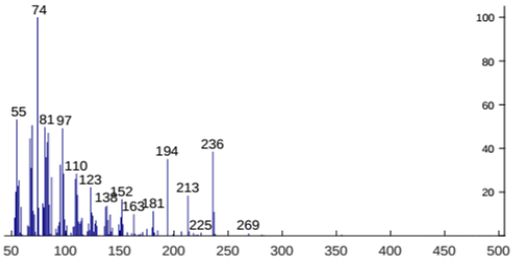

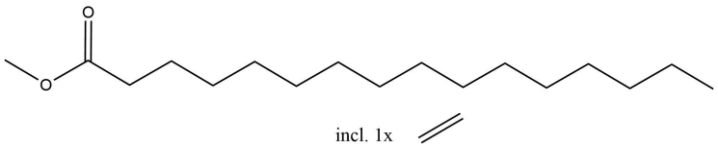

Short name: Br 16:0 (3Me)
Code: EOS-017
ECL: 15,3689
RT: 51,4641

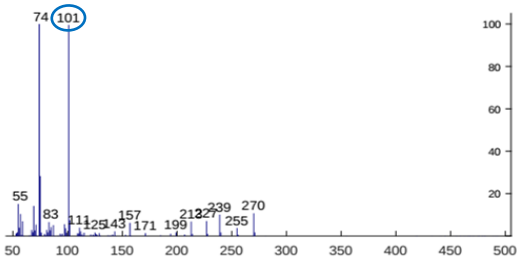

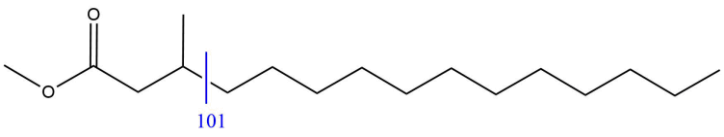

Short name: Br 16:0 (6Me)
Code: EOS-018
ECL: 15,4159
RT: 51,8789

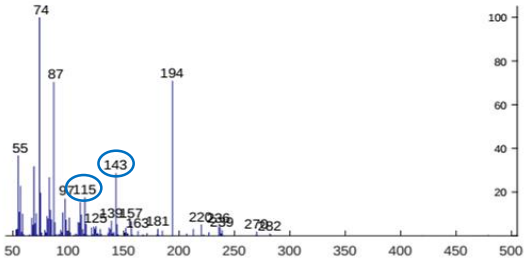

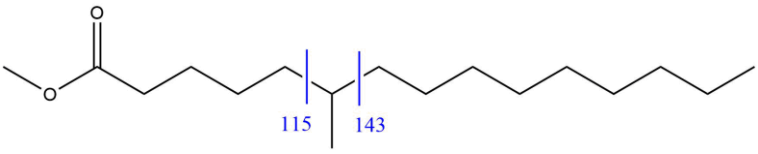

Short name: Br 16:0 (8Me)
Code: EOS-019
ECL: 15,4405
RT: 52,0962

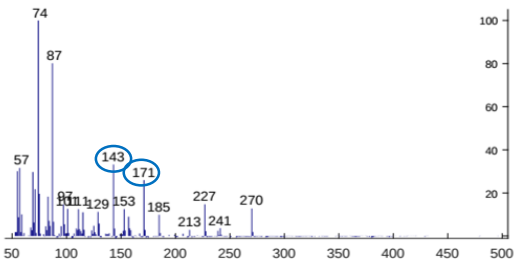

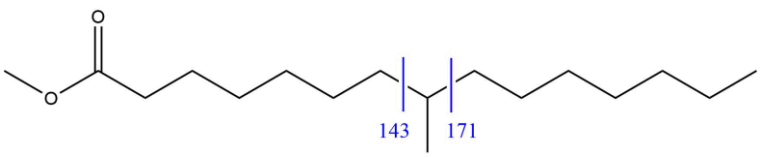

Short name: Br 16:0 (10Me)
Code: EOS-020
ECL: 15,4673
RT: 52,3332

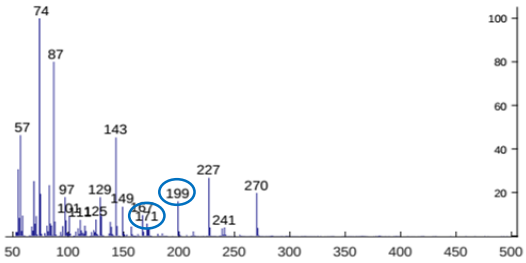

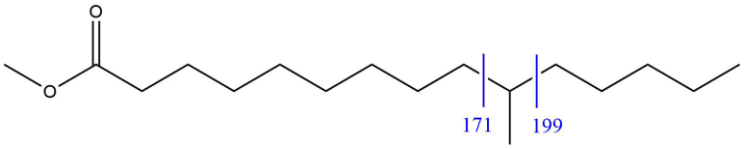

Short name: Br 16:0 (11Me)
Code: EOS-021
ECL: 15,5097
RT: 52,7085

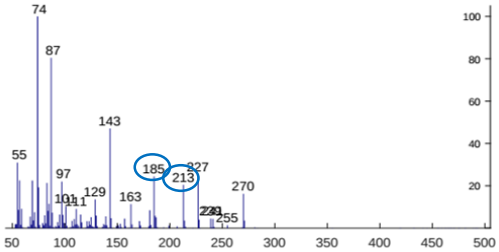

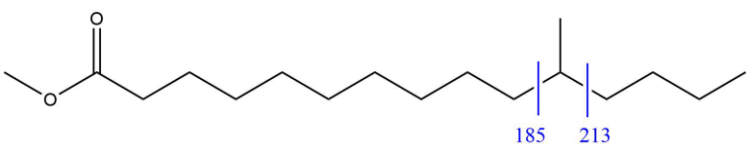

Short name: 16:2 n-6
Code: DIU-494
ECL: 15,6078
RT: 53,5776

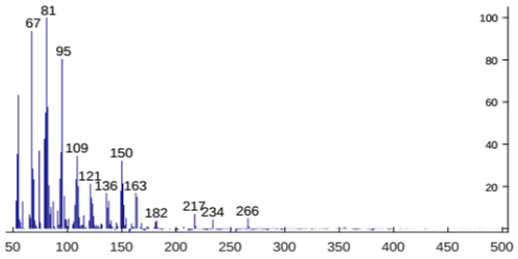

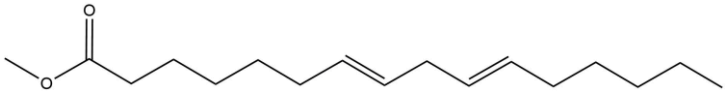

Short name: i-16:0
Code: SAB-072
ECL: 15,6256
RT: 53,7356

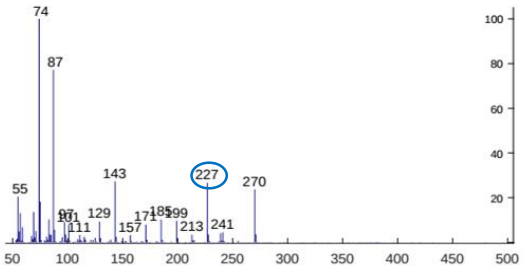

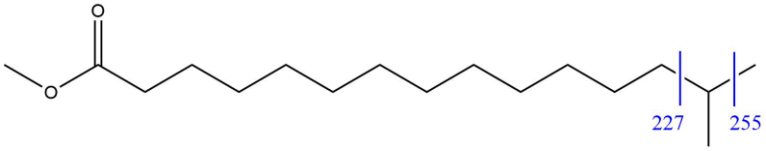

Short name: ai-16:0
Code: EOS-022
ECL: 15,7080
RT: 54,4664

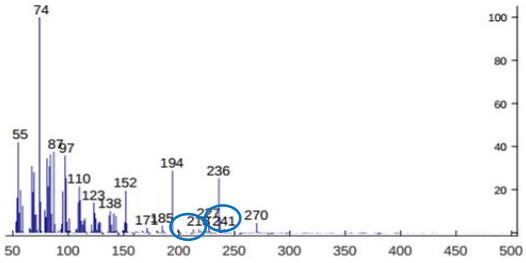

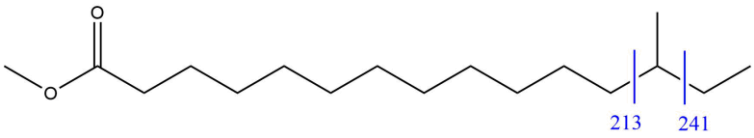

Short name: 16:1 n-9
Code: MOU-275
ECL: 15,7281
RT: 64,6442

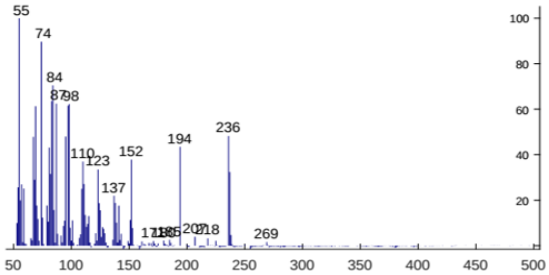

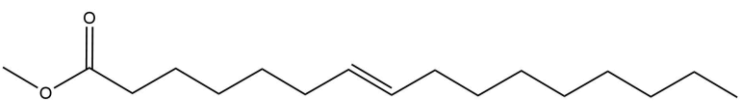

Short name: 16:1 n-7
Code: MOU-021
ECL: 15,7793
RT: 55,0985

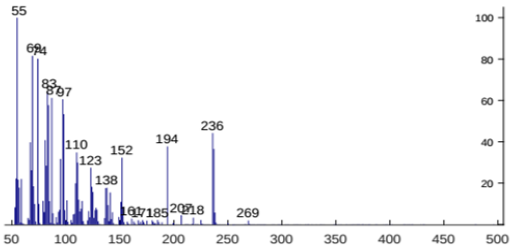

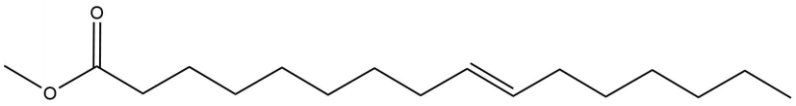

Short name: 16:1 n-5
Code: MOU-255
ECL: 15,8729
RT: 55,9281

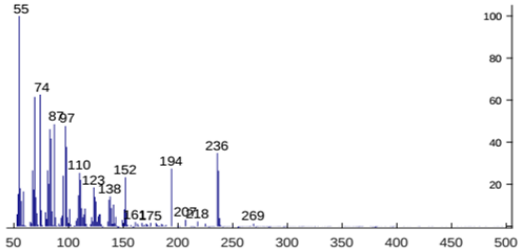

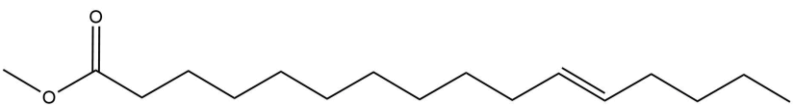

Short name: 16:0
Code: SAN-007
ECL: 16,0000
RT: 57,0539

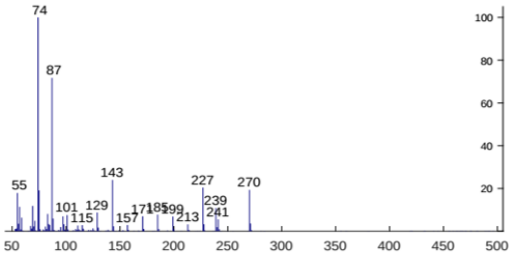

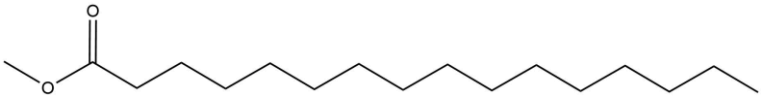

Short name: Br 17:0 (x,x DiMe/x Et)
Code: EOS-023
ECL: 16,0379
RT: 57,3897

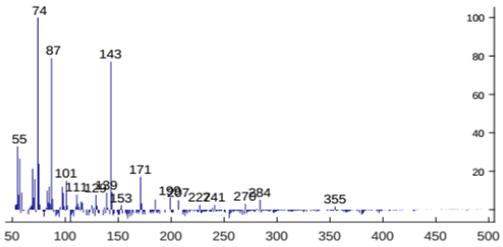

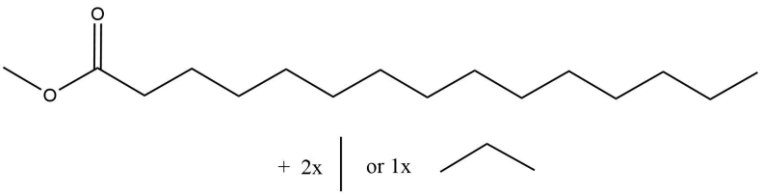

Short name: Br 17:0 (x,x DiMe/x Et)
Code: EOS-024
ECL: 16,0468
RT:57,4687

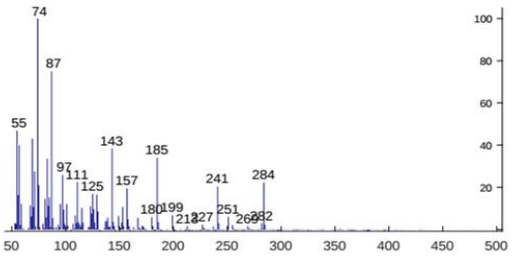

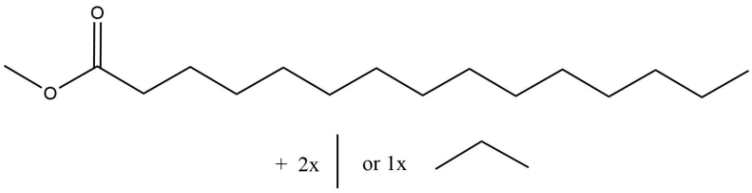

Short name: 17:1 n-x
Code: EOM-004
ECL: 16,0758
RT: 57,7255

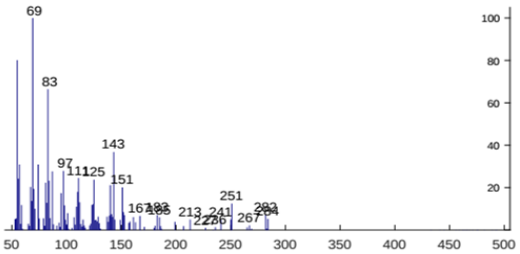

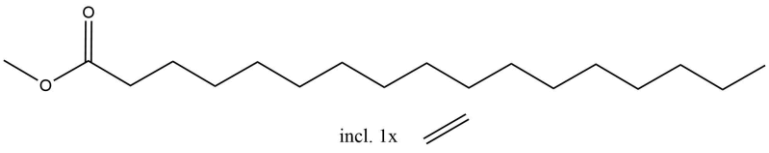

Short name:
Code: EOM-005
ECL: 16,1448
RT:58,3378

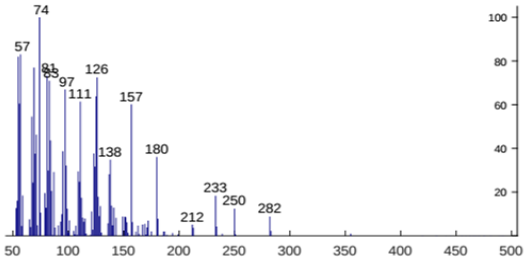

Short name: 16:1 n-x, 3Me
Code: EOM-006
ECL: 16,2382
RT: 59,1674

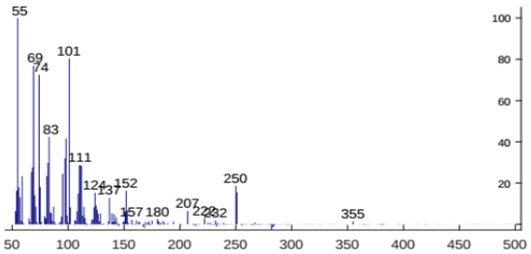

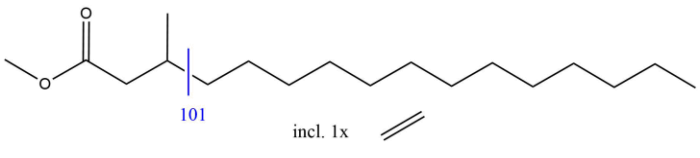

Short name: 16:1 n-x, xMe
Code: EOM-007
ECL: 16,2626
RT: 59,3846

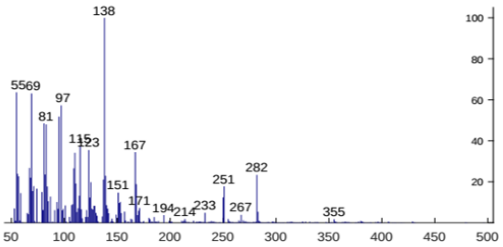

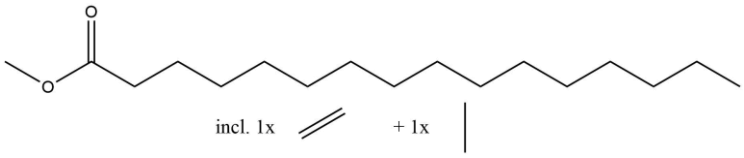

Short name:
Code: EOM-008
ECL: 16,3382
RT: 60,0562

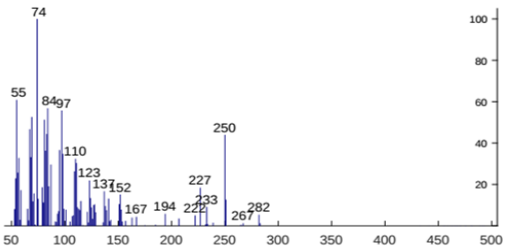

Short name: 17:1 n-7
Code: MOU-022
ECL: 16,3715
RT: 60,3525

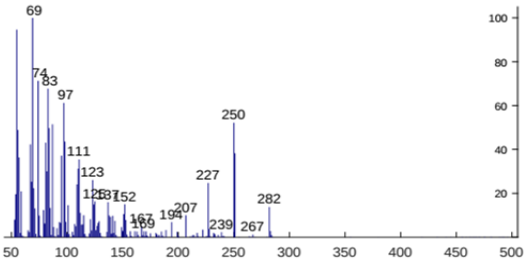

Short name: Br 17:0 (8Me)
Code: EOS-025
ECL: 16,4092
RT: 60,6882

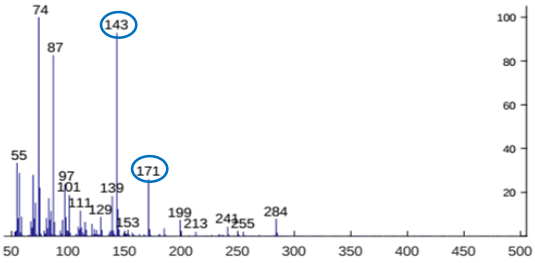

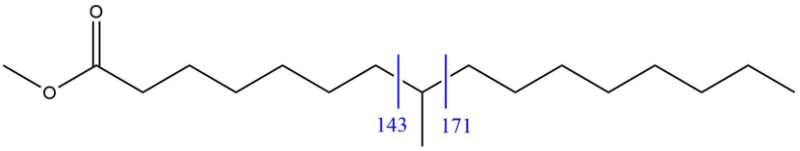

Short name: Br 17:0 (9Me)
Code: EOS-026
ECL: 16,4203
RT: 60,7870

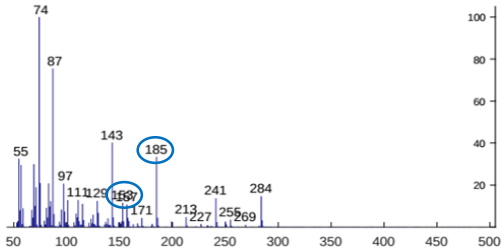

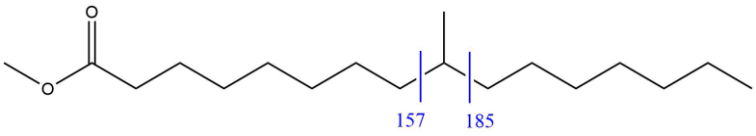

Short name: Br 17:0 (10Me)
Code: EOS-027
ECL: 16,4381
RT: 60,9450

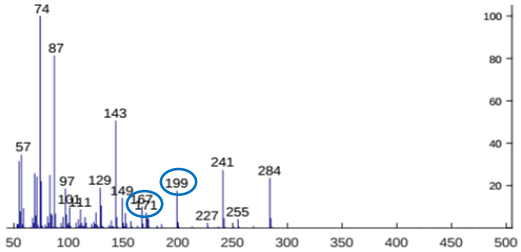

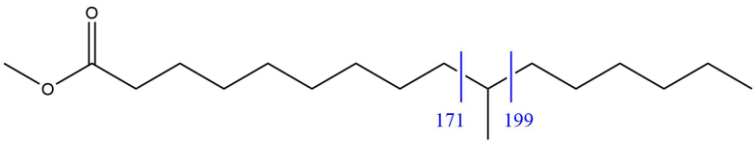

Short name: Br 17:0 (11Me)
Code: EOS-028
ECL: 16,4669
RT: 61,2018

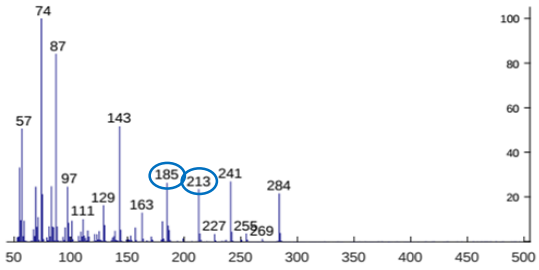

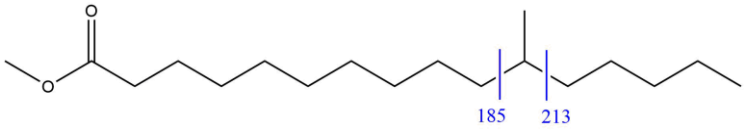

Short name: 16:1 n-10, 7Me
Code: MOB-286
ECL: 16,5380
RT: 61,8339

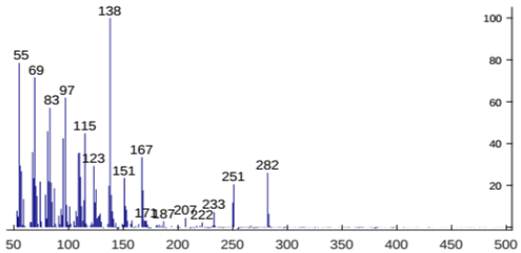

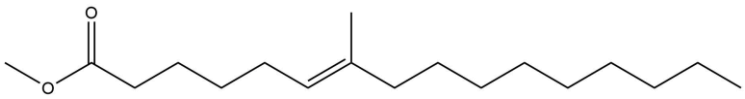

Short name: Br 17:0 (x,x DiMe/x Et)
Code: EOS-029
ECL: 16,6158
RT: 62,5252

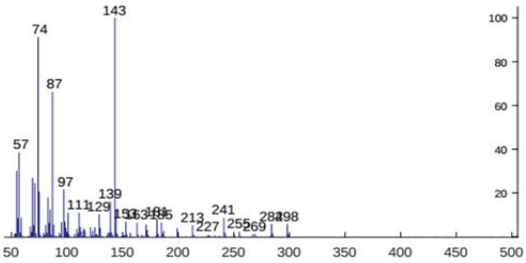

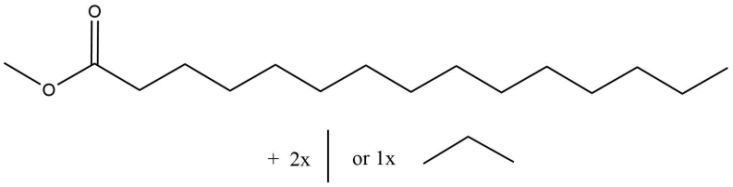

Short name: i-17:0
Code: SAB-074
ECL: 16,6269
RT: 62,6900

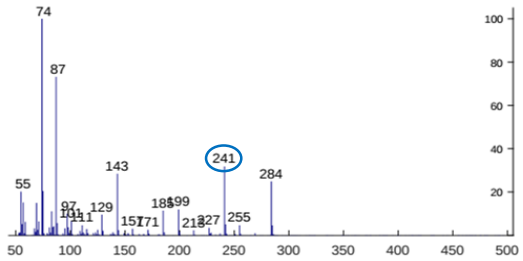

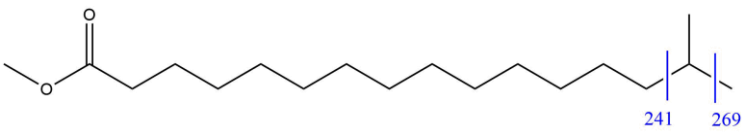

Short name: ai-17:0
Code: SAB-073
ECL: 16,7115
RT: 63,3745

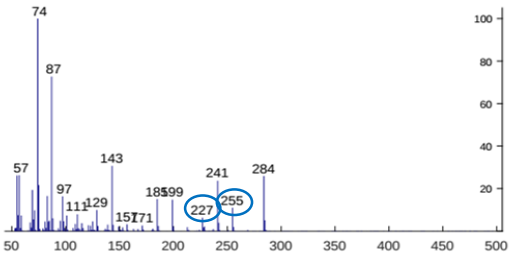

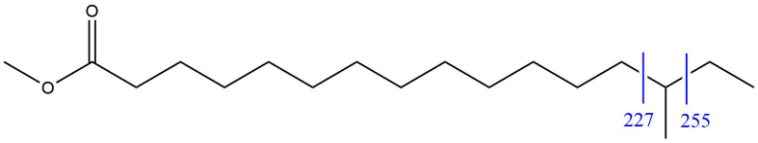

Short name: 17:1 n-8
Code: MOU-436
ECL: 16,7449
RT: 63,6708

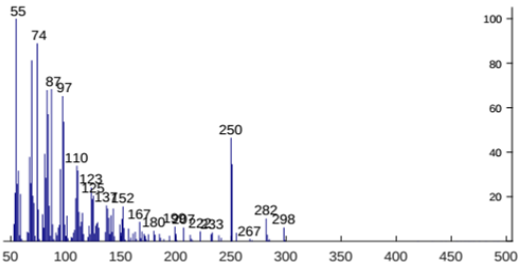

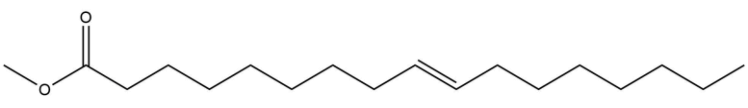

Short name: 18:2 n-x
Code: EOD-001
ECL: 16,9326
RT: 65,3299

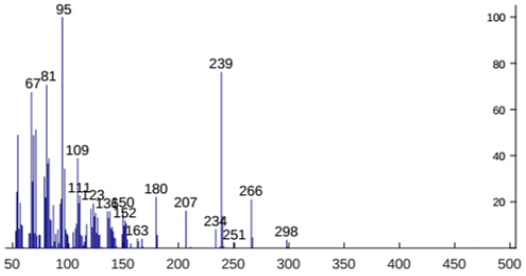

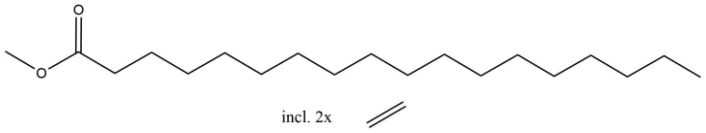

Short name: 17:0
Code: SAN-008
ECL: 16,9932
RT: 65,8632

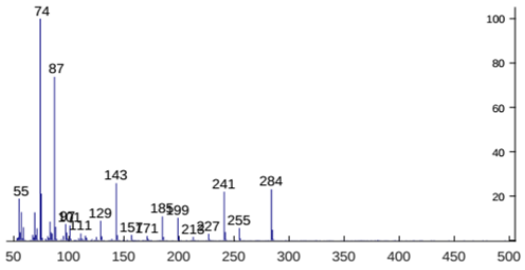

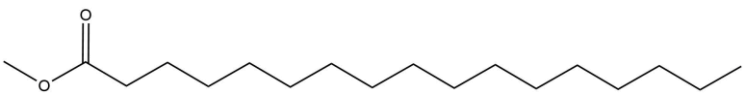

Short name: Br 18:0 (x,x DiMe/x Et)
Code: EOS-030
ECL: 17,0292
RT: 66,1793

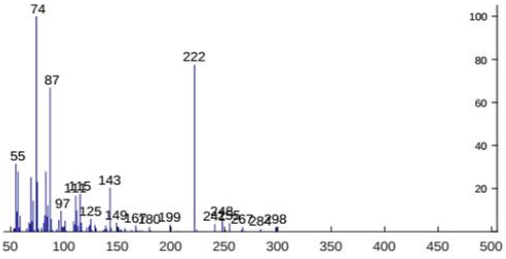

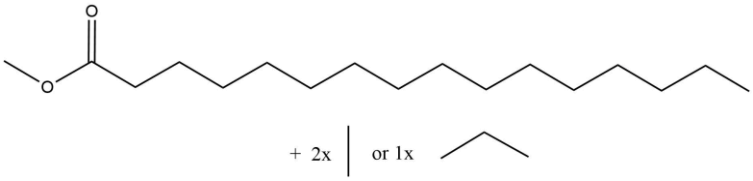

Short name: Br 18:0 (x,x DiMe/x Et)
Code: EOS-031
ECL: 17,0337
RT: 66,2188

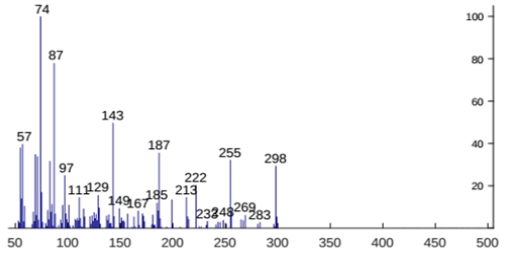

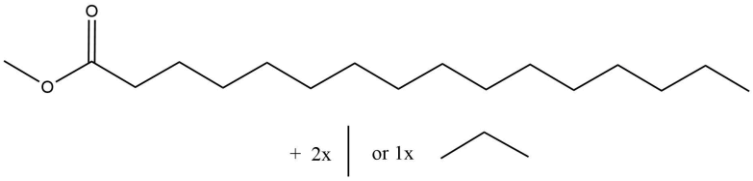

Short name: Br 18:0 (x,x DiMe/x Et)
Code: EOS-032
ECL: 17,0742
RT: 66,5743

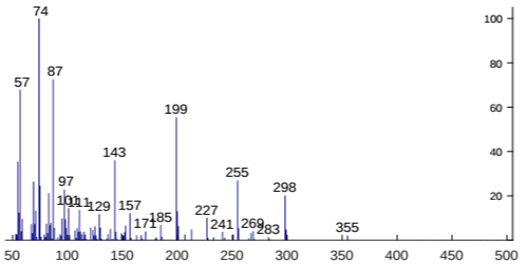

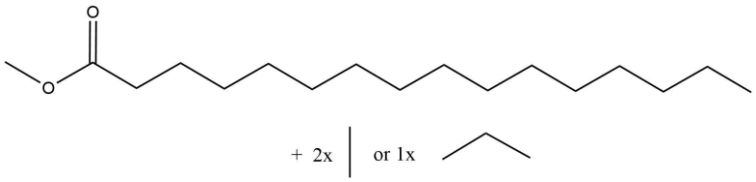

Short name: Br 18:0 (x,x DiMe/x Et)
Code: EOS-033
ECL: 17,1102
RT: 66,8903

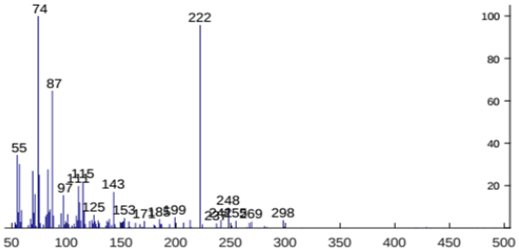

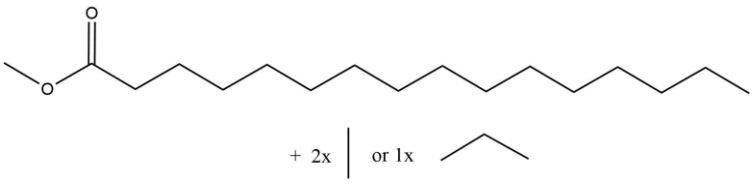

Short name: Br 18:0 (8Me)
Code: EOS-034
ECL: 17,3874
RT: 69,3198

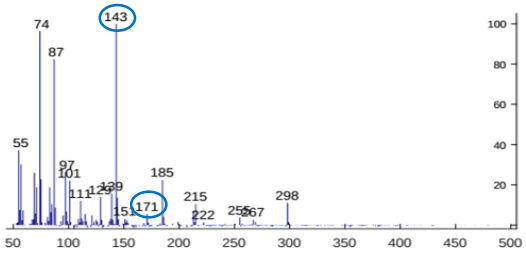

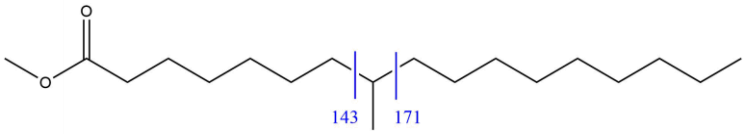

Short name: Br 18:0 (10Me)
Code: EOS-035
ECL: 17,4077
RT: 69,4976

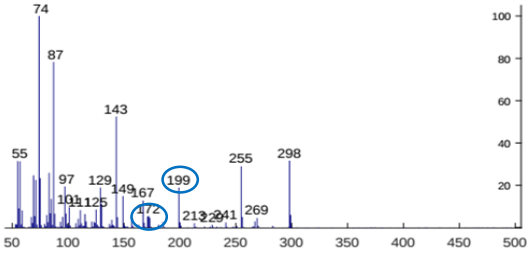

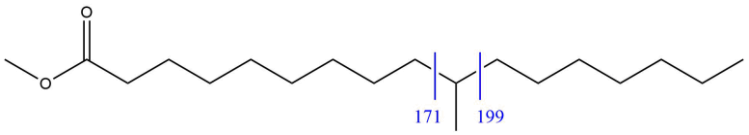

Short name: Br 18:0 (12Me)
Code: EOS-036
ECL: 17,4598
RT: 69,9519

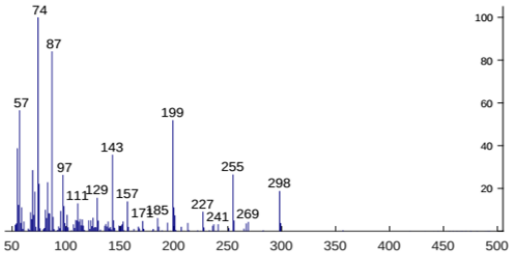

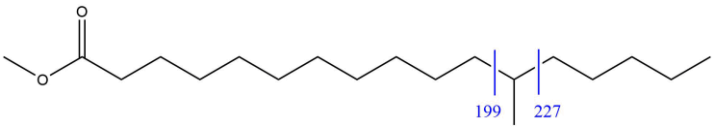

Short name: 16:0, 3OH
Code: SOH-769
ECL: 17,4801
RT: 70,1296

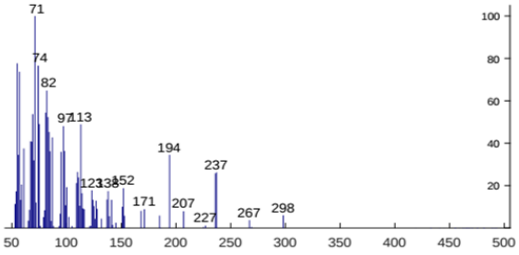

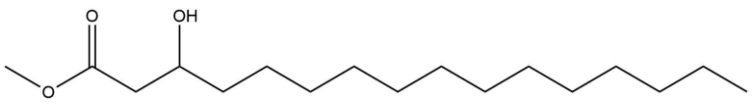

Short name: 18:2 n-6
Code: DIU-027
ECL: 17,5164
RT: 70,4457

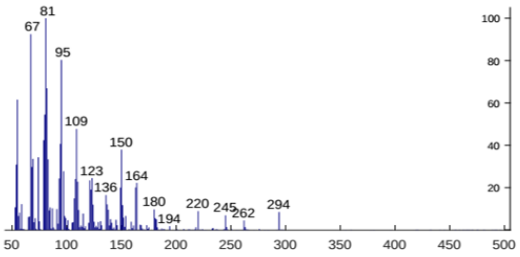

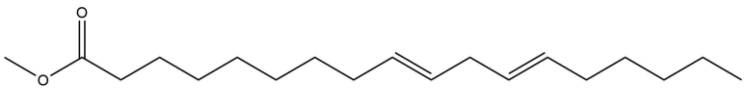

Short name: i-18:0
Code: EOS-037
ECL: 17,6252
RT: 71,3937

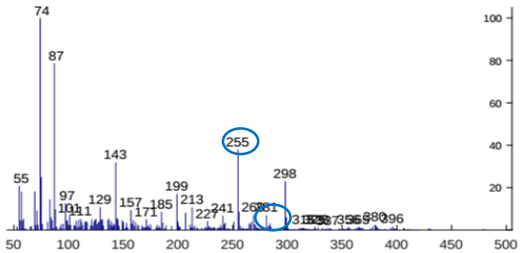

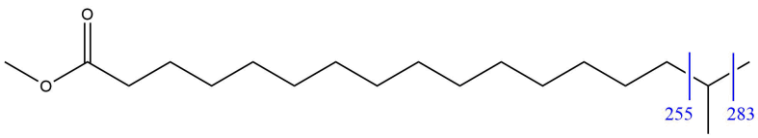

Short name: ai-18:0
Code: EOS-038
ECL: 17,7094
RT: 72,1246

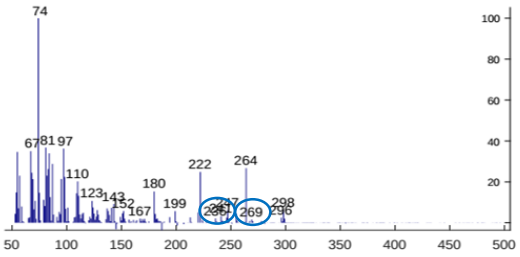

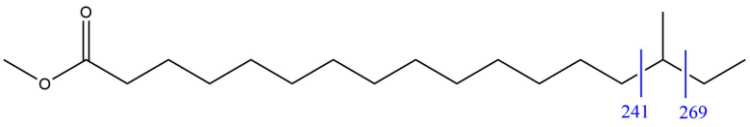

Short name: 18:1 n-9
Code: MOU-023
ECL: 17,7162
RT: 72,1838

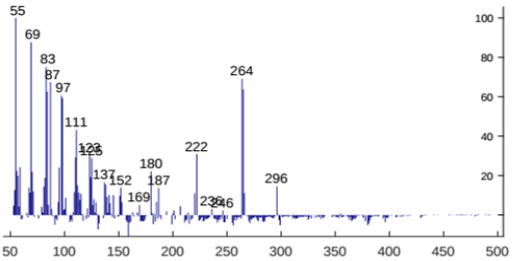

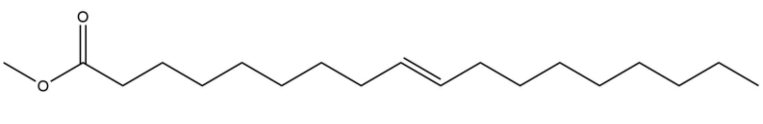

Short name:
Code: EOS-039
ECL: 17,7527
RT: 72,4998

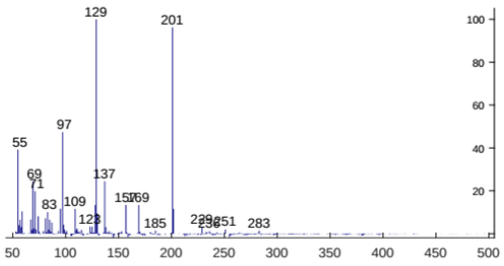

Short name: 18:1 n-7
Code: MOU-079
ECL: 17,7778
RT: 72,7171

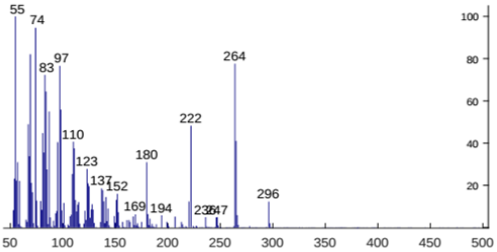

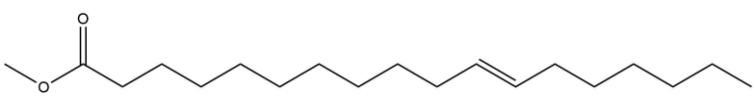

Short name: 19:1 n-x, xMe
Code: EOM-009
ECL: 17,8143
RT: 73,0332

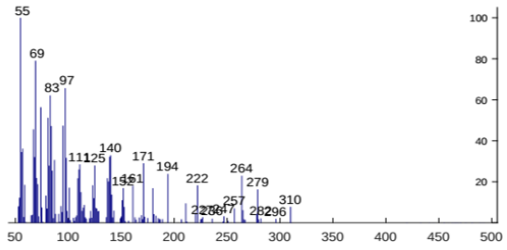

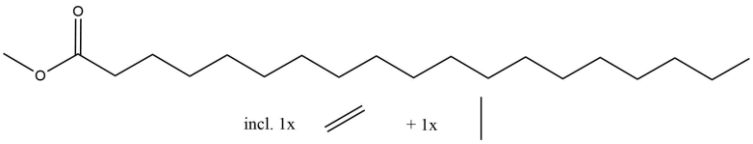

Short name: 18:1 n-5
Code: MOU-258
ECL: 17,8807
RT: 73,6060

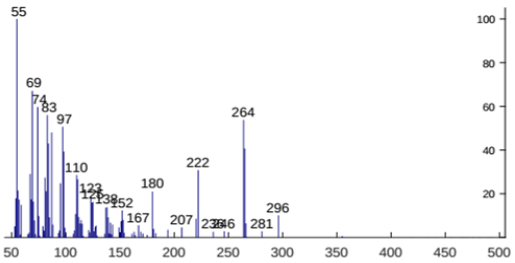

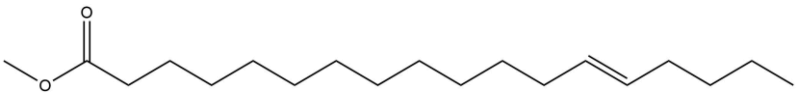

Short name: 18:0
Code: SAN-009
ECL: 18,0000
RT: 74,6330

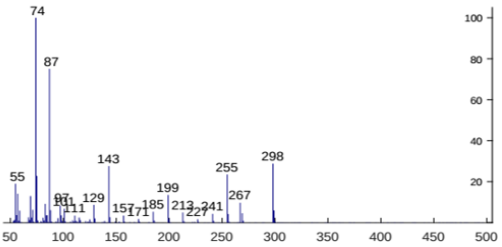

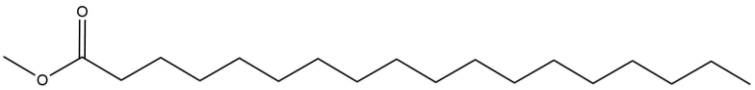

Short name:
Code: EOS-040
ECL: 18,0414
RT: 74,9886

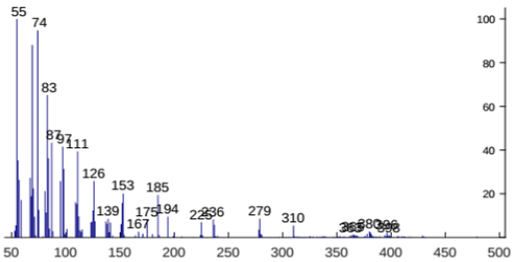

Short name: 18:1 n-6, 11Me
Code: EOM-010
ECL: 18,0598
RT: 75,1466

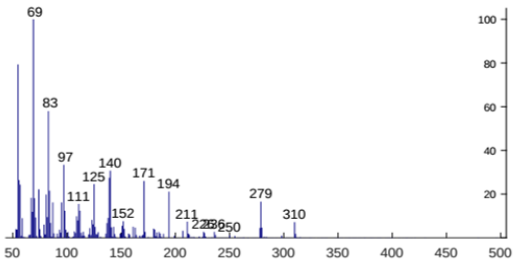

NIST suggestion:

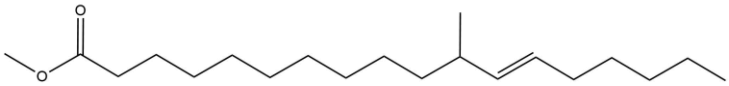

Short name: 19:1 n-x
Code: EOM-011
ECL: 18,0921
RT: 75,4231

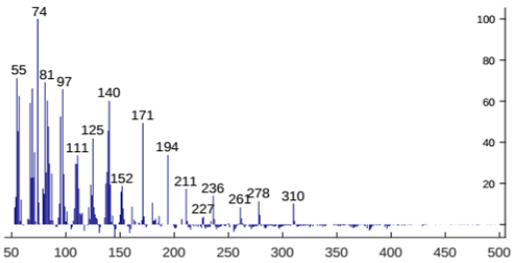

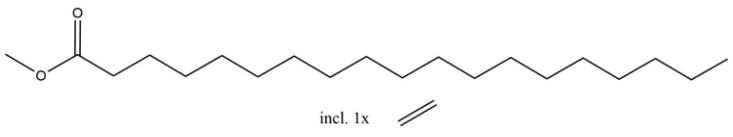

Short name: 19:2 n-x
Code: EOD-002
ECL: 18,1082
RT: 75,5614

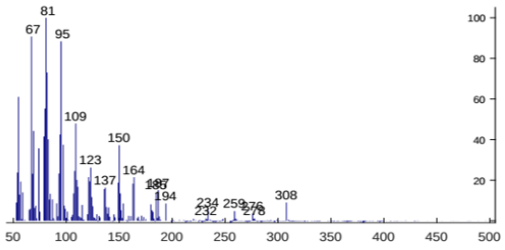

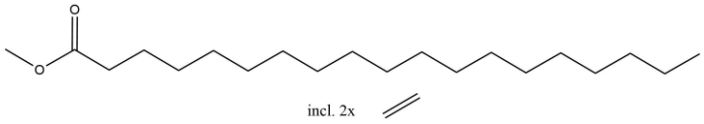

Short name:
Code: UNK-288
ECL: 18,1174
RT: 75,6404

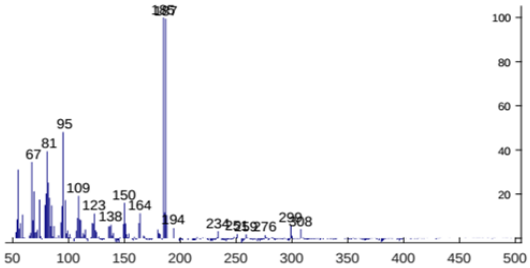

Short name: 19:1 n-x
Code: EOM-012
ECL: 18,1405
RT: 75,8379

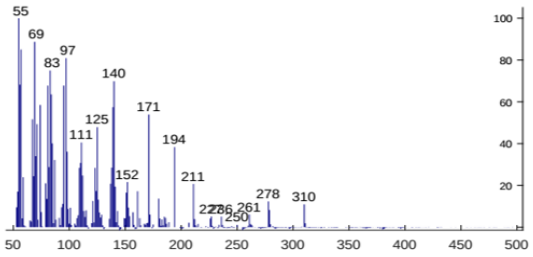

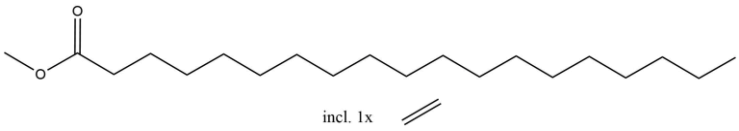

Short name: 19:1 n-x
Code: EOM-013
ECL: 18,1521
RT: 75,9367

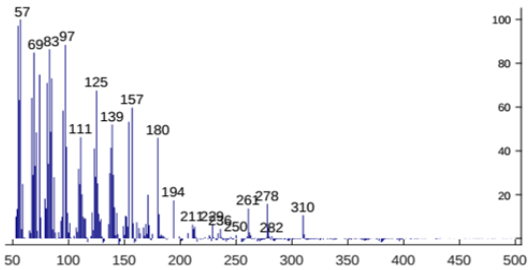

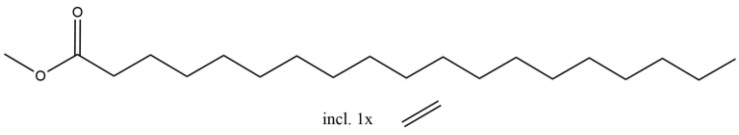

Short name: 19:1 n-x
Code: EOM-014
ECL: 18,1821
RT: 76,1934

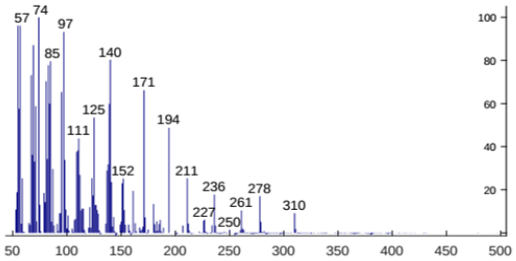

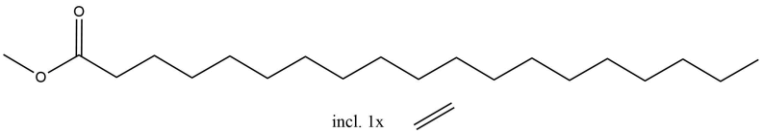

Short name: Br 19:0 (10Me)
Code: EOS-041
ECL: 18,3999
RT: 78,0501

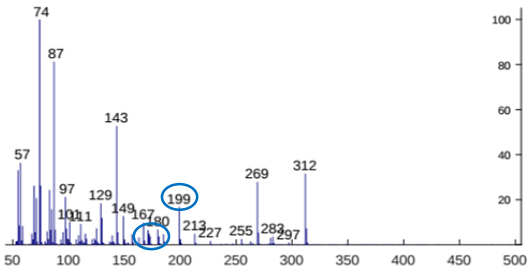

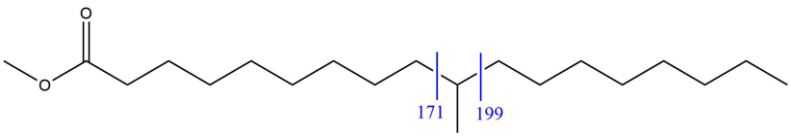

Short name: Br 19:0 (11Me)
Code: EOS-042
ECL: 18,4185
RT: 78,2081

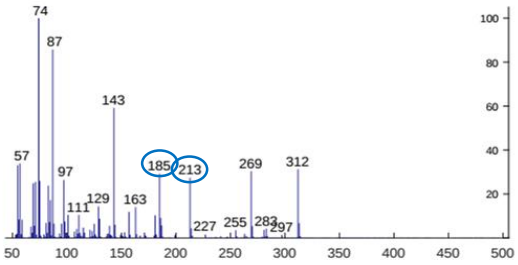

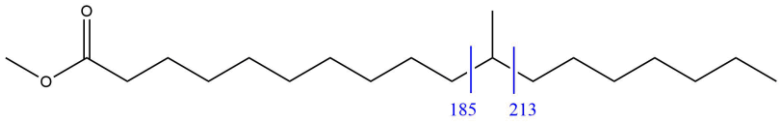

Short name:
Code: EOS-045
ECL: 18,5793
RT: 79,5710

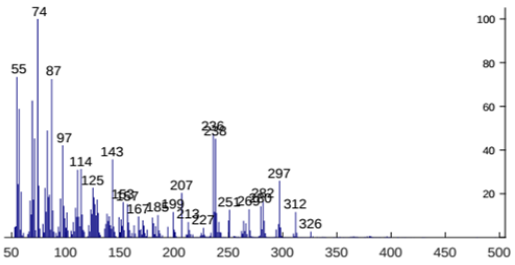

Short name:
Code: EOS-046
ECL: 18,5863
RT: 79,6303

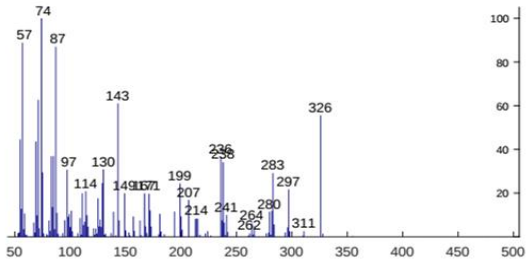

Short name: i-19:0
Code: EOS-043
ECL: 18,6260
RT: 79,9660

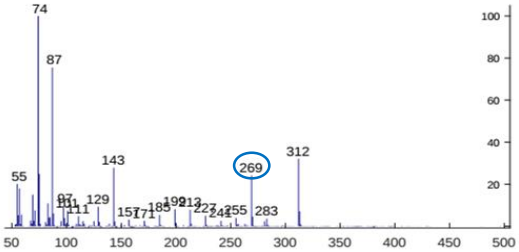

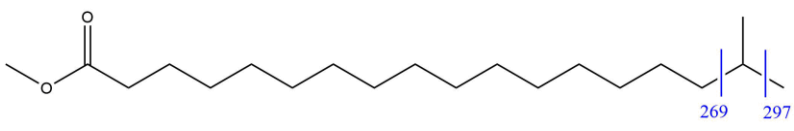

Short name: ai-19:0
Code: EOS-044
ECL: 18,7150
RT: 80,7166

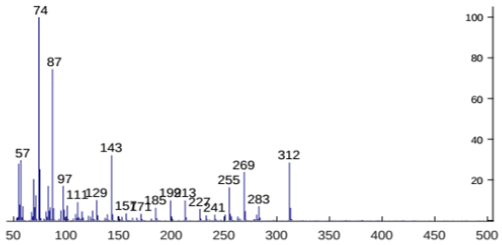

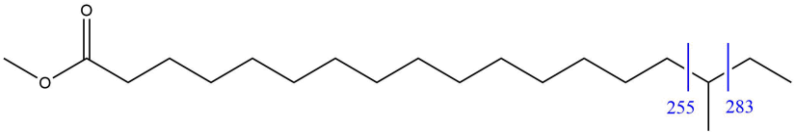

Short name: IS, 19:0
Code: SAN-010
ECL: 19,0710
RT: 83,6992

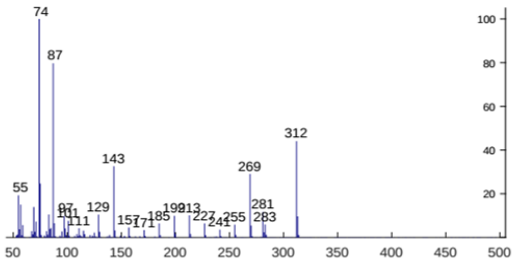

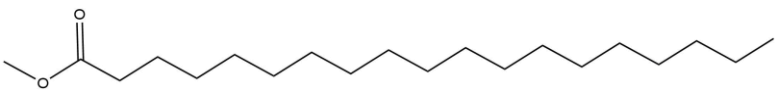

Short name: 20:4 n-6
Code: POU-035
ECL: 19,2775
RT: 85,4176

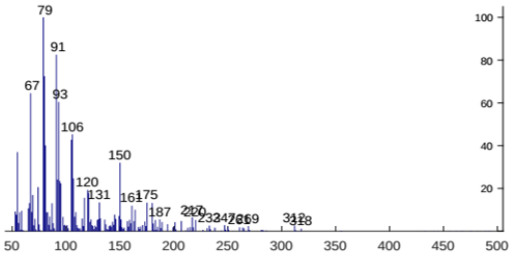

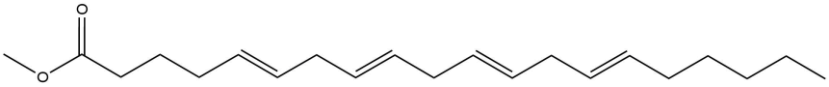

Short name: 20:5 n-3
Code: POU-036
ECL: 19,3346
RT: 85,8916

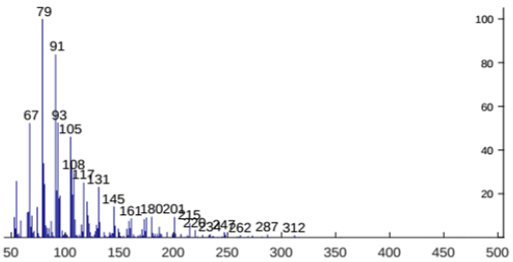

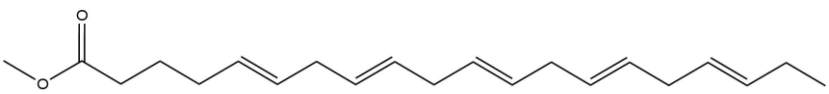

Short name: 20:2 n-6
Code: DIU-028
ECL: 19,5138
RT: 87,3730

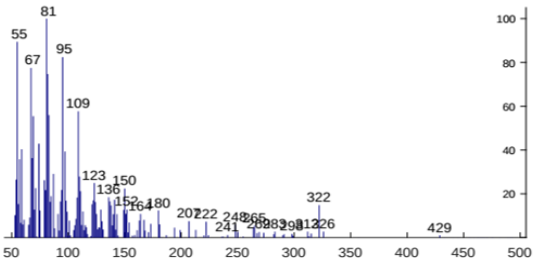

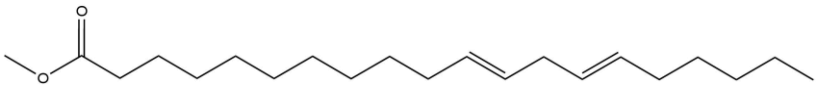

Short name:
Code: EOX-001
ECL: 19,6291
RT: 88,3211

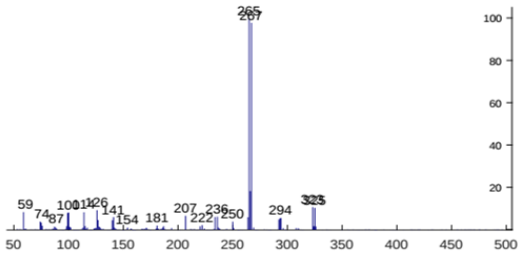

Short name: Br 20:0 (xMe)
Code: EOS-047
ECL: 19,7303
RT: 89,1506

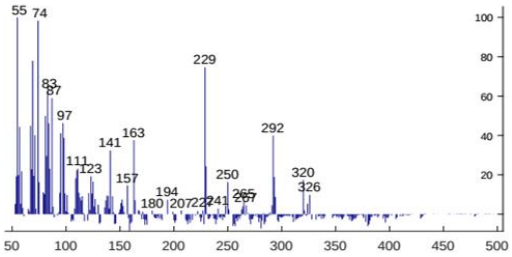

Short name:
Code: EOS-048
ECL: 19,7328
RT: 89,1704

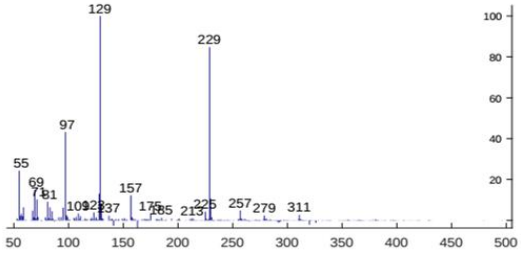

Short name: 20:0
Code: SAN-011
ECL: 19,9951
RT: 91,3036

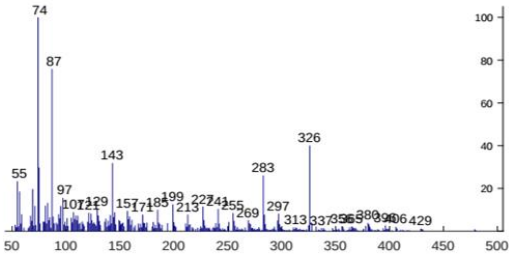

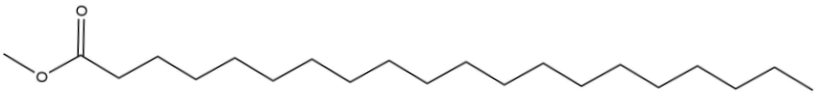

Short name:
Code: EOD-024
ECL: 20,0954
RT: 92,1134

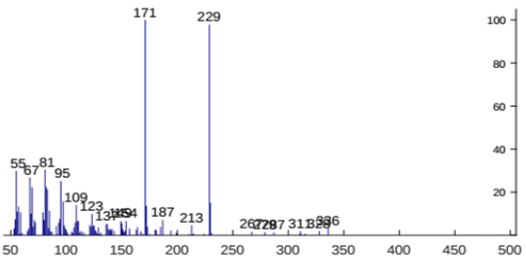

Short name:
Code: EOD-025
ECL: 20,1175
RT: 92,2912

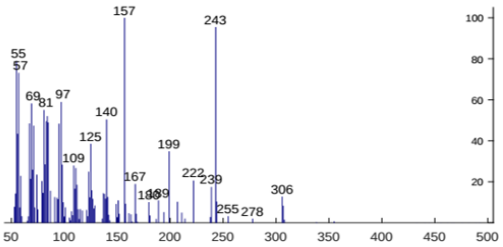

Short name:
Code: EOX-034
ECL: 20,3615
RT: 94,2466

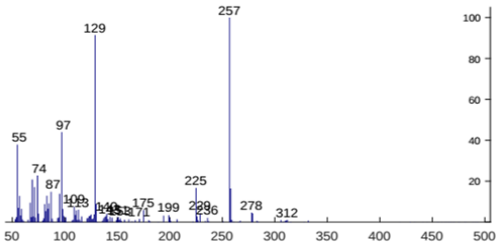

Short name: Br 21:0 (10Me or 12Me)
Code: EOS-049
ECL: 20,3739
RT: 94,3454

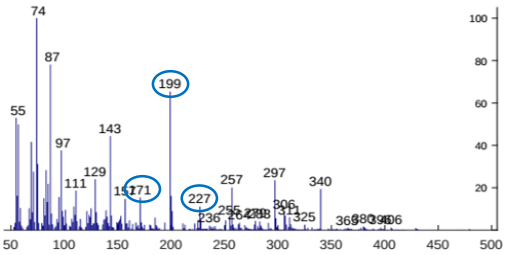

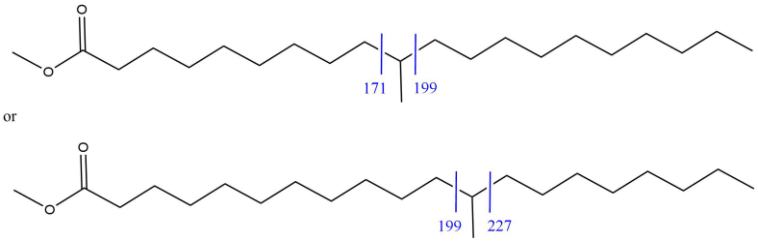

Short name:
Code: EOX-035
ECL: 20,5902
RT: 96,0638

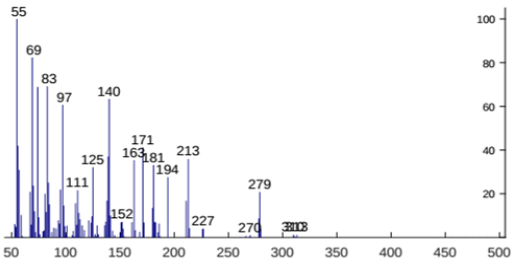

Short name:
Code: EOX-036
ECL: 20,5976
RT: 96,1231

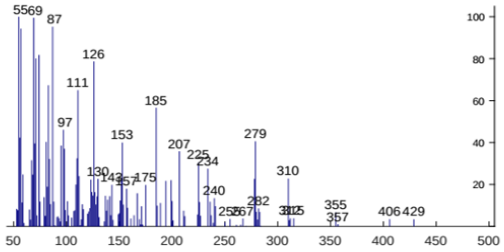

Short name: 21:0
Code: SAN-012
ECL: 20,9949
RT: 99,2438

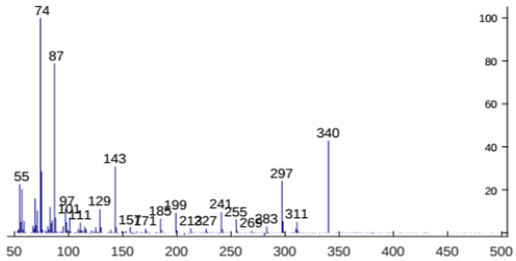

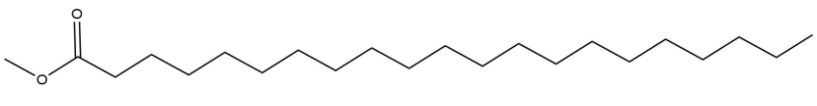

Short name: Br 21:0 (x,x DiMe/x Et)
Code: EOS-050
ECL: 21,0634
RT: 99,7772

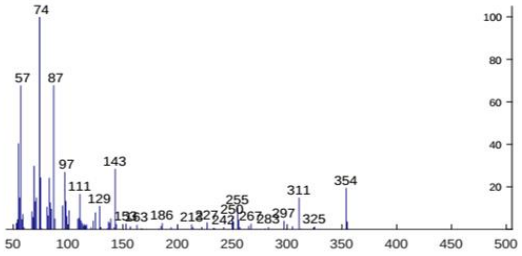

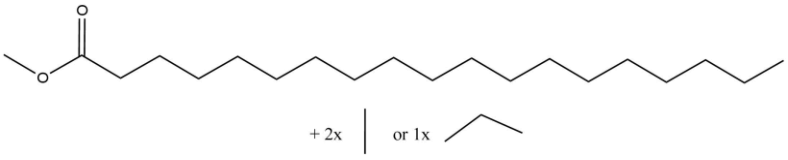

Short name: Br 21:0 (x,x DiMe/x Et)
Code: EOS-051
ECL: 21,0710
RT: 99,8364

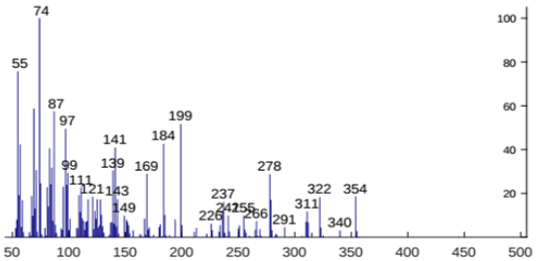

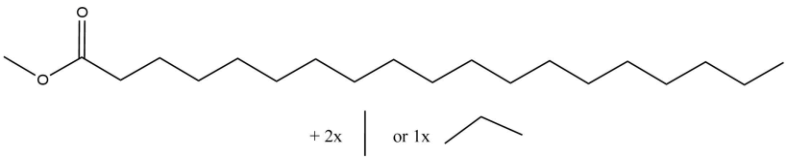

Short name: 22:5 n-6
Code: POU-066
ECL: 21,1015
RT: 100,0734

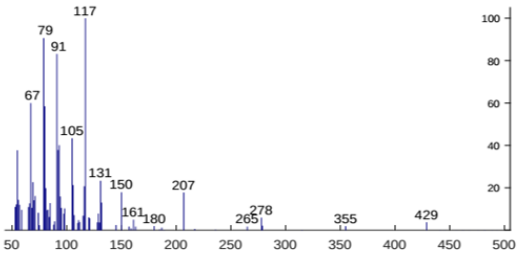

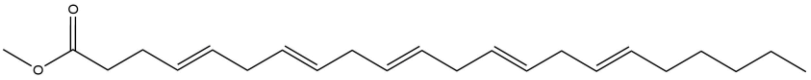

Short name: 22:6 n-3
Code: POU-039
ECL: 21,1727
RT: 100,6265

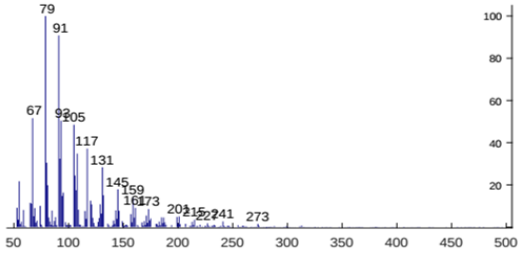

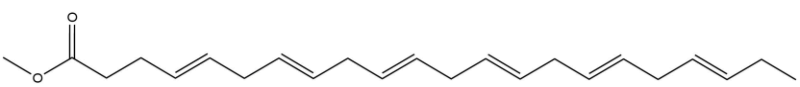

Short name:
Code: EOX-002
ECL: 21,2621
RT: 101,3178

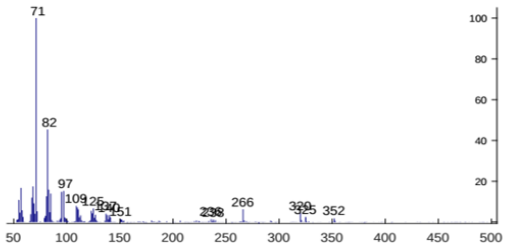

Short name:
Code: EOX-003
ECL: 21,2876
RT: 101,5153

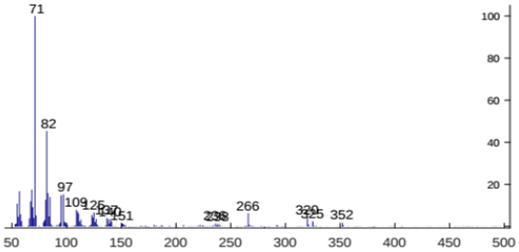

Short name: 22:5 n-3
Code: POU-038
ECL: 21,3158
RT: 101,7326

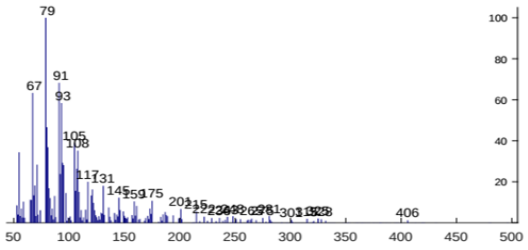

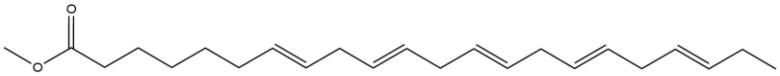

Short name:
Code: EOX-004
ECL: 21,6299
RT: 104,1423

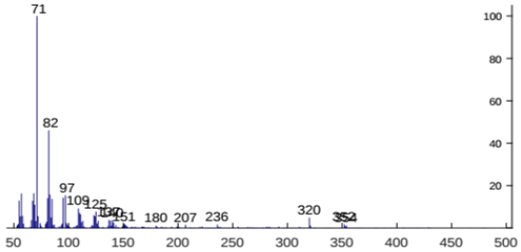

Short name:
Code: EOX-005
ECL: 21,6558
RT: 104,3398

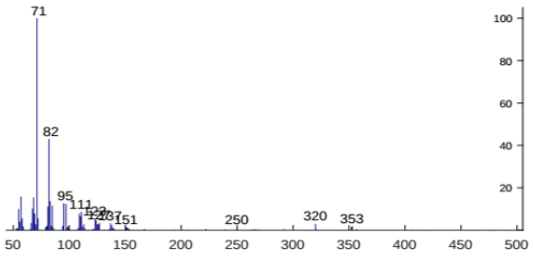

Short name: 22:0
Code: SAN-013
ECL: 22,0026
RT: 106,9668

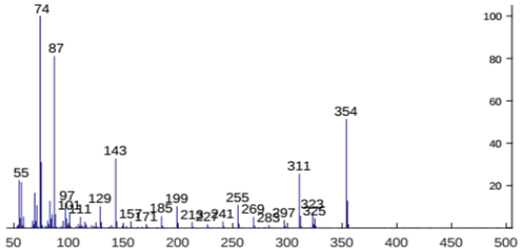

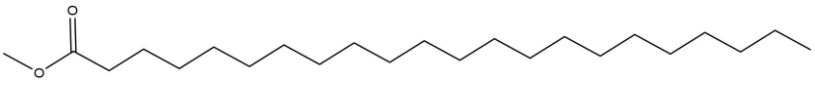

Short name:
Code: EOX-006
ECL: 22,2580
RT: 108,8827

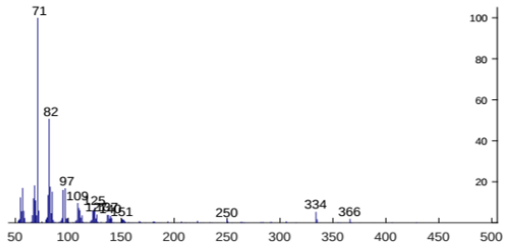

Short name: Br 23:0 (xMe)
Code: EOS-052
ECL: 22,3719
RT: 109,7321

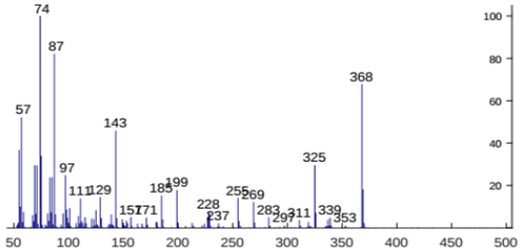

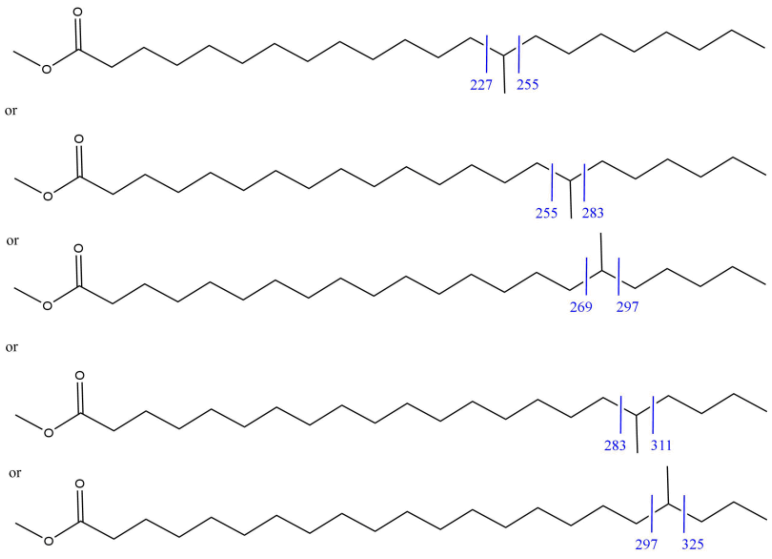

Short name: Br 23:0 (xMe)
Code: EOS-053
ECL: 22,4170
RT: 110,0679

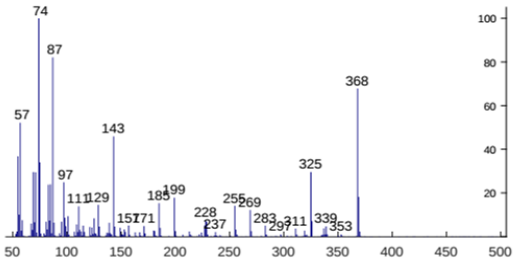

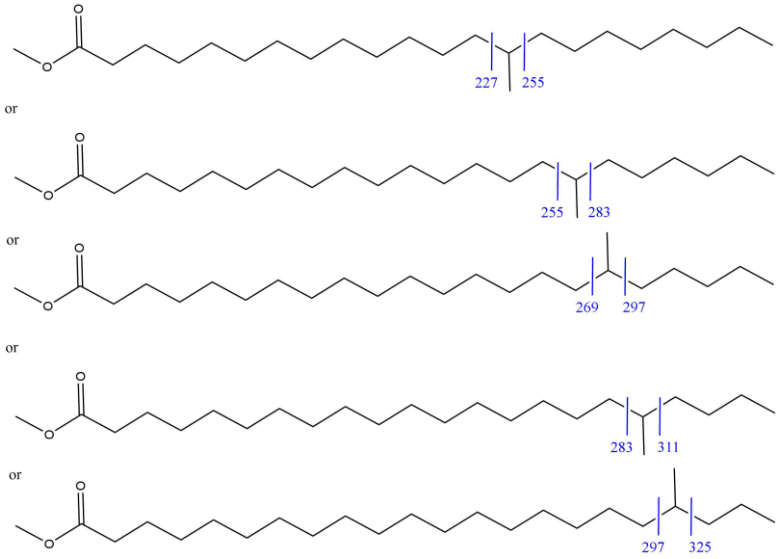

Short name: i-23:0
Code: EOS-054
ECL: 22,6356
RT: 111,6875

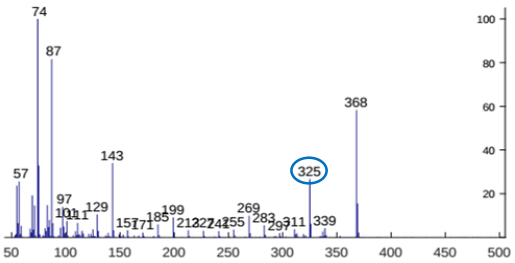

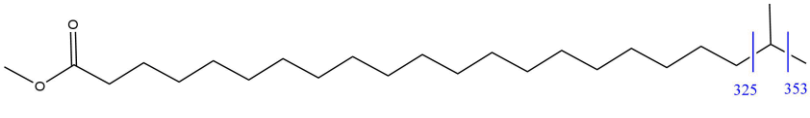

Short name: ai-23:0
Code: EOS-055
ECL: 22,7267
RT: 112,3591

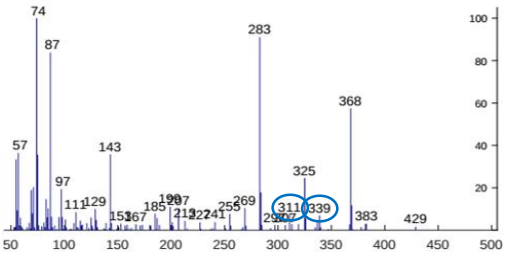

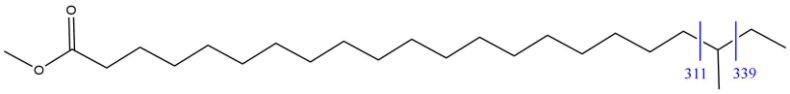

Short name:
Code: EOX-007
ECL: 22,8396
RT: 113,1886

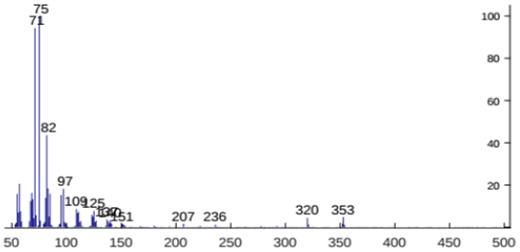

Short name:
Code: EOX-008
ECL: 22,8666
RT: 113,3862

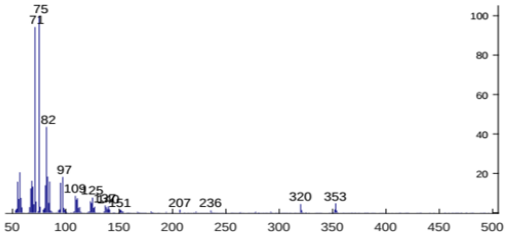

Short name: 23:0
Code: SAN-014
ECL: 22,9963
RT: 114,3343

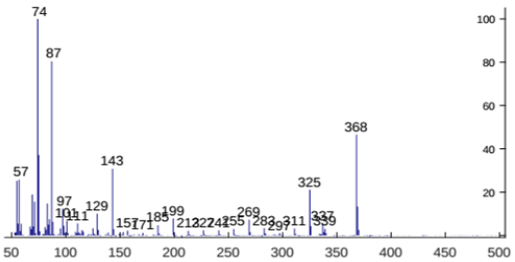

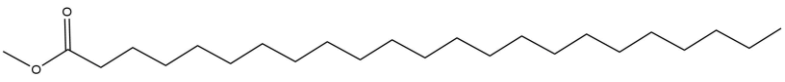

Short name:
Code: EOX-009
ECL: 23,0044
RT: 114,3935

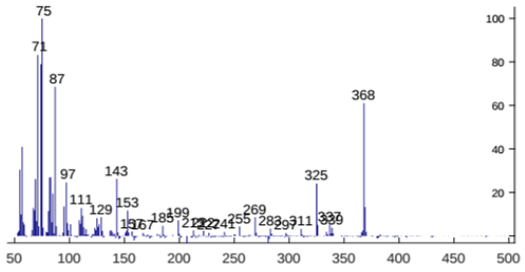

Short name: Br 24:0 (x,x DiMe/x Et)
Code: EOS-056
ECL: 23,0641
RT: 114,8281

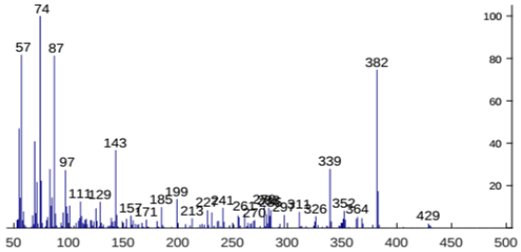

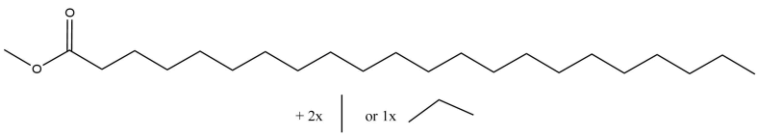

Short name:
Code: EOX-010
ECL: 23,2547
RT: 116,2107

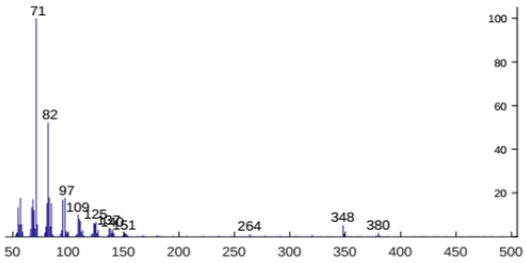

Short name: Br 24:0 (17Me)
Code: EOS-057
ECL: 23,3862
RT: 117,1588

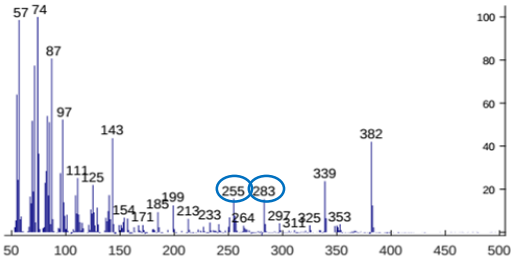

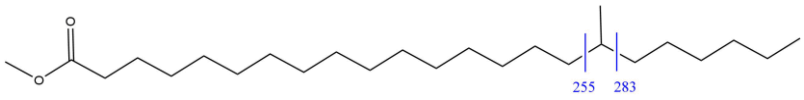

Short name:
Code: EOX-037
ECL: 23,3972
RT: 117,2378

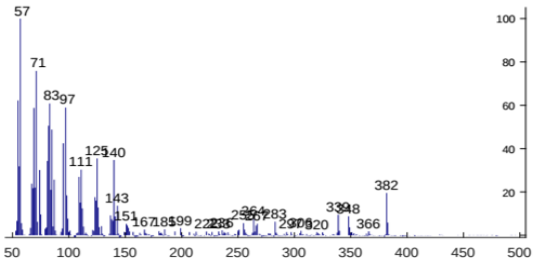

Short name:
Code: EOX-011
ECL: 23,6261
RT: 118,8772

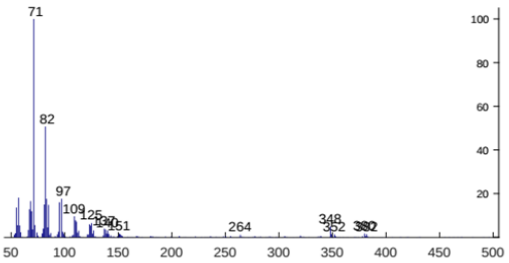

Short name: ai-24:0
Code: EOS-057
ECL: 23,7233
RT: 119,5685

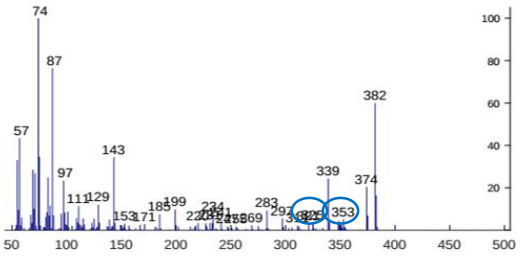

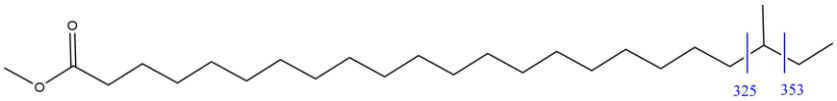

Short name: 24:1 n-x
Code: MOU-571
ECL: 23,8124
RT: 120,2006

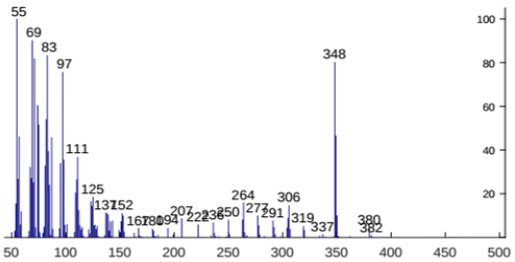

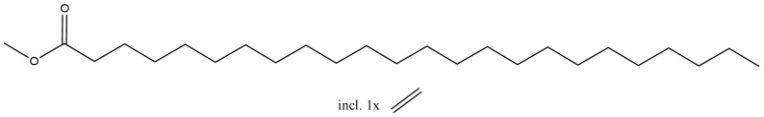

Short name:
Code: EOX-012
ECL: 23,8319
RT: 120,3388

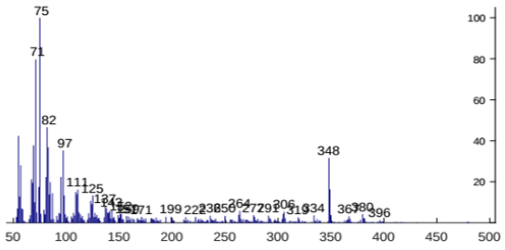

Short name: 24:1 n-x
Code: EOM-015
ECL: 23,9242
RT: 120,9906

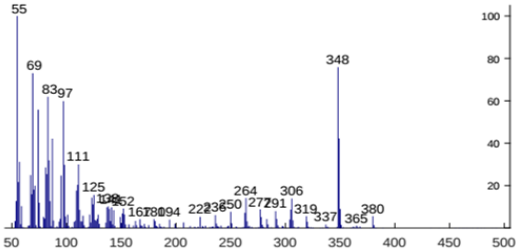

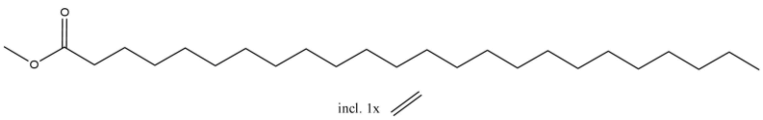

Short name: 24:0
Code: SAN-015
ECL: 24,0000
RT: 121,5239

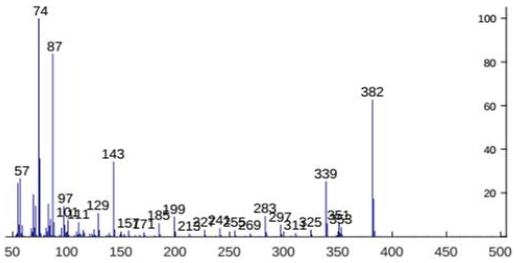

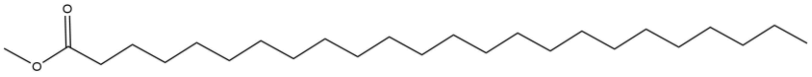

Short name: 25:2 n-x
Code: EOD-003
ECL: 24,1577
RT: 122,6300

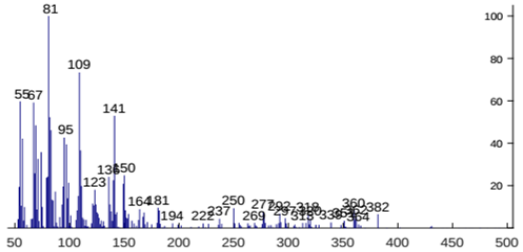

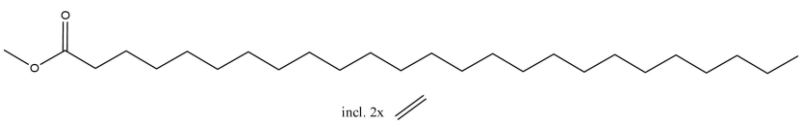

Short name: Br 25:0 (xMe)
Code: EOS-059
ECL: 24,3902
RT: 124,2497

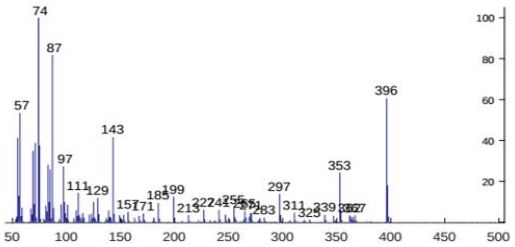

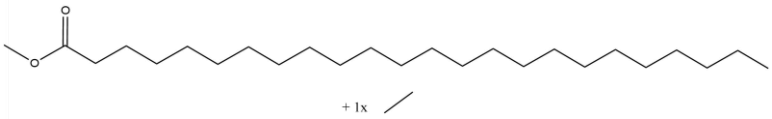

Short name: 25:1 n-x
Code: EOM-016
ECL: 24,4129
RT: 124,4077

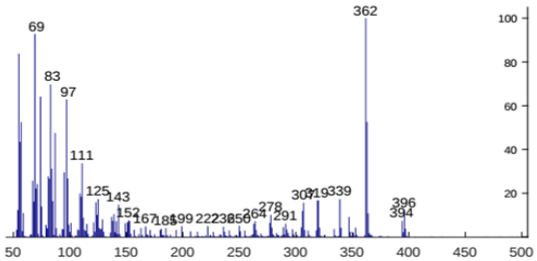

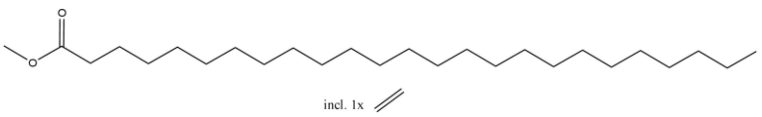

Short name: 25:2 n-x, xMe
Code: EOD-004
ECL: 24,5414
RT: 125,2965

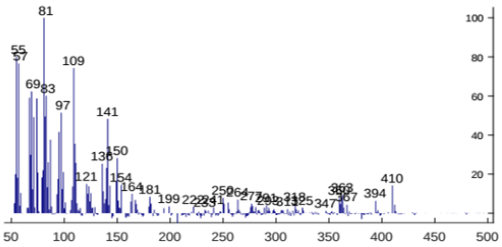

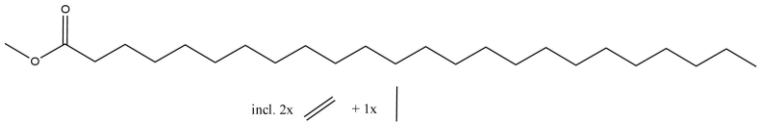

Short name:
Code: EOS-060
ECL: 24,5557
RT: 125,3953

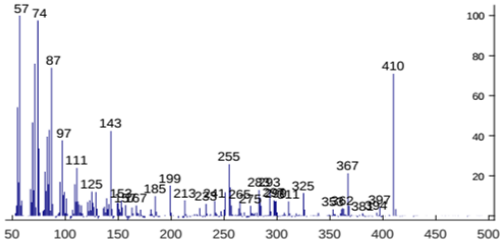

Short name: i-25:0
Code: EOS-061
ECL: 24,6273
RT: 125,8891

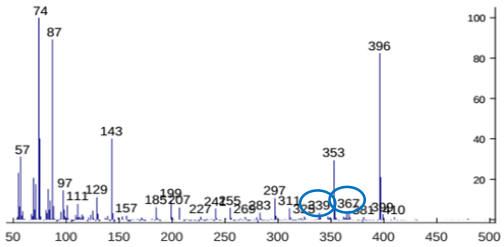

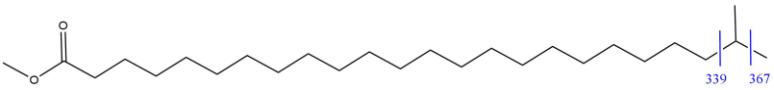

Short name: ai-25:0
Code: EOS-062
ECL: 24,7279
RT: 126,5804

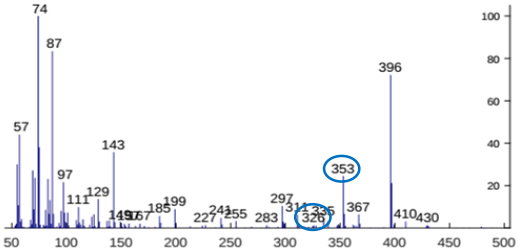

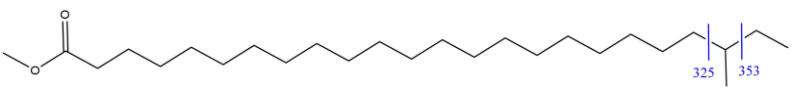

Short name:
Code: EOX-013
ECL: 24,8347
RT: 127,3112

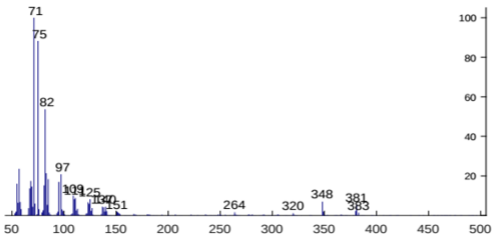

Short name:
Code: EOX-014
ECL: 24,8434
RT: 127,3705

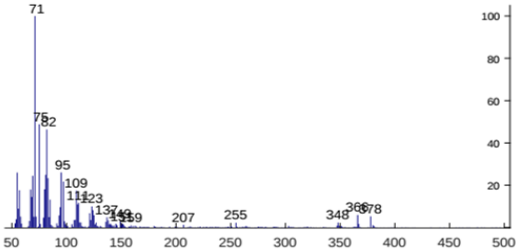

Short name:
Code: EOX-015
ECL: 24,9942
RT: 128,3976

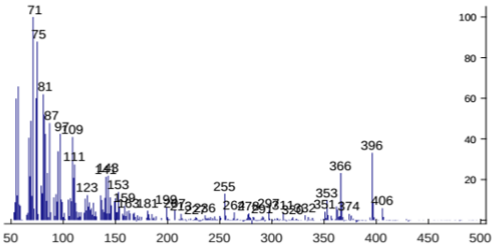

Short name:
Code: EOD-005
ECL: 25,0087
RT: 128,4963

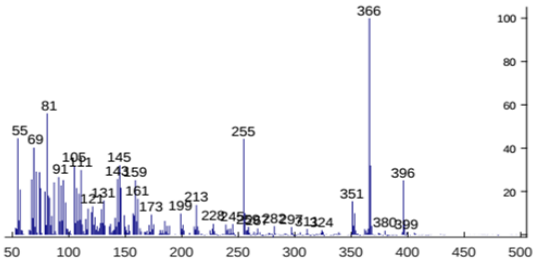

Short name: (Br) 26:2 n-x
Code: EOD-006
ECL: 25,0465
RT: 128,7531

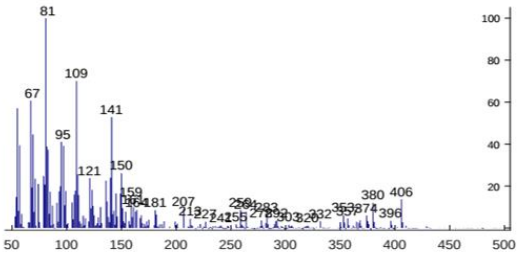

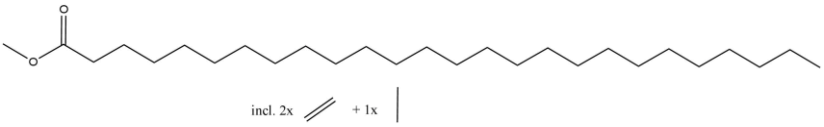

Short name: (Br) 26:2 n-x
Code: EOD-007
ECL: 25,1721
RT: 129,6024

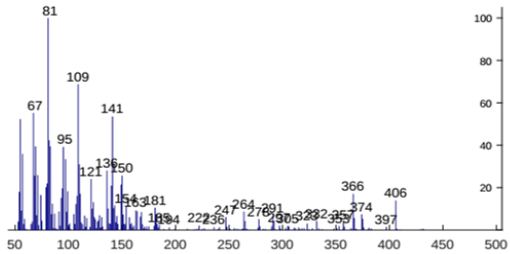

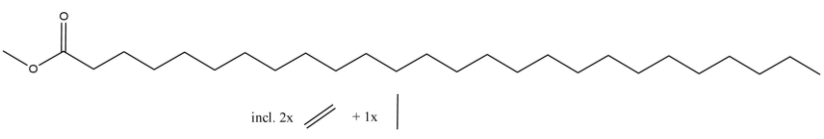

Short name:
Code: EOD-008
ECL: 25,3807
RT: 131,0048

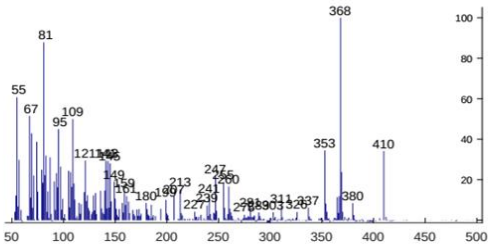

Short name: (Br) 26:2 n-x
Code: EOD-009
ECL: 25,5167
RT: 131,9134

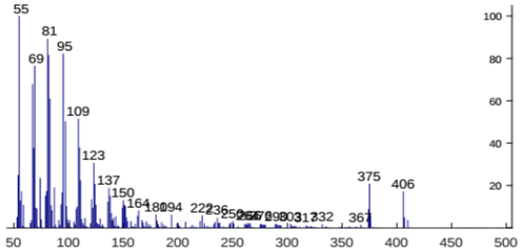

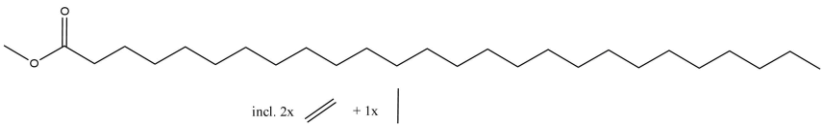

Short name: (Br) 26:2 n-x
Code: EOD-010
ECL: 25,5670
RT: 132,2492

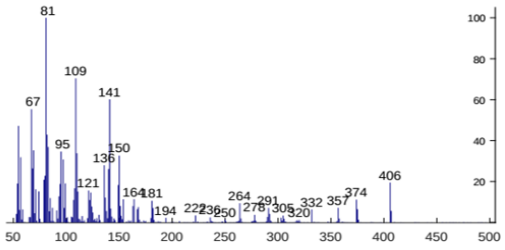

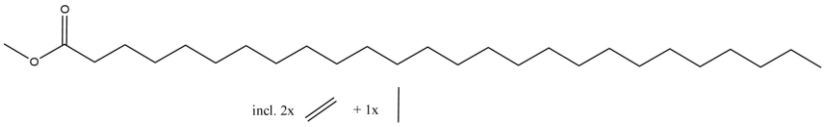

Short name:
Code: EOD-024
ECL: 25,8411
RT: 134,0663

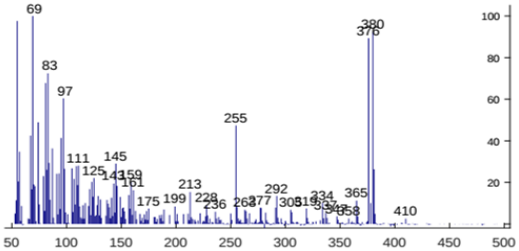

Short name: (Br) 27:2 n-x
Code: EOD-011
ECL: 25,9459
RT: 134,7577

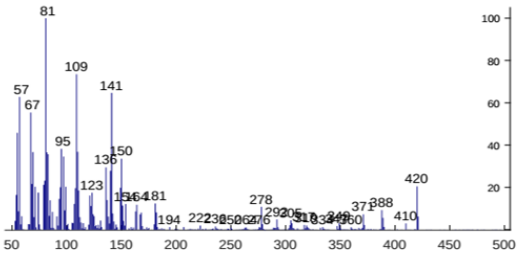

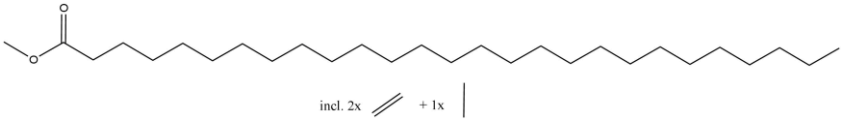

Short name: (Br) 27:2 n-x
Code: EOD-012
ECL: 25,9880
RT: 135,0342

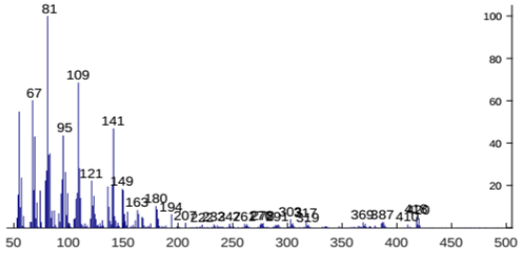

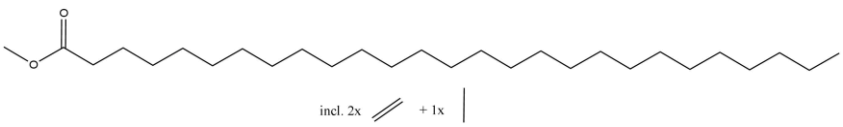

Short name: (Br) 27:2 n-x
Code: EOD-013
ECL: 26,0210
RT: 135,2515

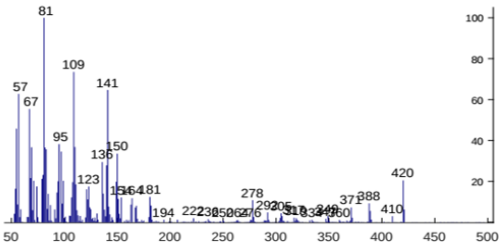

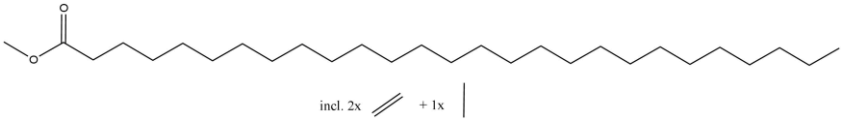

Short name: (Br) 27:2 n-x
Code: EOD-014
ECL: 26,1113
RT: 135,8440

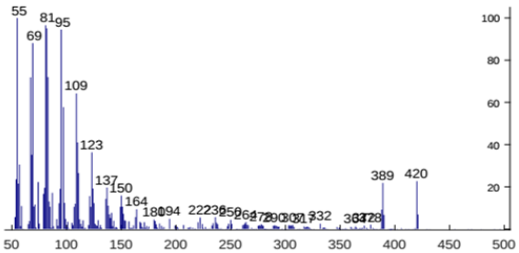

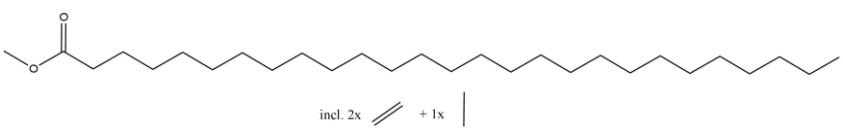

Short name: (Br) 27:2 n-x
Code: EOD-015
ECL: 26,1898
RT: 136,3576

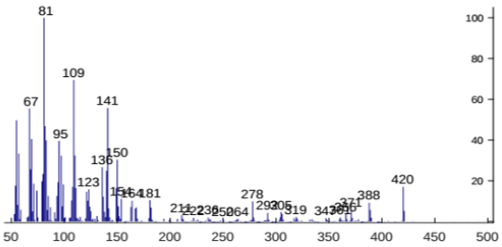

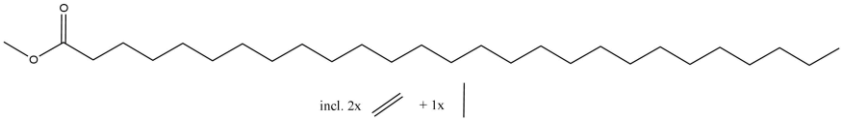

Short name:
Code: EOD-016
ECL: 26,2988
RT: 137,0686

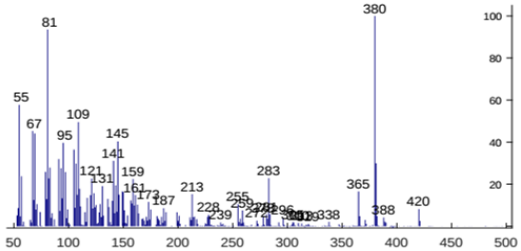

Short name:
Code: EOD-017
ECL: 26,3291
RT: 137,2661

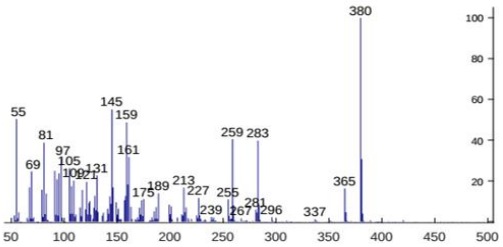

Short name:
Code: EOD-018
ECL: 26,3777
RT: 137,5822

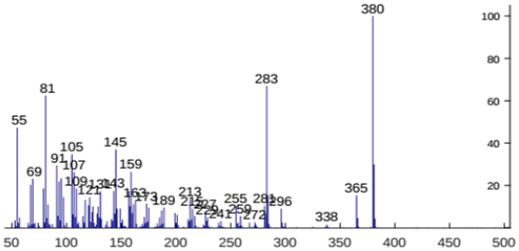

Short name: (Br) 27:2 n-x
Code: EOD-019
ECL: 26,5727
RT: 138,8463

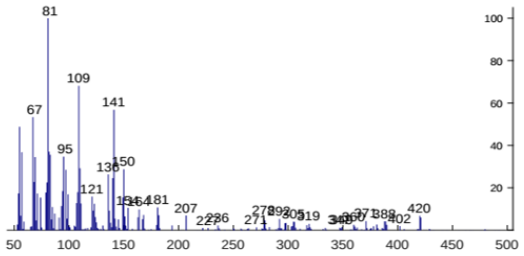

Short name: (Br) 27:2 n-x
Code: EOD-020
ECL: 26,6277
RT: 139,2018

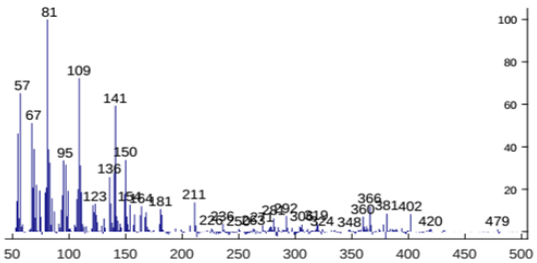

Short name: Sterol
Code: EOX-16
ECL: 26,9752
RT: 141,4338

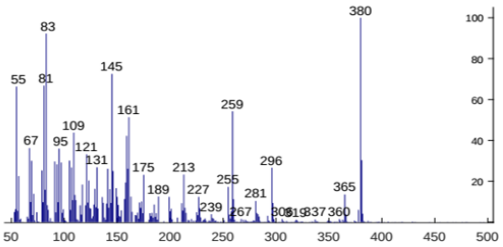

Short name: Sterol
Code: EOX-017
ECL: 27,0278
RT: 141,7696

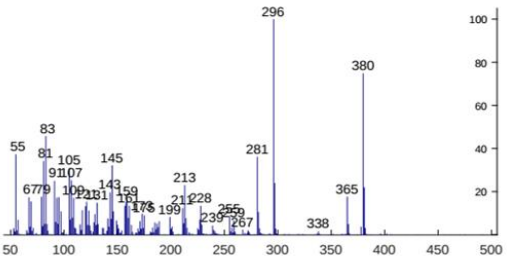

Short name: Sterol
Code: EOX-18
ECL: 27,3605
RT: 143,8830

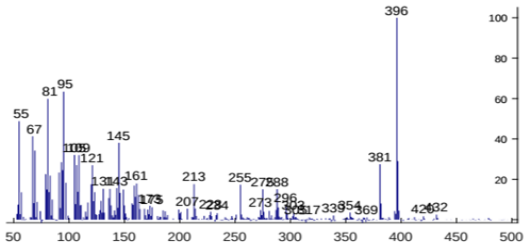

Short name:
Code: EOD-021
ECL: 27,5076
RT: 144,8113

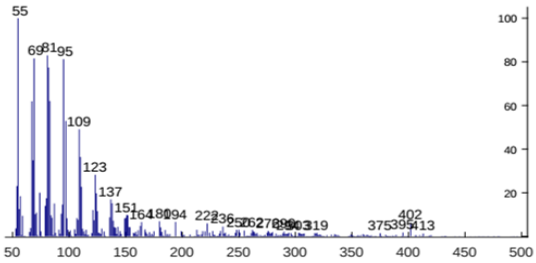

Short name: Sterol
Code: EOX-019
ECL: 27,7909
RT: 146,5890

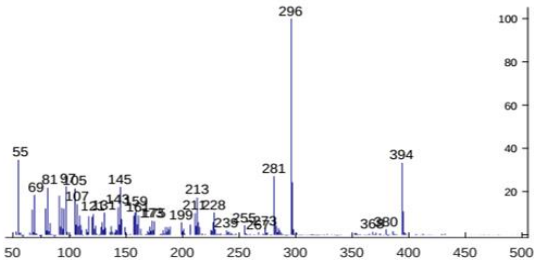

Short name:
Code: EOD-022
ECL: 27,9587
RT: 147,6359

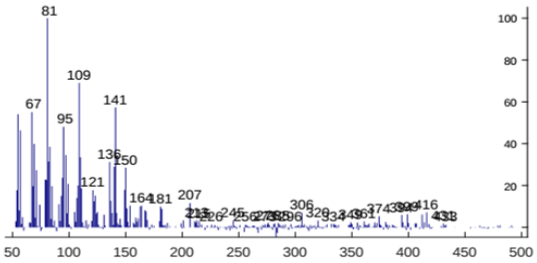

Short name:
Code: EOD-023
ECL: 27,9746
RT: 147,7346

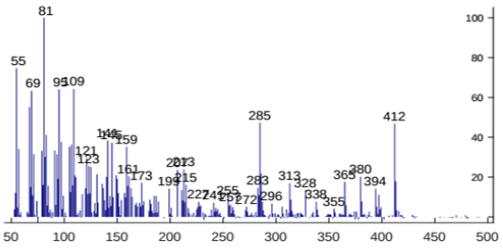

Short name: Sterol
Code: EOX-020
ECL: 27,9936
RT: 147,8531

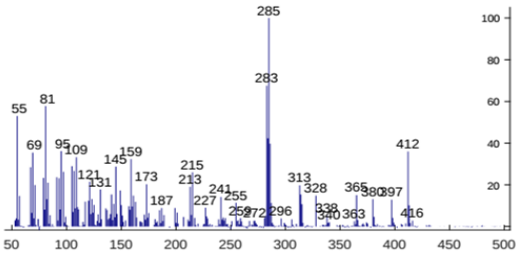

Short name: Sterol
Code: EOX-021
ECL: 28,0540
RT: 148,2284

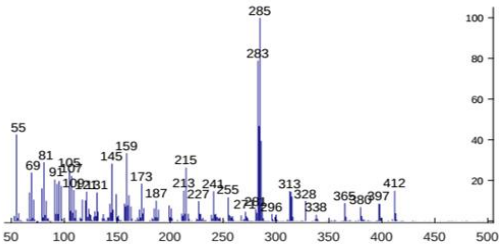

Short name: Sterol
Code: EOX-022
ECL: 28,5182
RT: 151,0924

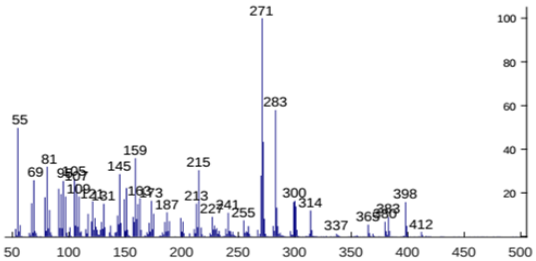

Short name: Sterol
Code: EOX-023
ECL: 28,5730
RT: 151,4282

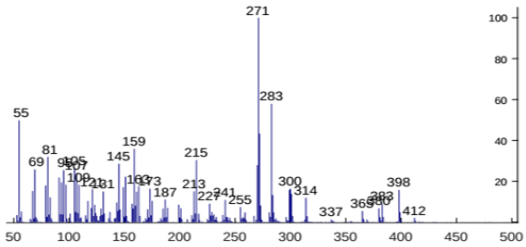

Short name: Sterol
Code: EOX-024
ECL: 28,6052
RT: 151,6257

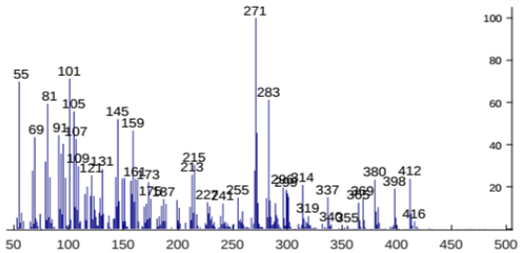

Short name: Sterol
Code: EOX-025
ECL: 28,6568
RT: 151,9418

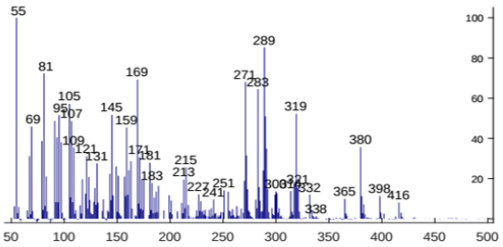

Short name: Sterol
Code: EOX-026
ECL: 28,7022
RT: 152,2183

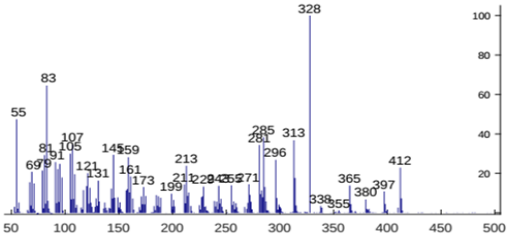

Short name: Sterol
Code: EOX-027
ECL: 29,2396
RT: 155,4773

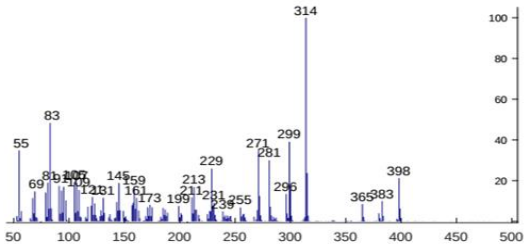

Short name: Sterol
Code: EOX-028
ECL: 29,3217
RT: 155,9711

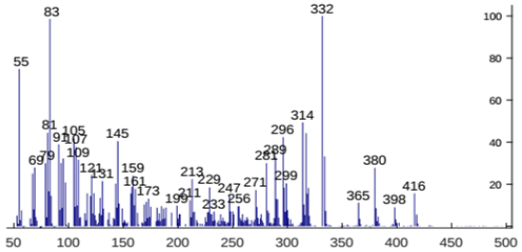

Short name:
Code: EOX-029
ECL: 31,9517
RT: 171,2986

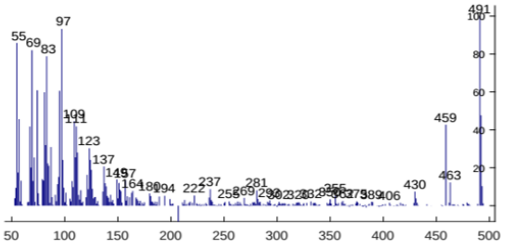

Short name:
Code: EOX-030
ECL: 32,1407
RT: 172,3652

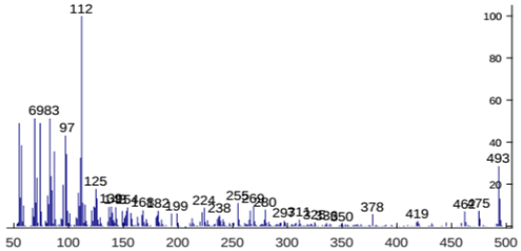

Appendix D

PCA Score and loading plots of the individual treatments and the individual sampling points.

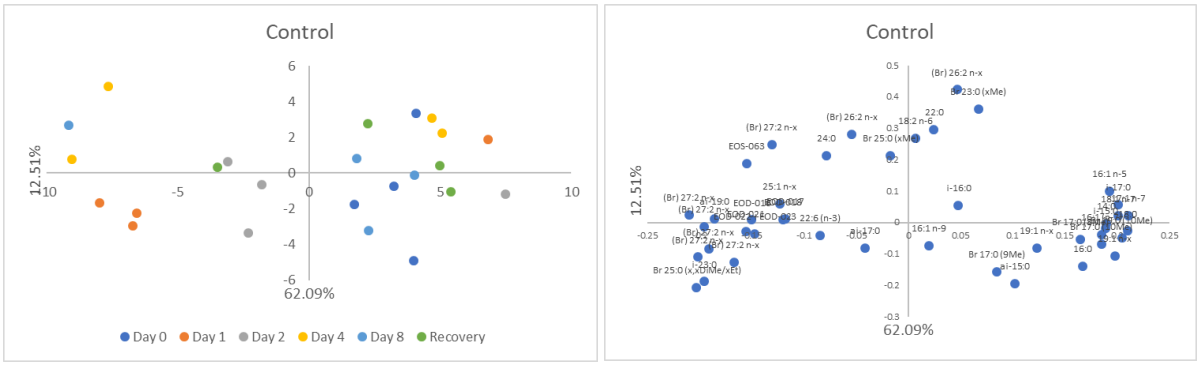

Figure D1: PCA score and loading plot of the control sponges.

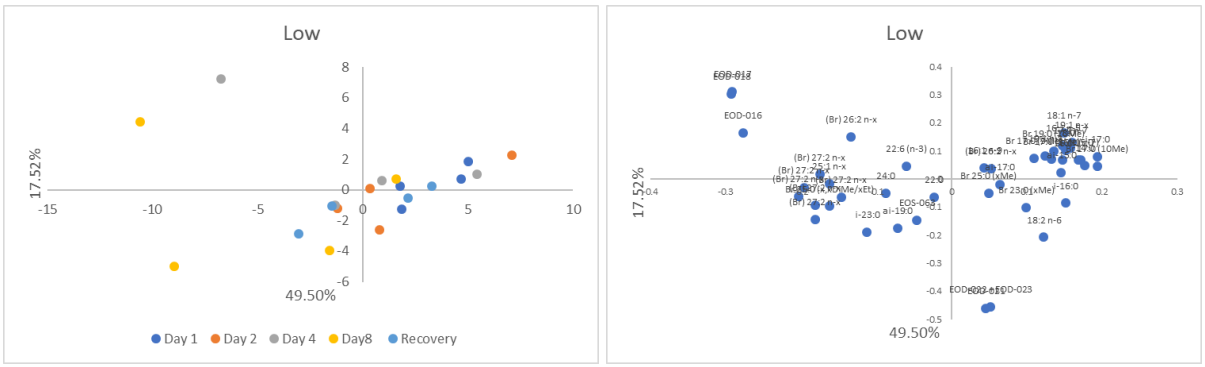

Figure D2: PCA score and loading plot of the sponges exposed to low concentrations of PAH.

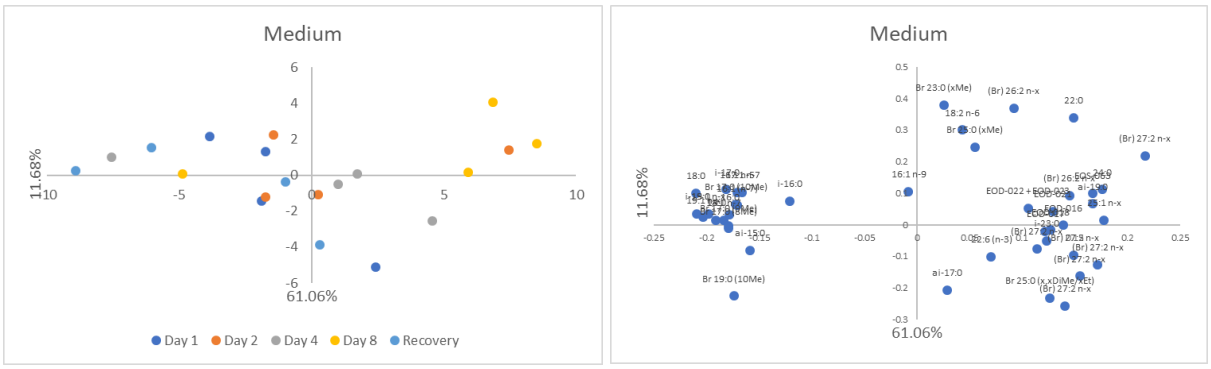

Figure D3: PCA score and loading plot of the sponges exposed to medium concentrations of PAH.

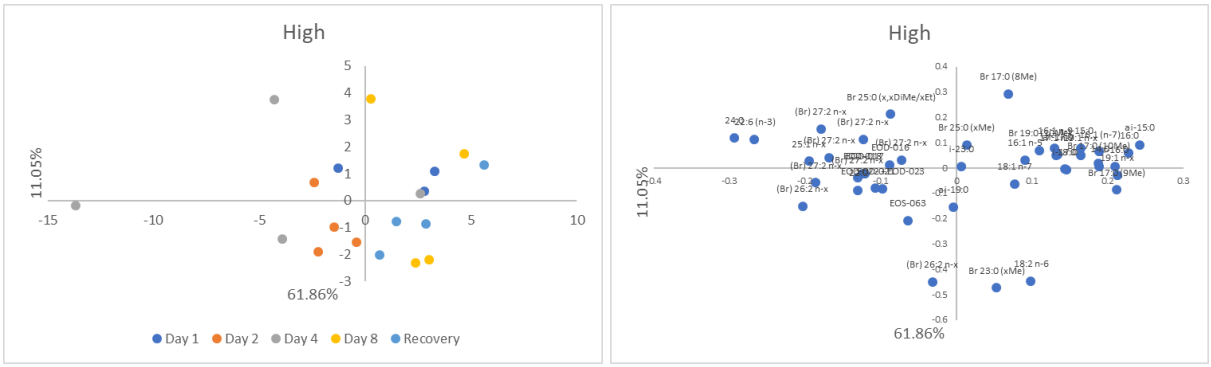

Figure D4: PCA score and loading plot of the sponges exposed to high concentrations of PAH.

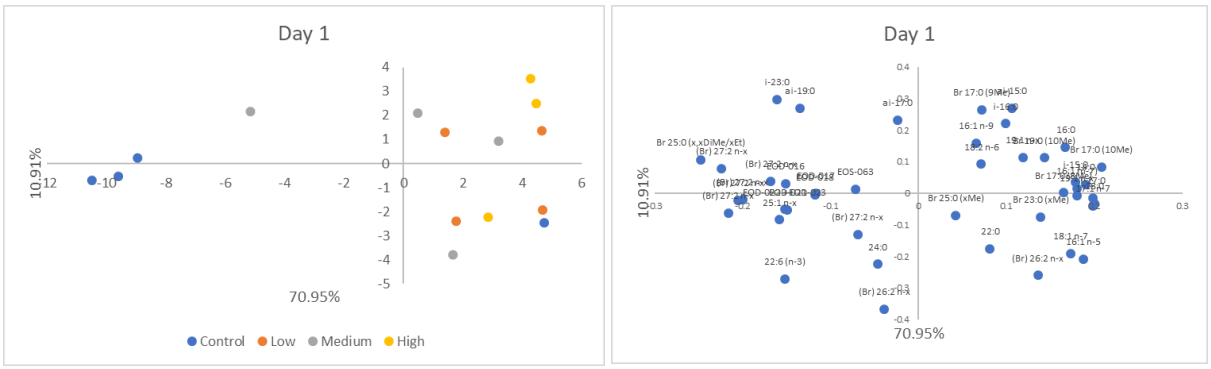

Figure D5: PCA score and loading plot of the sponges exposed to dispersed oil for one day.

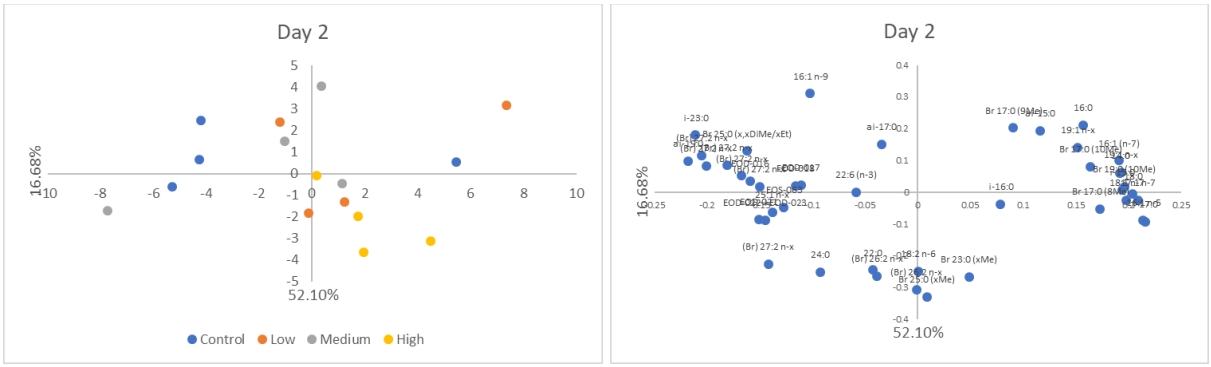

Figure D6: PCA score and loading plot of the sponges exposed to dispersed oil for two days.

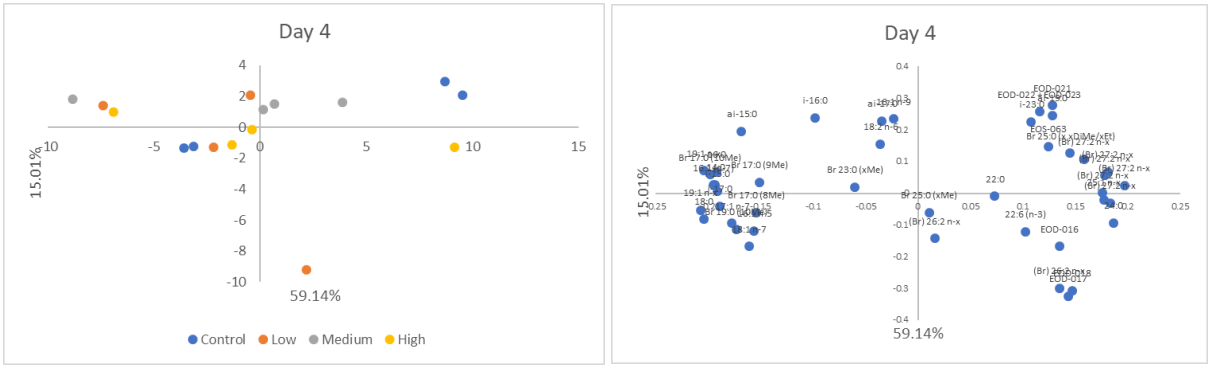

Figure D7: PCA score and loading plot of the sponges exposed to dispersed oil for four days.

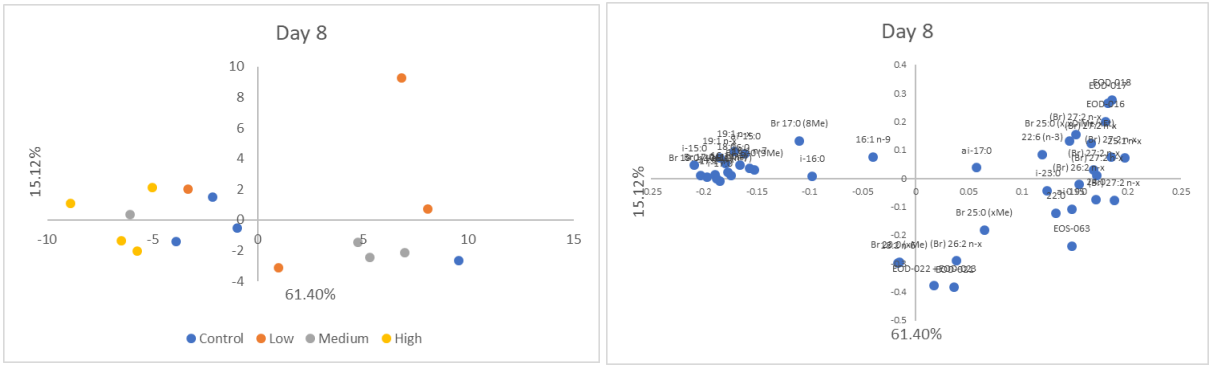

Figure D8: PCA score and loading plot of the sponges exposed to dispersed oil for eight days.

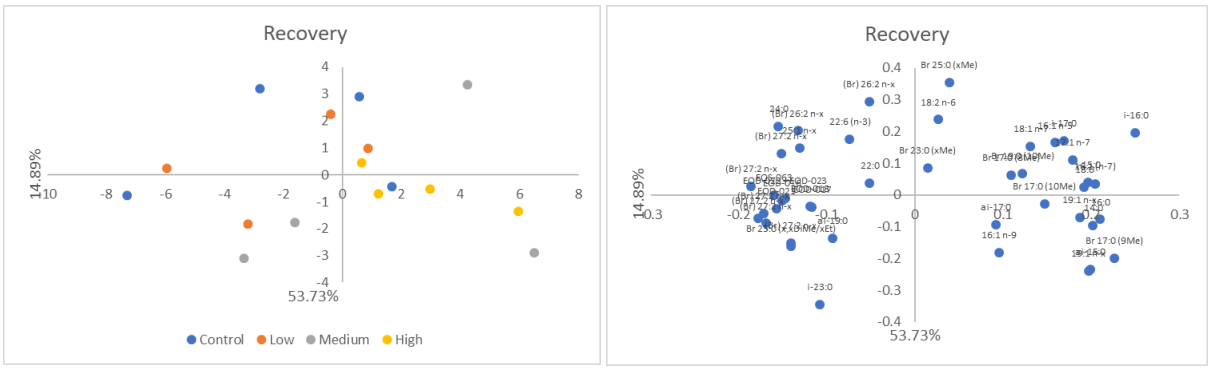

Figure D9: PCA score and loading plot of the sponges exposed to dispersed oil for eight days, then left for a 30-day recovery.

Appendix E

Presentation of the FA accounting for more than 1% of the total FA. Mean values and standard deviations are calculated from all control samples (n=20) and all high samples (n=19). Some sterols and unknowns are also pose more than 1% of the total lipids, but are not included in this table.

Code:	Short name:	Control:	High:	Significant difference (t-test, $p \leq 0.05$):
SAN-005	14:0	4.10 ± 1.10	5.23 ± 0.82	TRUE, higher
SAB-078	i-15:0	3.55 ± 1.10	4.70 ± 0.72	TRUE, higher
SAB-077	ai-15:0	4.90 ± 0.74	5.90 ± 1.08	TRUE, higher
SAB-072	i-16:0	9.30 ± 0.48	10.10 ± 0.98	TRUE, higher
SAN-007	16:0	6.40 ± 1.02	7.42 ± 1.00	TRUE, higher
EOS-025	Br 17:0 (8Me)	2.80 ± 1.04	3.36 ± 1.19	FALSE
EOS-026	Br 17:0 (9Me)	2.41 ± 0.77	3.46 ± 1.10	TRUE, higher
EOS-027	Br 17:0 (10Me)	6.05 ± 1.12	7.04 ± 0.84	TRUE, higher
SAB-074	i-17:0	4.93 ± 1.17	5.94 ± 0.66	TRUE, higher
SAB-073	ai-17:0	15.51 ± 1.02	15.36 ± 0.79	FALSE
SAN-009	18:0	5.01 ± 1.19	6.09 ± 0.66	TRUE, higher
EOS-042	Br 19:0 (10Me)	4.12 ± 1.19	5.05 ± 0.66	TRUE, higher
EOS-044	ai-19:0	8.34 ± 1.17	7.56 ± 0.67	TRUE, lower
SAN-013	22:0	13.77 ± 1.21	13.33 ± 0.87	FALSE
EOS-052	Br 23:0 (xMe)	10.69 ± 1.08	11.08 ± 0.91	FALSE
EOS-054	i-23:0	7.01 ± 1.35	6.45 ± 0.63	FALSE
SAN-015	24:0	10.59 ± 0.67	9.89 ± 1.31	FALSE
EOS-063		7.87 ± 1.21	7.34 ± 0.70	FALSE
EOS-059	Br 25:0 (xMe)	11.55 ± 0.85	11.36 ± 0.53	FALSE
EOS-060	Br 25:0 (x,xDiMe/xEt)	4.48 ± 1.32	3.46 ± 0.59	TRUE, lower
MOU-275	16:1 n-9	4.07 ± 1.14	4.03 ± 0.73	FALSE
MOU-021	16:1 n-7	5.89 ± 1.09	6.98 ± 0.88	TRUE, higher
MOU-255	16:1 n-5	2.77 ± 1.21	3.75 ± 0.56	TRUE, higher
MOU-022	17:1 n-7	3.08 ± 1.22	4.17 ± 0.65	TRUE, higher
MOU-070	18:1 n-7	7.50 ± 1.19	8.25 ± 0.58	TRUE, higher
EOM-013	19:1 n-x	4.01 ± 1.14	5.06 ± 0.74	TRUE, higher
EOM-014	19:1 n-x	3.65 ± 0.86	4.69 ± 0.98	TRUE, higher
EOM-016	25:1 n-x	9.35 ± 0.99	8.23 ± 0.88	TRUE, lower
DIU-027	18:2 n-6	9.07 ± 0.75	9.49 ± 0.96	FALSE
EOD-009	(Br) 26:2 n-x	7.81 ± 0.88	7.08 ± 1.09	TRUE, lower
EOD-010	(Br) 26:2 n-x	9.49 ± 1.12	9.55 ± 0.92	FALSE
EOD-011	(Br) 27:2 n-x	12.39 ± 1.04	11.72 ± 0.83	TRUE, lower
EOD-012	(Br) 27:2 n-x	4.29 ± 1.33	3.34 ± 0.52	TRUE, lower
EOD-013	(Br) 27:2 n-x	5.60 ± 1.09	4.55 ± 0.83	TRUE, lower
EOD-014	(Br) 27:2 n-x	5.21 ± 1.11	4.10 ± 0.77	TRUE, lower
EOD-015	(Br) 27:2 n-x	4.63 ± 1.21	3.55 ± 0.69	TRUE, lower
EOD-016		6.75 ± 0.89	5.92 ± 0.57	TRUE, lower
EOD-017		5.28 ± 0.70	4.60 ± 0.55	TRUE, lower
EOD-018		5.40 ± 0.71	4.72 ± 0.56	TRUE, lower
EOD-020	(Br) 27:2 n-x	5.63 ± 1.18	4.60 ± 0.68	TRUE, lower
EOD-021		6.64 ± 0.99	5.96 ± 0.67	TRUE, lower

EOD-022 + EOD-023		6.59 ± 0.99	5.86 ± 0.68	TRUE, lower
POU-039	22:6 (n-3)	3.47 ± 1.02	2.70 ± 1.24	FALSE

Appendix F

A presentation of the chromatograms of the total FA and fractions 1-9. Chromatograms were obtained using an Agilent 7890A GC coupled with a FID detector. The GC column was an Agilent 122-5062 DB-5 (60 m · 0.25 mm · 0.25 µm) and the carrier gas was helium at a constant flow rate of 1 mL/min. 5-12.5 µL samples (depending on lipid content) were injected at 280°C using an automatic liquid sampler. The oven temperature was held at 60°C and ramped to 130°C at a rate of 60°C/min, then ramped to 325°C at 1°C/min rate and held at this temperature for 7 min. The detector temperature was 300°C.

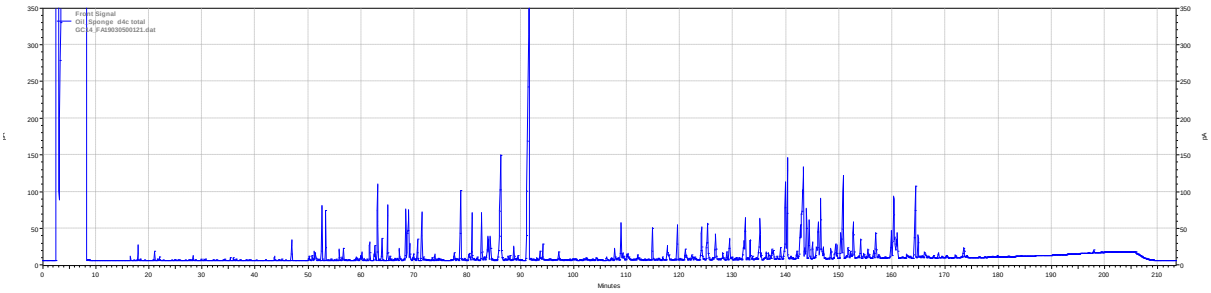

Figure F1: Chromatogram of the total lipid extract.

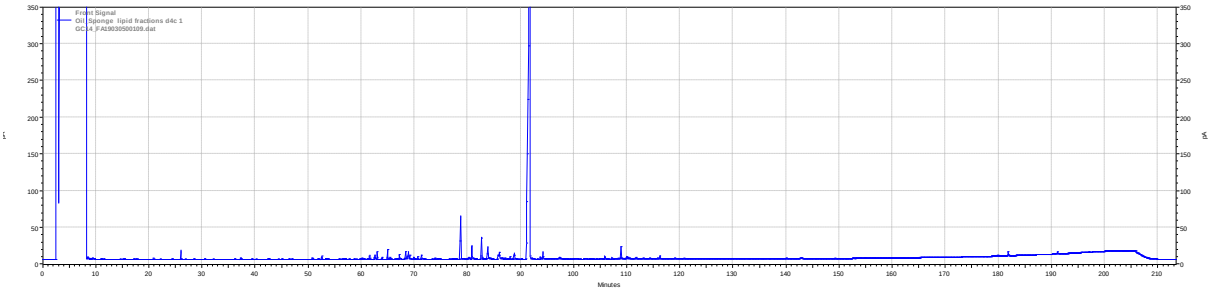

Figure F2: Chromatogram of fraction 1 from the total lipid extract.

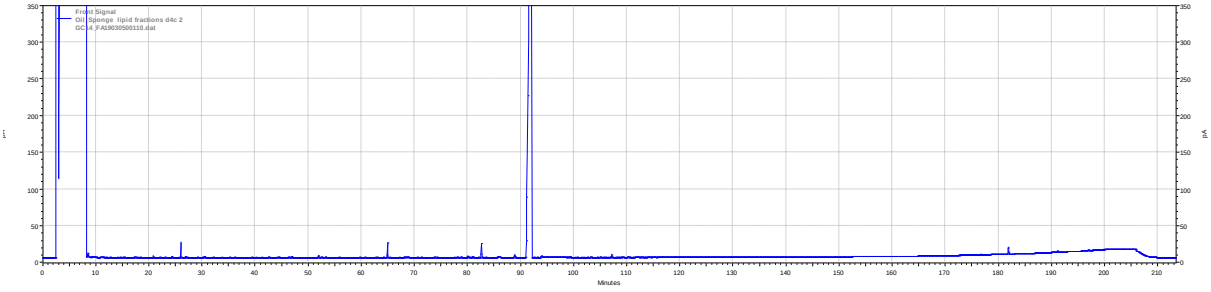

Figure F3: Chromatogram of fraction 2 from the total lipid extract.

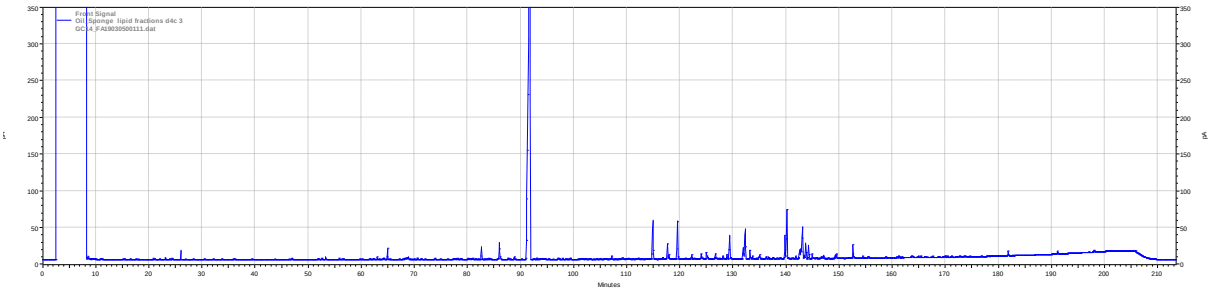

Figure F4: Chromatogram of fraction 3 from the total lipid extract.

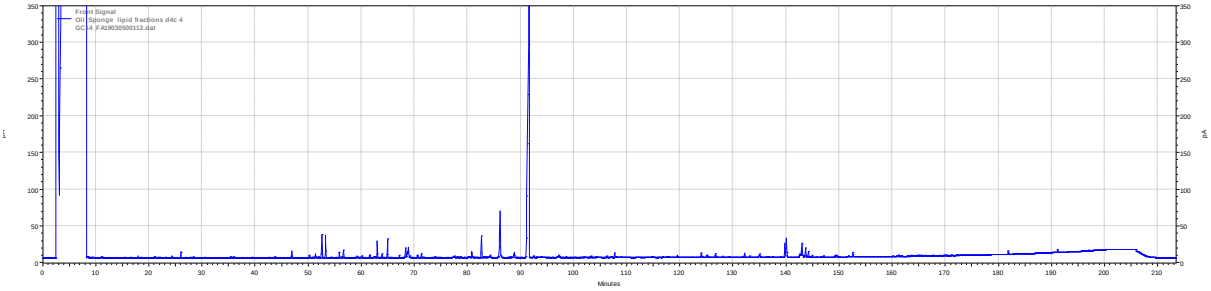

Figure F5: Chromatogram of fraction 4 from the total lipid extract.

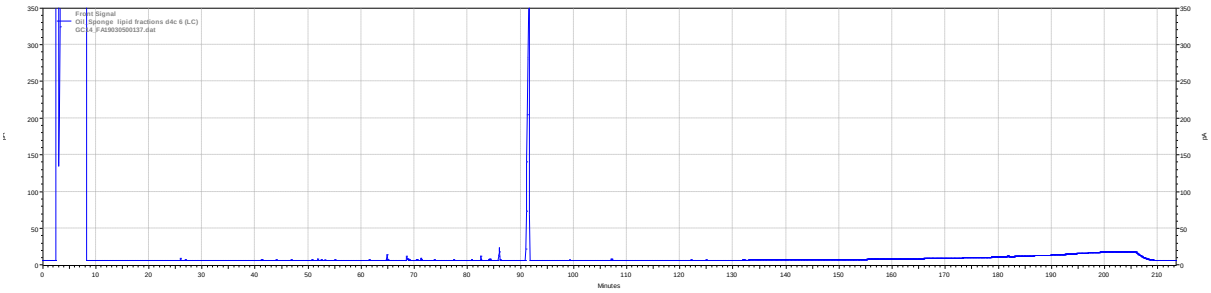

Figure F6: Chromatogram of fraction 5 from the total lipid extract.

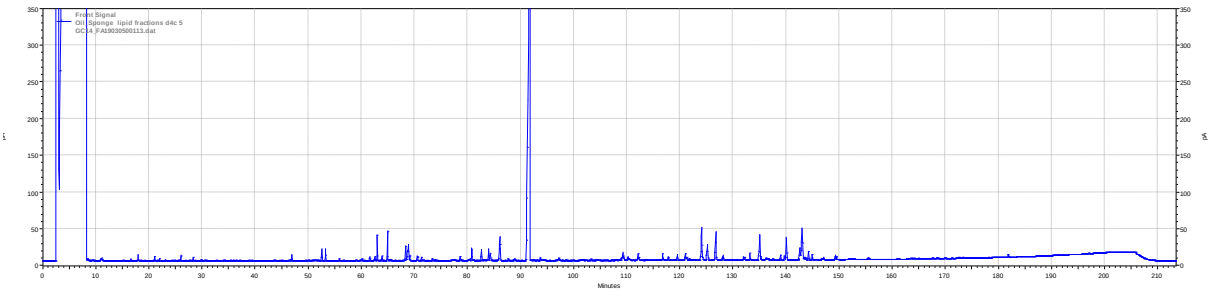

Figure F7: Chromatogram of fraction 6 from the total lipid extract.

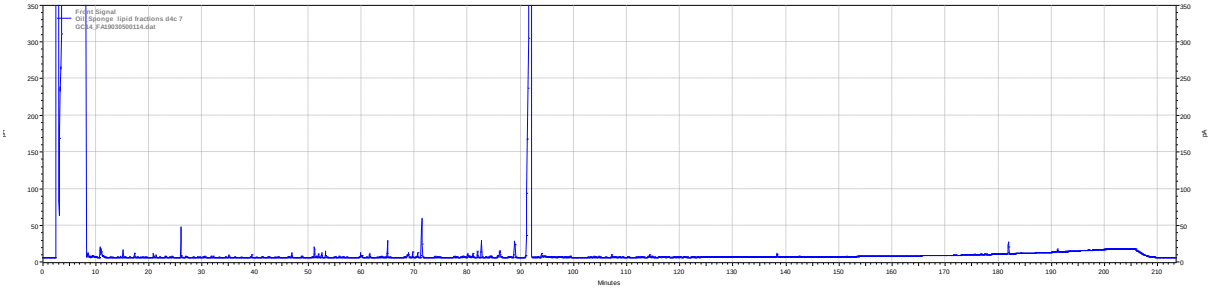

Figure F8: Chromatogram of fraction 7 from the total lipid extract.

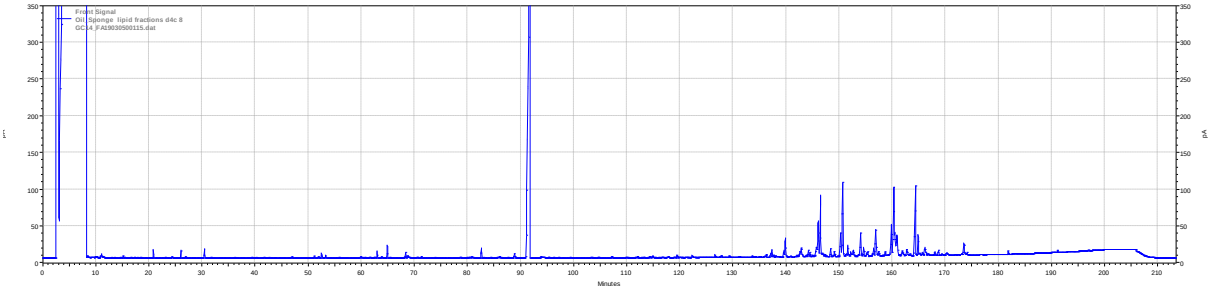

Figure F9: Chromatogram of fraction 8 from the total lipid extract.

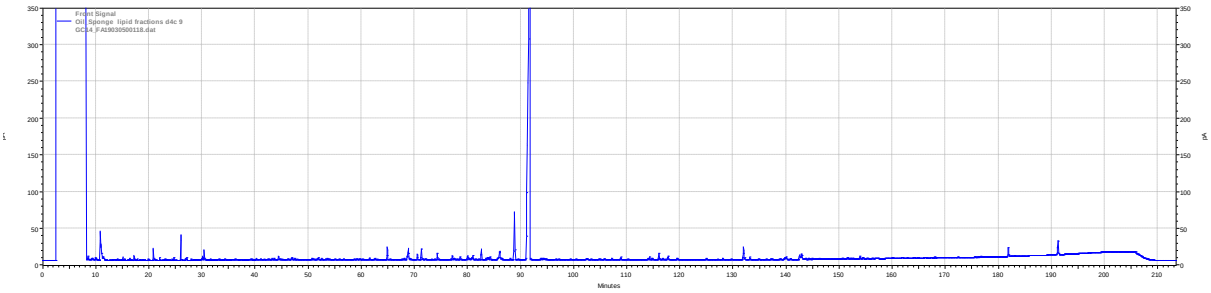

Figure F10: Chromatogram of fraction 9 from the total lipid extract.